SUPPLEMENTAL MATERIAL

Analytical techniques

U-Pb Geochronology

Separation of heavy minerals from all samples followed standard crushing, heavy liquid, and magnetic separation techniques. Zircon crystals were picked in ethanol under a binocular microscope and were selected based on their morphology, color, clarity, and lack of inclusions. Sample locations are presented in Figure 2. Zircons selected for U-Pb analysis were placed in quartz beakers and annealed in a muffle furnace at 900 ± 20 °C for 60 hours. When possible, individual grains to be dated were selected for image analysis. In some samples, zircons were too small to be both imaged and dated. In this case, representative grains were selected for imaging. All zircon images are grouped by sample number and are presented in Figs. S1-S49. Zircons were mounted in epoxy and polished to approximately half their original thickness. Cathodoluminescence (CL) imaging of grain mounts was done with the MIT JEOL 733 Superprobe electron microprobe. Image analysis was carried out with a 15 kV accelerating voltage and 10-30 nA beam current. If the size of the grain allowed, zircon grains were removed from the mount after CL imaging for U-Pb analysis. Zircons selected for analysis were chemically abraded using a modified version of the technique of (Mattinson, 2005). Grains were loaded in 300 µl Teflon FEP microcapsules, placed in a Parr vessel, and leached in ~120 µl of 29 M HF for 12 hours at 220 °C. Following the leach step, grains were fluxed in HNO_3 for 30 minutes and then sonicated for 45 minutes. After this step, grains were rinsed two times in ultrapure water and fluxed in 6 M HCl for 30 minutes and sonicated for 45 minutes. Grains were each rinsed two more times in ultrapure water and then loaded into individual microcapsules with ~120 µl of 29 M HF and a mixed ^{205}Pb-^{233}U-^{235}U spike (ET535). Zircons were dissolved at 220 °C for 48 hours, dried to salts, and re-dissolved in ~120 µl of 6 M HCl at 180 °C for at least 12 hours. Pb and U were separated from the sample using HCl-based anion exchange columns modified from (Krogh, 1973).

Pb and U were analyzed by thermal ionization mass spectrometry on the MIT VG Sector 54 multicollector mass spectrometer or the MIT Isotopx X62 multicollector mass spectrometer. Both Pb and U were loaded onto degassed single zone-refined Re filaments with a silica gel-H_3PO_4 mixture (Gerstenberger and Haase, 1997). Pb was measured by peak-hopping on a single Daly detector. U was measured in static Faraday mode. Isotope ratios Pb were corrected for mass fractionation during analysis using the ET535 tracer solution (McLean et al., 2015; Condon et al., 2015). Data aquisiton and

reduction was accomplished using the Tripoli and U-Pb Redux software packages (McLean et al., 2011; Bowring et al., 2011).

Zircon U-Pb data from the Midnight Peak Formation and the BPIC are summarized in Table 1 and reported at the 95% confidence levels in Table 2. U-Pb zircon data from these samples typically yield clusters of dates on or near concordia ($^{206}Pb/^{238}U = {}^{207}Pb/^{235}U = {}^{207}Pb/^{206}Pb$). Final solidification ages are interpreted using the $^{206}Pb/^{238}U$ dates, which give the highest possible precision for rocks of this general age range. The $^{206}Pb/^{238}U$ dates are calculated with the decay constants of (Jaffey et al., 1971) and the present day $^{238}U/^{235}U$ ratio recommended by (Hiess et al., 2012); errors were calculated using the algorithms of (McLean et al., 2011). All dates are corrected for initial ^{230}Th disequilibrium using an average whole rock Th/U ratio of 2.6 ± 0.15, calculated from three whole-rock samples (Chan, 2012). Altering this value by 50% changes the $^{206}Pb/^{238}U$ date by less than 10 ka. As we are concerned with duration of magmatism, the errors of the weighted mean dates are the internal errors based on analytical uncertainties only, including counting statistics, spike subtraction, and blank subtraction.

In-situ trace element analysis

In-situ trace element analyses of zircons from eleven samples (MAF, PX10-76, PX11-284, PX10-261A, PX10-34A, SCP, PX10-175, WCG, PX10-86, PX10-221, PX10-236) were acquired using the sensitive high-resolution ion microprobe (SHRIMP-RG) located at the U.S. Geological Survey-Stanford Ion Probe Laboratory (Mazdab and Wooden, 2006). Zircons selected for analysis were mounted in epoxy, polished to approximately half their thickness, and imaged using a cathodoluminescence (CL) detector on a scanning electron microscope. These images were used to guide selection of points for analysis. Isotopic analysis was conducted using a ~15 μm diameter, 1-2 nA O_2^- primary beam. Grains were analyzed for Li, Be, B, F, P, Ti, V, Y, all the REE, Hf, Pb, Th, and U. Trace element concentrations were standardized against Madagascar Green (MAD) zircons (Mazdab and Wooden, 2006). Spot locations are presented in Figs. S10, S15, S16, S18, S19, S22-24, S27, S29-S32, S34, S37, S38, S42, S43, S48, S49, S51, S54, S55, S57. Data can be found in Table S1.

Sm-Nd isotopic analysis

Sm-Nd isotopic analyses were done for six samples from the Black Peak intrusive complex (PX10-13B, PX10-148, PX10-148B, PX10-251, PX10-236, WCG). Approximately 100 mg of powdered whole rock from each sample was spiked with a mixed ^{149}Sm-^{150}Nd tracer and completely dissolved in 3 mL of concentrated HF and 0.5 mL of 7 M HNO_3 in Teflon pressure vessels at 220 °C for 48 h. Separation of Nd

and Sm was carried out using a standard two-stage column chemistry procedure. The REEs were isolated in 8 cm^3 columns containing Biorad AG50W-X8 cation-exchange resin, followed by separation of Nd and Sm from the REEs in 5 cm^3 columns containing Eichrom LN-spec resin, using 0.3 M HCl and 0.5 M HCl, respectively. Once separated, Sm was loaded onto single Ta filaments with ~1 μL of 1 M H_3PO_4 and analyzed as metal ions in static mode on the Sector X62 TIMS at MIT. Nd was loaded onto triple Re laments with ~1 μL of 1 M H_3PO_4 and analyzed as metal ions in dynamic multicollector mode with a ^{144}Nd signal intensity of 1.5 $x10^{-11}$ A. Sm and Nd data were corrected for fractionation using an exponential law and normalizing to $^{152}Sm/^{147}Sm$=1.783 and $^{146}Nd/^{144}Nd$=0.7219, respectively. Details of internal and external reproducibility of the data are given in the footnote to Table S2. Data from all samples are given in Table S2 and presented in Fig. 10.

Oxygen Isotopic Analysis

High spatial resolution zircon $\delta^{18}O$ values were analyzed using the UCLA CAMECA ims 1270 high-resolution ion microprobe using the same mounts made for trace element analysis. All analyses were conducted during a single session settings and conditions were similar to those described in the supplementary data to Schmitt (2006). Because the USGS-Stanford SHRIMP uses an oxygen primary beam, mounts were first polished to remove analysis pits that may have contained implanted oxygen. CL images were used to analyze approximately the same region for both trace element and oxygen isotopic measurements. Our data are reported relative to the R33 internal standard (5.55 ± 0.04 ‰; Valley, 2003). Data are presented in Table S3 and Fig. 11.

Sample and zircon descriptions

Midnight Peak Formation

BPX10-110. One sample, BPX10-110, was analyzed from the Midnight Peak Formation. As stated in the main text, this sample was collected <100 m from the nearest outcrop of the BPIC (Fig. 2). BPX10-110 is a fine-grained andesite with plagioclase and augite phenocrysts, and has been statically metamorphosed in the greenschist facies. Zircons are extremely rare in this sample; however, two small, stubby zircons yielded ages that overlapped within uncertainty. A weighted mean of these analyses gives an age of 94.166 ± 0.077 Ma (Figs. 4, S58a).

Crescent Mtn unit

MAF-1.Twelve whole grains of zircon were analyzed from sample MAF, a coarse-grained gabbro, collected near the eastern margin with the Twisp Valley schist (Fig. 2). Thin section analysis indicates zircons are present as inclusions in hornblende, plagioclase, and quartz. All zircons were selected from a population of euhedral stubby prisms. CL images from dated and representative grains show very thin bright rims surrounding concentrically-zoned cores (Figs. S9-S10). Analysis of chemically abraded grains yielded a range of dates that exceeds analytical uncertainty, indicating an older component. Older analyses range up to 91.95 ± 0.4 Ma. Analysis of the youngest eight grains yielded a weighted mean date of 91.755 ± 0.040 Ma (MSWD=0.97, n=8) (Figs. 4, S58b).

PX10-34B. Seven whole grains and fragments of zircon were analyzed from sample PX10-34B, a coarse-grained gabbro, collected along the contact between the Crescent Mtn unit and the Stiletto Mtn unit (Fig. 2). Zircons from this sample were euhedral and stubby. Thin section analysis indicates zircons are present as inclusions in plagioclase and quartz. Some grains showed bright rims surrounding sector or oscillatory zoned cores while others showed oscillatory zoning from core to rim (Fig. S11). Analysis of seven grains yielded a weighted mean date of 91.587 ± 0.027 Ma (MSWD=1.1, n=7) (Figs. 4, S58c).

PX10-54. Seven whole zircon grains were analyzed from sample PX10-54, a biotite tonalite collected along the eastern contact of the Crescent Mtn unit with the Triassic Twisp Valley schist (Fig. 2). CL images from a representative population of grains show concordant oscillatory zoning from rim to core with some grains containing structural cores, although not all of these grains have older ages (Fig. S12). A population of six dates overlap and yield a weighted mean date of 91.378 ± 0.036 Ma (MSWD=1.3, n=6); one grain is slightly older with a date of 91.904 ± 0.084 Ma (Fig. 4, S58d).

PX10-13b. Eight zircon grains, selected from a population of colorless, clear euhedral prisms, were analyzed from sample PX10-13b, a medium-grained quartz diorite collected in the central part of the Crescent Mtn unit (Fig. 2). Thin section analysis suggests that zircons are present as inclusions near the rims of plagioclase grains and in quartz. CL images from nearly all grains reveal grains with oscillatory zoning that appears concordant between cores and rims with rare truncations of the zoning pattern (Fig. S13). Sector zoning was also present in some grains. The eight grains yielded a range of dates that do not overlap within uncertainty from 91.47 ± 0.14 Ma to 91.18 ± 0.12 Ma, our estimate for the timing of final solidification (Fig. 4, S58e).

Stiletto Mtn unit

PX10-76. Seventeen whole grains were analyzed from sample PX10-76, a medium-grained hornblende granodiorite collected approximately 100 m west of the contact with the ~94 Ma Midnight Peak formation (Fig. 2). CL images of representative zircons suggest that distinct cores are not uncommon (Figs. S14-S16). Grains are generally small and sub-euhedral and thin section analysis indicates zircon is present as inclusions in plagioclase and quartz. One grain from PX10-76 is 90.69 ± 0.20 Ma, slightly older than the weighted mean date of the youngest sixteen grains 90.345 ± 0.030 Ma (MSWD =1.1, n=16) (Figs. 5, S59a).

PX10-34A. Nine whole grains were analyzed from sample PX10-34A, a medium-grained hornblende granodiorite (Color index (CI) ~35) collected from the eastern Stiletto Mtn unit along the contact with the Crescent Mtn unit (sample PX10-34B) (Fig. 2). Along the contact the two phases show mingling relationships at the outcrop-scale. Zircons from PX10-34A are clear, colorless, and euhedral and thin section analysis indicates zircons are present as inclusions in plagioclase rims and quartz. CL images from dated and representative grains show many distinct cores, likely from mixing and assimilation of the Crescent Mtn unit (Figs. S17-S18). Dates within PX10-34A range up to 90.975 ± 0.064 Ma, suggesting an inherited component from the Crescent Mtn unit (Figs. 5, S59b). The two youngest grains in the sample have simple oscillatory zoning and yield a weighted mean date of 90.292 ± 0.053 Ma (MSWD=0.82, n=2).

GP-322.Nine whole grains were analyzed from sample GP-322, a medium-grained hornblende tonalite collected near the contact between the eastern Stiletto Mtn unit and the Midnight Peak formation (Fig. 2). CL images of a representative population of grains indicate most grains have concentric zoning from core to rim, many grains also have sector zoning. Obvious cores are rare in CL images of zircons (Fig. S20). Zircons are generally euhedral, clear, colorless, small (<70 μm) and stubby. Zircons from GP-322 have dates that range from 90.219 ± 0.080 Ma to 90.400 ± 0.058 Ma (Fig. 5, S59c). The youngest two grains yield a weighted mean date of 90.238 ± 0.065 Ma (MSWD=0.72, n=2).

PX10-289. Four grains were analyzed from PX10-289, a fine-grained biotite hornblende granodiorite collected along the northeastern edge of the Stiletto unit (Fig. 2). Grains were selected from population of clear, colorless euhedral equant zircons and yield a weighted mean date 90.132 ± 0.075 Ma (MSWD=1.1, n=4), interpreted as the crystallization age (Figs. 5, S59d).

K26. Seven grains and grain fragments were analyzed from sample K26, a fine- to medium-grained hornblende tonalite collected from the Stiletto transect (Fig. 2b). CL images of representative grains suggest that cores are rare and sector zoning is present in all imaged grains (Figs. S21-S22). Zircons from

K26 are clear, colorless, euhedral equant or elongate grains. A weighted mean of the youngest five analyses gives a date of 90.110 ± 0.036 Ma (MSWD= 1.1, n=5). Older grains range up to 90.29 ± 0.41 Ma (Figs. 5, S59e).

K55. Six whole grains and grain fragments were analyzed from sample K55, a coarse-grained biotite tonalite collected along the Stiletto transect (Fig. 2). CL images of dated and representative grains show simple sector and concentric zoning patterns with little evidence for older cores (Figs. S23-24). In plain light, zircons are clear, colorless elongate or equant grains. Most analyses overlap within uncertainty, but one grain did not, giving a date of 90.155 ± 0.062 Ma (Figs. 5, S59f). A weighted mean of the youngest five analyses gives a date of 90.075 ± 0.027 Ma (MSWD=0.80, n=5).

PX10-251. Seven whole grains were analyzed from sample PX10-251, collected along the northeastern Stiletto Mtn unit (Fig. 2). Here, the Stiletto Mtn unit is intruded by the Eocene Golden Horn granite, obscuring any contact relationships with host rocks. PX10-251 is a medium-grained granite with euhedral hornblende. Thin section analysis indicates zircons are present as inclusions in hornblende, biotite, plagioclase, and quartz. CL images of grains from PX10-251 suggest that distinct, discordant cores are relatively uncommon; most grains are concentrically zoned from core to rim (Fig. S25). Dates from PX10-251 show some scatter outside of analytical uncertainty and range up to 90.48 ± 0.33 Ma (Figs. 5, S59g). A weighted mean of the youngest six analyses gives a date of 90.076 ± 0.070 Ma (MSWD =0.32, n=4).

K16B. Five whole grains and grain fragments were analyzed from sample K16B, a coarse-grained biotite tonalite collected from a weakly sheeted zone along the Stiletto transect (Fig. 2b). CL images of dated and representative grains show homogeneous light-colored cores surrounded by concentrically-zoned rims (Figs. S26-S27). Zircons from K16B are clear, colorless, and euhedral elongate or equant grains. A weighted mean of all five analyses gives a date of 90.066 ± 0.053 Ma (MSWD=0.17, n=5) (Figs. 5, 59h).

K9. Eight whole grains and grain fragments were analyzed from sample K9, a fine- to medium-grained biotite tonalite collected along the Stiletto transect (Fig. 2b). Zircons are sub-euhedral equant or stubby grains. Dates from K9 range up to 90.131 ± 0.048 Ma (Fig. 5, S59i). A weighted mean of the youngest six analyses gives a date of 90.063 ± 0.030 Ma (MSWD=0.68, n=6).

PX10-236. Eight grains were analyzed from sample PX10-236, a medium-grained hornblende diorite collected along the eastern Stiletto Mtn unit (Fig. 2). Thin section analysis indicates that zircons are present as inclusions in plagioclase and quartz. CL images of dated and representative grains show

simple twinning, sector zoning, or concentric zoning from core to rim with no obvious cores (Figs. S28-30). Dates from PX10-236 range up to 90.47 ± 0.11 Ma, indicating an older component in the zircon population (Figs., 5, S59j). A weighted mean of the youngest five analyses from PX10-236 gives a date of 90.050 ± 0.028 Ma (MSWD=0.77, n=6).

K42B. Seven whole grains and grain fragments were analyzed from sample K42B a fine to medium-grained biotite tonalite collected along the Stiletto transect (Fig. 2b). This sample was obtained from a heterogeneous outcrop of tonalite with varying biotite and hornblende content. Zircon morphology is sub-euhedral and ranges from elongate to stubby. CL images from dated and representative grains suggests that xenocrystic cores are present in many grains. Other grains show concentrically-zoned rims and cores or zoned rims surrounding homogeneous, light-colored cores (Figs. S31-S32). Our geochronology supports this conclusion; dates from K42B range from 89.63 ± 0.23 Ma to 90.33 ± 0.20 Ma (Figs. 6, S59k). A weighted mean of the youngest four analyses gives a date of 89.710 ± 0.043 Ma (MSWD=0.27, n=4).

PX10-86. Sample PX10-86, a medium-grained biotite tonalite, was collected from the western half of the Stiletto Mtn unit (Fig. 2). This sample shows significant solid state deformation, likely caused by movement along the Gabriel Peak fault zone. Zircons are euhedral, clear, colorless, and small. Thin section analysis indicates zircons are present in quartz and plagioclase grains. CL images of dated and representative grains suggest that most zircons have concentrically-zoned rims surrounding large, homogeneous light-colored cores (Figs. S33-S34). Dated grains range from 89.15 ± 0.14 Ma to 90.01 ± 0.13 Ma (Figs. 6, S59l). A weighted mean of the four youngest grains give a date of 89.183 ± 0.067 Ma (MSWD=0.33, n=4).

GP-309-1. Six whole grains were dated from sample GP-309-1, a highly deformed biotite tonalite collected directly east of the Gabriel Peak fault zone (Fig. 2). Zircons from GP-309-1 are euhedral, clear, colorless, and small and thin section analyses indicate that zircons are present as inclusions in plagioclase and quartz. CL images of representative zircons show concentrically-zoned rims and cores and some grains have a notable dark band between these regions (Fig. S35). Dates show scatter outside of analytical uncertainty and range from 89.85 ± 0.14 Ma to 88.81 ± 0.30 Ma (Figs. 6, S59m).

Louis Lake heterogeneous zone

PX11-261A. Seven whole grains were dated from sample PX11-261A, a coarse-grained hornblende tonalite with a color index ~40. This sample was collected from an outcrop containing many fine-grained

enclaves (which were not present in the dated sample) and cut by grey tonalite and leucotonalite dikes (Fig. 2c). Zircons are stubby, clear, colorless, and euhedral. CL images of dated and representative grains suggest relatively simple growth patterns; grains are typified by large, dark-colored cores surrounded by concentrically-zoned rims (Figs. S36-S38). A weighted mean of all seven grains gives a date of 89.762 ± 0.033 Ma (MSWD=1.6, n=7) (Figs. 6, S60a).

PX10-209. Eight whole grains and grain fractions were dated from PX10-209, a fine-grained, grey-colored biotite tonalite collected from a 10-m-thick dike cross-cutting an outcrop of coarse-grained biotite tonalite (Fig. 2c). Zircons are euhedral, clear, and colorless; grain morphology varies between stubby and equant. Thin section analysis of PX10-209 indicate that zircon is present at inclusions in plagioclase and quartz. CL images of dated and representative grains show core to rim oscillatory zoning or large homogeneous dark-colored cores surrounded by concentrically-zoned rims (Fig. S39). Dates from PX10-209 range from 89.933 ± 0.064 Ma to 89.475 ± 0.054 Ma (Figs. 6, S60b).

PX11-263C. Seven whole grains were dated from sample PX11-263C, a fine-grained, grey-colored biotite tonalite collected from a dike cutting a complex outcrop of coarse-grained biotite tonalite and medium-fine grained biotite tonalite (Fig. 2c). Zircons are stubby to equant, euhedral, clear, and colorless. CL images of representative grains show that grains can have simple sector or concentric zoning or more complex zoning patterns (Fig. S40). One older grain is present in our sample set, giving a date of 89.504 ± 0.060 Ma (Figs. 6, S60c). A weighted mean of the youngest six analyses gives a date of 89.400 ± 0.037 Ma (MSWD=1.4, n=6).

PX11-284. Ten whole grains were dated from sample PX11-284, a medium- to fine-grained biotite tonalite with minor hornblende collected directly outside the heterogeneous zone (Fig. 2c). Overall the outcrop is homogeneous, but is cut by a small dikelet of grey tonalite, which is in turn cut by a pegmatite filling in a small fault. Zircons are stubby to equant, euhedral, clear, and colorless. CL images of dated and representative grains show little evidence for distinct cores; grains are generally concentrically zoned from rim to core (Figs. S41-S42). However, our U-Pb dates show scatter outside of analytical uncertainty, dated grains range from 90.44 ± 0.12 Ma to 89.345 ± 0.093 Ma (Figs. 6, S60d).

PX11-270. Seven whole grains were dated from sample PX11-270, a medium-grained felsic tonalite cut by dikes of leucotonalite and grey tonalite (Fig. 2c). Zircons from PX11-270 are stubby to equant, euhedral, clear, and colorless. Our U-Pb dates from this sample show scatter outside analytical uncertainty, ranging from 90.875 ± 0.052 Ma to 89.027 ± 0.093 Ma (Figs. 6, S60e).

PX11-268. Five whole grains were dated from sample PX11-268, a coarse-grained leucotonalite dike cross-cutting an outcrop of medium-fine grained biotite tonalite (Fig. 2c). The dike of leucotonalite cuts the boundary between a mixed zone and a more homogeneous zone within the tonalite, which is not uncommon for leucotonalite dikes. Zircons from PX11-268 are generally colorless, clear, sub-euhedral equant grains. As with most samples in the heterogeneous zone, PX11-268 shows significant evidence for an older component in its zircon population. Dates from PX11-268 range from 89.786 ± 0.055 Ma to 89.017 ± 0.072 Ma (Fig. 6, S60f).

Reynolds Peak unit

PX10-96. Eight whole grains and grain fragments were dated from sample PX10-96, a medium-grained hornblende-biotite tonalite collected along the northern end of the Reynolds Peak unit (Fig. 2). CL images of dated grains show homogeneous light-colored cores surrounded by concentrically-zoned rims that comprise >90% of the grain (Fig. S43-S44). In plain light, zircons are sub-euhedral, clear, and colorless. Thin section analysis indicates that most zircons are present as inclusions in plagioclase and quartz, but some are present in hornblende and biotite. U-Pb analyses show scatter outside of analytical uncertainty, dates range from 88.38 ± 0.11 Ma to 88.74 ± 0.11 Ma (Figs. 7, S61a). A weighted mean date of the youngest five analyses is 88.467 ± 0.031 Ma (MSWD=1.0, n=5).

PX10-103B. Ten whole grains and grain fragments were dated from sample PX10-103B, a medium-grained leucotonalite collected from the same outcrop as PX10-103A (Fig. 2). Zircons were stubby to equant, euhedral, clear, and colorless. Thin section analysis indicates zircons are present in plagioclase, potassium feldspar, biotite, and quartz. CL images of dated and representative grains show grains with concentric zoning from core to rim or with homogeneous light-colored cores surrounded by concentrically-zoned rims (Fig. S45). Dated grains range from 90.910 ± 0.079 Ma to 88.28 ± 0.11 Ma, (Figs. 7, S61b). A weighted mean of the youngest three analyses gives a date of 88.403 ± 0.042 (MSWD=0.35, n=3)

GP-158-10. Thirteen whole grains were dated from sample GP-158-10, a medium-grained biotite tonalite collected from the southern part of the Reynolds Peak unit (Fig. 2). Zircons are equant, euhedral, clear, and colorless and thin section analysis suggests that most grains are present in plagioclase or quartz. CL images of dated and representative grains suggest indicate that most grains have concentrically-zoned rims surrounding homogeneous, light-colored cores (Fig. S46). Dated grains

range from 88.359 ± 0.078 Ma to 93.38 ± 0.12 Ma (Figs. 7, S61c). A weighted mean of the youngest seven grains gives a date of 88.382 ± 0.035 Ma (MSWD=0.23, n=7).

SCP. Ten whole grains and grain fragments were dated from sample SCP, a medium-grained leucotonalite collected from the eastern portion of the Reynolds Peak unit (Fig. 2). Zircons are equant to elongate, euhedral, clear, and colorless and present as inclusions in potassium feldspar, plagioclase, quartz, and biotite. CL images of dated and representative grains suggest that most zircons are concentrically-zoned from core to rim (Figs. S47-S49). Dates range from 88.220 ± 0.071 Ma to 88.84 ± 0.25 Ma (Figs. 7, S61d). A weighted mean of the youngest two dated grains give a date of 88.221 ± 0.050 Ma (MSWD= 0.00053, n=2).

PX10-221. Eleven whole grains were dated from sample PX10-221, a medium- to fine-grained granite collected from the central part of the Reynolds Peak unit (Fig. 2). Zircons are stubby to equant, euhedral, clear, and colorless and present as inclusions in plagioclase, potassium feldspar, biotite, and quartz. CL images of zircons are generally have concentrically zoned rims surrounding light-colored cores (Figs. S50-51). Dated grains show significant scatter outside of analytical uncertainty. Dates range from 88.590 ± 0.083 Ma to 87.872 ± 0.065 Ma (Figs. 7, S61e).

PX10-103A. Ten whole grains and grain fragments were dated from sample PX10-103A, a medium- to fine-grained biotite tonalite collected from an outcrop close to the contact with the eastern Stiletto Mtn unit (Fig. 2) Zircons are stubby to equant, euhedral, clear, and colorless. Thin section analysis indicates zircons are present as inclusions in plagioclase, potassium feldspar, and quartz. CL images of dated and representative grains show large, light-colored cores surrounded by concentrically zoned rims (Fig. S52). Dated grains range from 87.69 ± 0.14 Ma up to 92.14 ± 0.14 Ma (Figs. 7, S61f). The weighted mean of dates from two pieces from the same grain give date of 87.565 ± 0.072 Ma (MSWD=1.4, n=2).

War Creek unit

WCG. Twelve whole grains were analyzed from sample WCG, a fine-grained biotite tonalite gneiss collected from the western margin of the War Creek unit (Fig. 2). Zircons are equant, euhedral, clear, and colorless and present as inclusions in plagioclase and quartz. CL images of dated and representative grains show concentrically zoned cores, some embayed, surrounded by darker rims (Figs. 53-55). Dates range up to 161.43 ± 0.11 Ma but the majority of analyses are <91 Ma (Figs. 8, S62a-b). The youngest analyzed grain gives a date of 87.474 ± 0.052 Ma.

PX10-175. Eleven whole grains and grain fragments were analyzed from sample PX10-175, a fine-grained biotite tonalite gneiss collected along the sheeted western margin of the War Creek unit (Fig. 2). Zircons are equant, euhedral, clear, and colorless. Thin section analysis indicates zircon is present as inclusions in plagioclase and quartz. CL images of dated and representative grains show concentrically zoned cores surrounded by darker rims (Figs. 56-57). Dates range up to 123.07 ± 0.12 Ma but the majority of analyses are <88 Ma (Figs. 8, S62c-d). A weighted mean date of the youngest three analyses gives a date of 86.862 ± 0.062 Ma (MSWD=0.61, n=3).

SUPPLEMENTARY REFERENCES CITED

Bowring, J.F., McLean, N.M., and Bowring, S.A., 2011, Engineering cyber infrastructure for U-Pb geochronology: Tripoli and U-Pb_Redux: Geochemistry Geophysics Geosystems, v. 12, p. Q0AA19, doi: 10.1029/2010GC003479.

Chan, C.F., 2012, Constructing a Sheeted Magmatic Complex within the Lower Arc Crust: Insights from the Tenpeak Pluton, North Cascades, Washington [M.S. Thesis]: Corvallis, University of Oregon, 315 p.

Condon, D.J., Schoene, B., McLean, N.M., Bowring, S.A., 2015, Metrology and traceability of U-Pb isotope dilution geochronology (EARTHTIME Tracer Calibration Part I): Geochimica et Cosmochimica Acta, v. 164, p. 464-480, doi:10.1016/j.gca.2015.02.040.

Gerstenberger, H., and Haase, G., 1997, A highly effective emitter substance for mass spectrometric Pb isotope ratio determinations: Chemical Geology, v. 136, p. 309–312.

Hiess, J., Condon, D.J., McLean, N., and Noble, S.R., 2012, 238U/235U Systematics in terrestrial uranium-bearing minerals.: Science (New York, N.Y.), v. 335, p. 1610–1614, doi: 10.1126/science.1215507.

Jaffey, A.H., Flynn, K.F., and Glendenin, L.E., 1971, Precision measurement of half-lives and specific activities of ^{235}U and ^{238}U: Physical Review C, v. 4, p. 1889–1906.

Krogh, T.E., 1973, A low-contamination method for hydrothermal decomposition of zircon and extraction of U and Pb for isotopic age determinations: Geochimica et Cosmochimica Acta, v. 37, p. 485–494.

Mattinson, J.M., 2005, Zircon U–Pb chemical abrasion (“CA-TIMS”) method: Combined annealing and multi-step partial dissolution analysis for improved precision and accuracy of zircon ages: Chemical Geology, v. 220, p. 47–66, doi: 10.1016/j.chemgeo.2005.03.011.

Matzel, J., 2004, Rates of tectonic and magmatic processes in the North Cascades continental magmatic arc: 249 p.

Mazdab, F., and Wooden, J., 2006, Trace element analysis in zircon by ion microprobe (SHRIMP-RG): Technique and applications: Geochimica et Cosmochimica Acta, v. 70, p. A405.

McLean, N.M., Bowring, J.F., and Bowring, S.A., 2011, An algorithm for U-Pb isotope dilution data reduction and uncertainty propagation: Geochemistry Geophysics Geosystems, v. 12, p. 1–26, doi: 10.1029/2010GC003478.

McLean, N.M., Condon, D.J., Schoene, B., Bowring, S.A., 2015, Evaluating uncertainties in the calibration of isotopic reference materials and multi-element isotopic tracers (EARTHTIME Tracer Calibration Part II): Geochimica et Cosmochimica Acta, v. 164, p. 481-480, doi: 10.1016/j.gca.2015.02.040.

Schmitt, A.K., 2006, Laacher See revisited: High-spatial-resolution zircon dating indicates rapid formation fo a zoned magma chamber: Geology, v. 34, p. 597–600, doi: 10.1130/G22533.1.

Valley, J.W., 2003, Oxygen Isotopes in Zircon, *in*, Hanchar, J.M., and Hoskin, P.W.O, eds., Zircon: Reviews in Mineralogy and Geochemistry 53, p. 343–385.

Fig. S1: Contact between the Twisp Valley schist and intrusions in the Crescent Mtn pluton. Note the blunt-tipped intrusion of the tonalite into the schist and how intrusions wrap around the host rock.

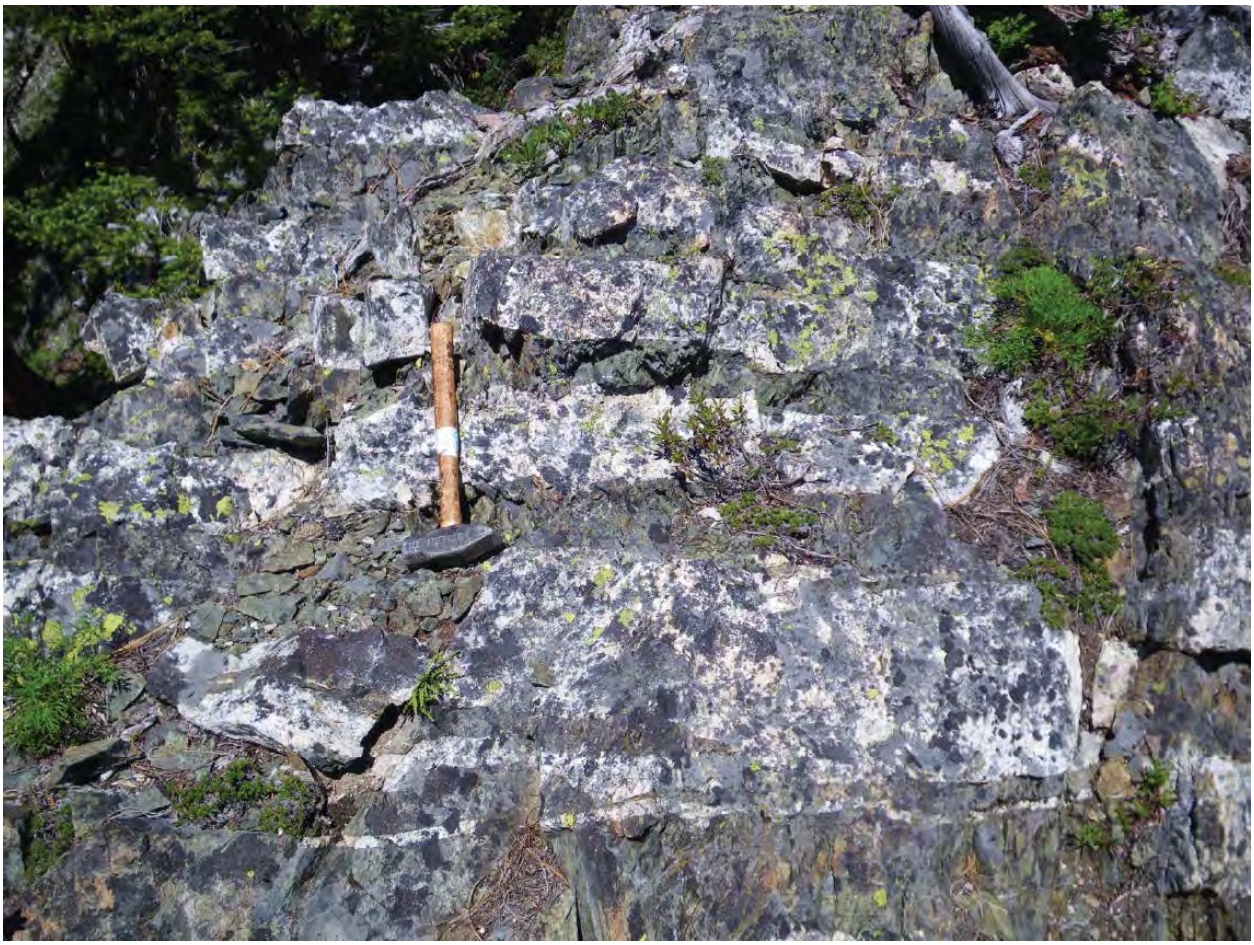

Fig. S2: Sheeted intrusions of tonalite (Stiletto Mtn pluton) in diorite (Crescent Mtn pluton). Hammer for scale. Note the sharp contact between the diorite and tonalite and the small dikelets of tonalite in diorite.

Fig. S3: Granodiorite (Stiletto Mtn pluton) intruding gabbro (Crescent Mtn pluton). Sample PX10-34A was collected from the granodiorite. PX10-34B was collected from the gabbro. Hammer for scale.

Fig. S4: Disaggregation of Midnight peak formation by intrusion of the Stiletto Mtn tonalite. Pen for scale.

Fig. S5: Outcrop in the Louis Lake heterogeneous zone showing complex relations between different magma types. Pen for scale.

Fig. S6: Mingling between magmas in the Louis Lake heterogeneous zone. Pen for scale.

Fig. S7: Older hornblende tonalite (PX11-261A) intruded by younger biotite tonalite (PX11-270). Dashed lines indicate contacts.

Fig. S8: Layering in the War Creek pluton. Hammer for scale.

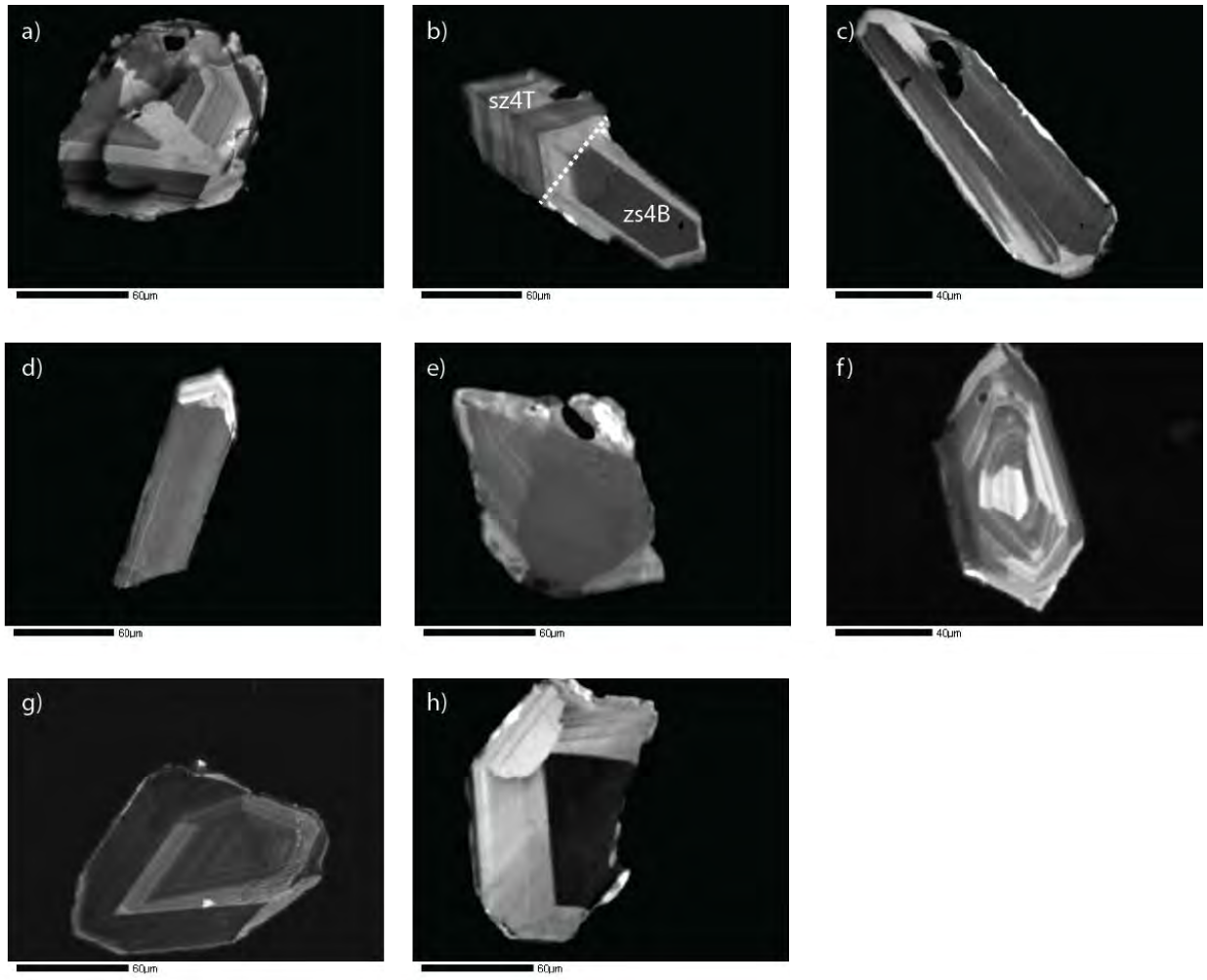

Fig. S9: CL images of representative and dated grains from sample MAF-1. Asterisk indicates dated grain. a) zM71* b) sz4T*, zs4b* c) s2* d) s3 e) zM1* f)- h) representative grains

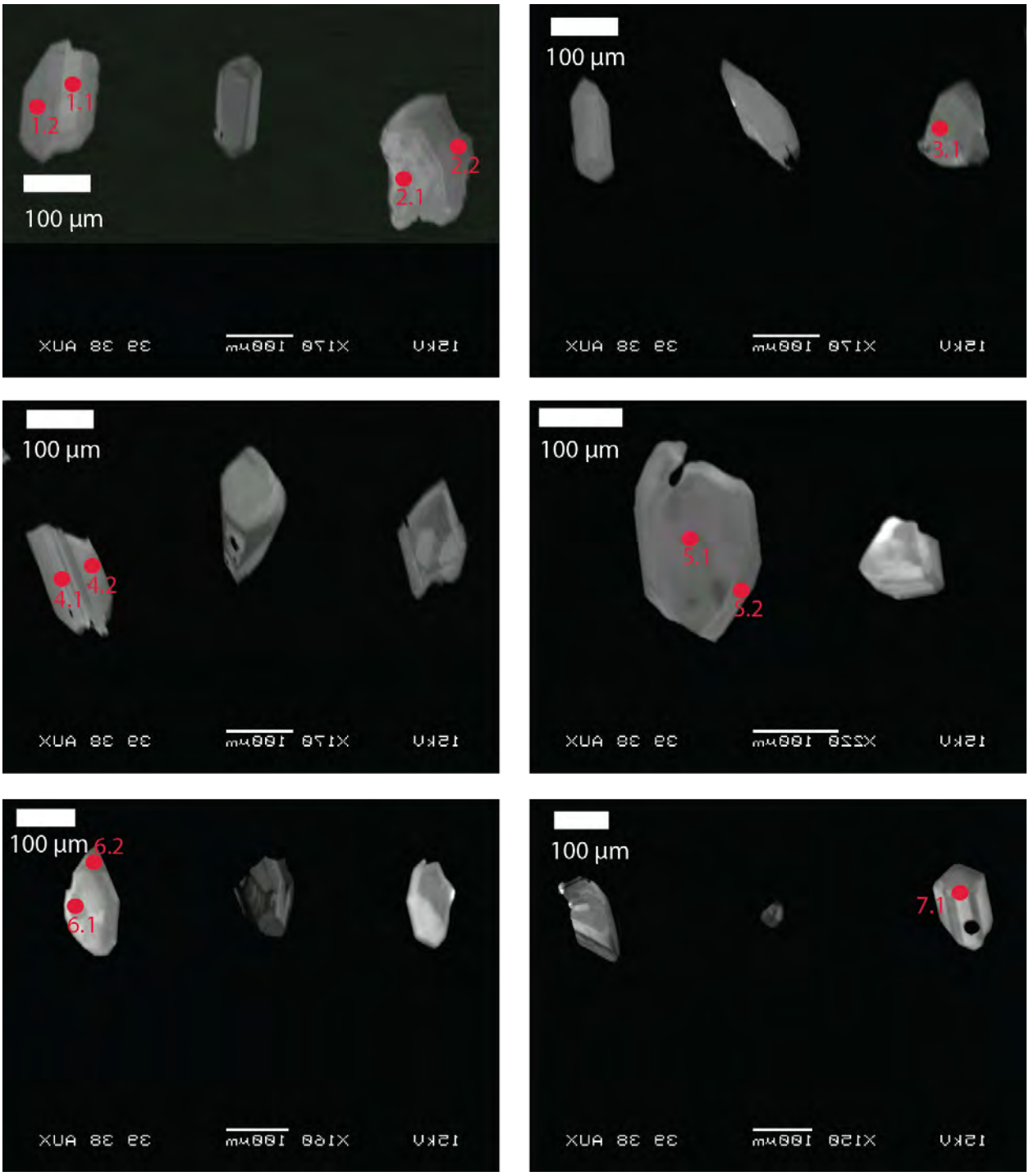

Fig. S10: CL images of SHRIMP and oxygen isotope spots from sample MAF-1. Scale bars are on the left side of each image. Spots are denoted by red dots with the spot number nearby.

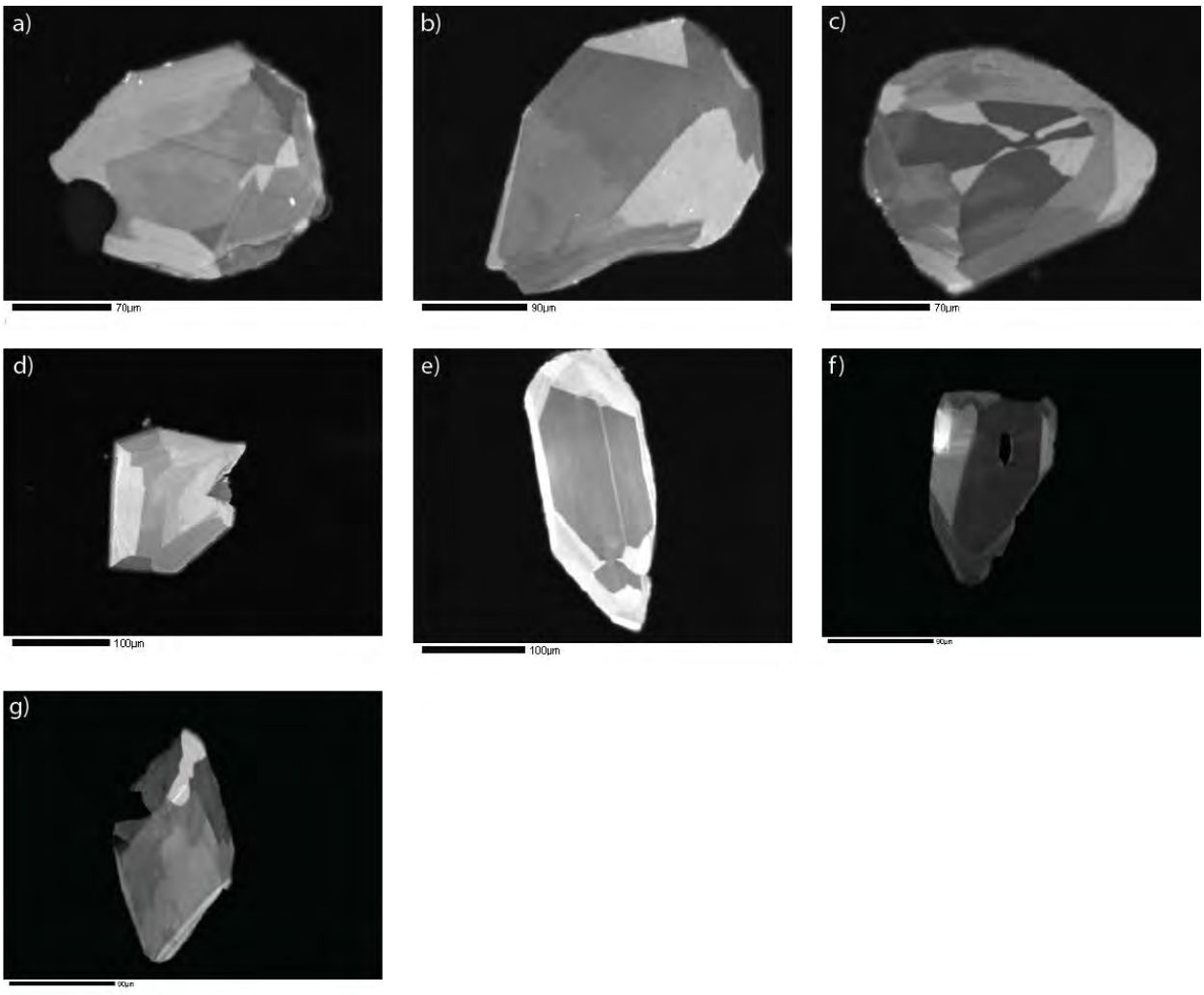

Fig. S11: CL images of dated grains from PX10-34B. a) zL1 b) zL4 c) zL5 d) zL6 e) zM5 f) zM11 g) zM12

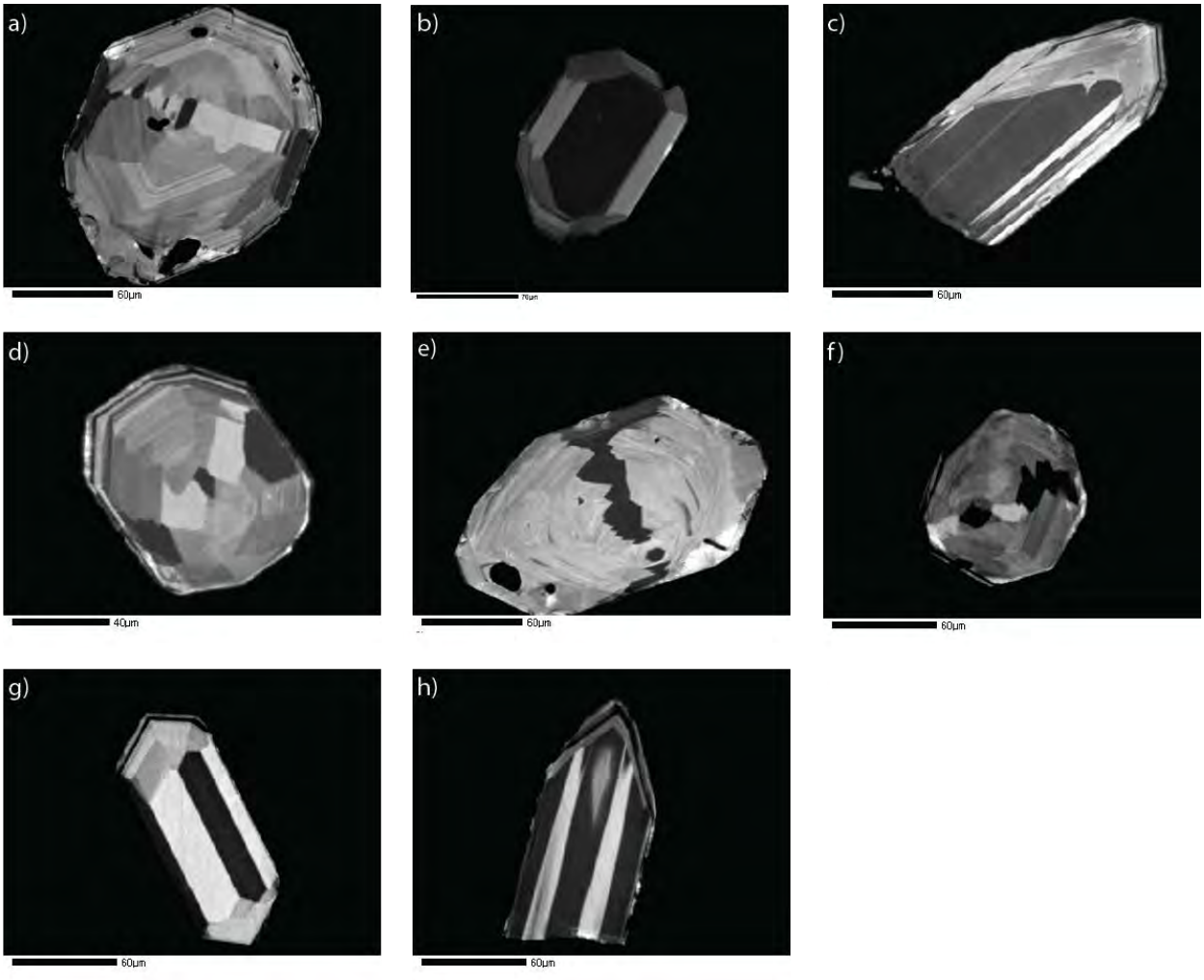

Fig. S12: CL images of representative and dated grains from sample PX10-54. Asterisk indicates dated grain. a) zM1A* b)-i) representative grains

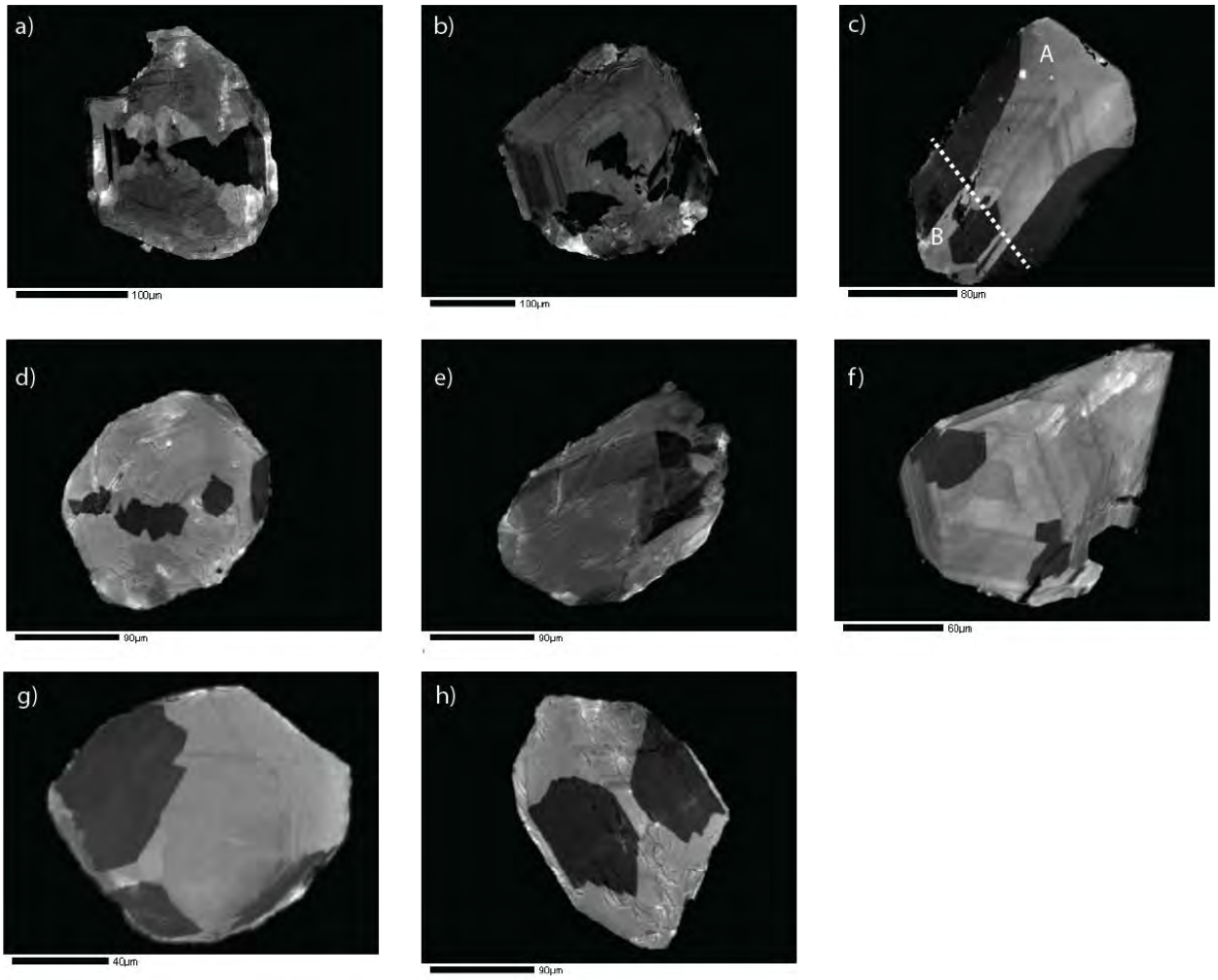

Fig. S13: CL images of dated grains from PX10-13b. Asterisk indicates dated grain. a) zL3 b) zL7 c) zM2A, zM2B* d) zM3 e) zM4 f) zM6 g) zM9 h) zM11

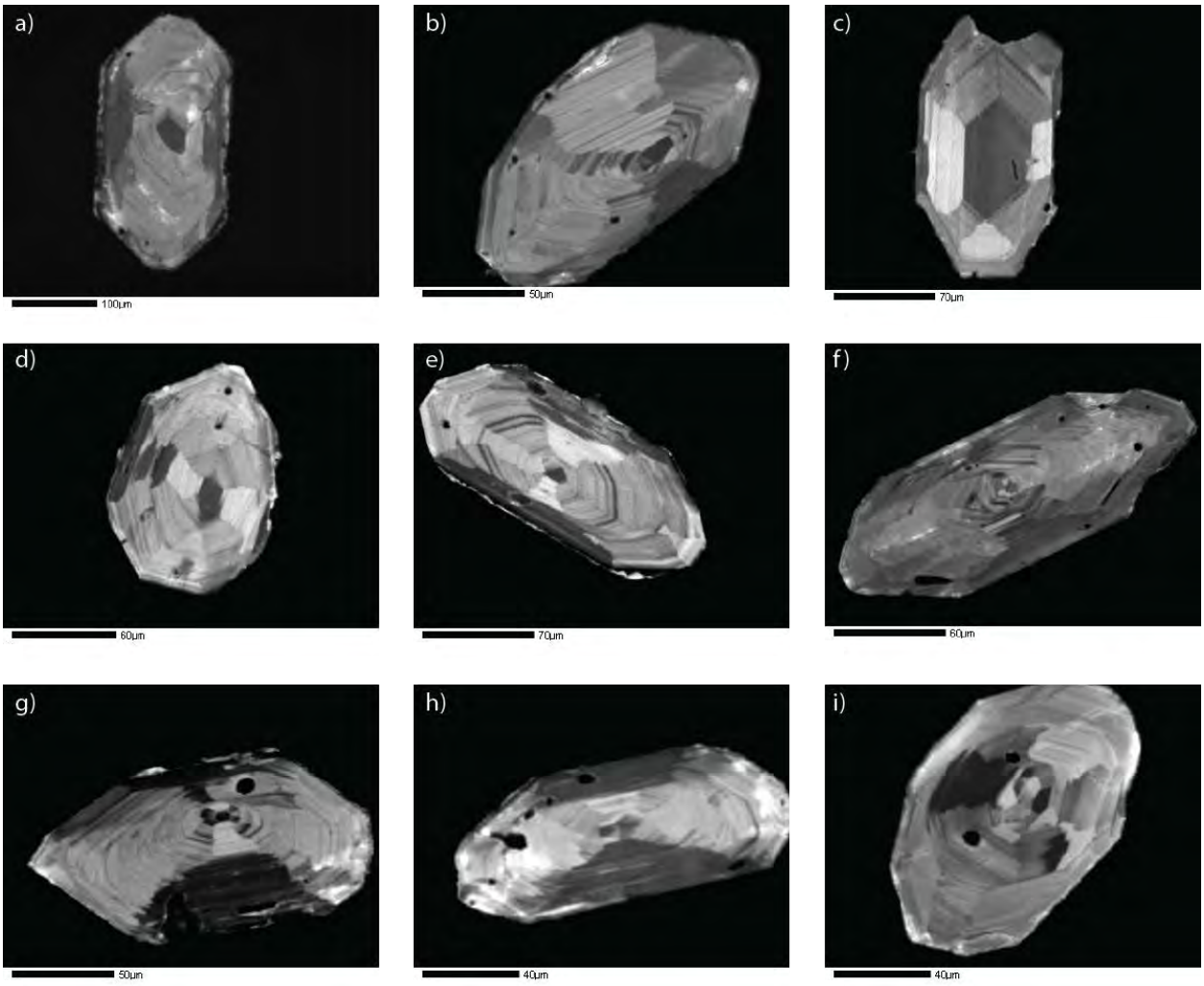

Fig. S14: CL images of dated and representative grains from sample PX10-76. a)-i) representative grains

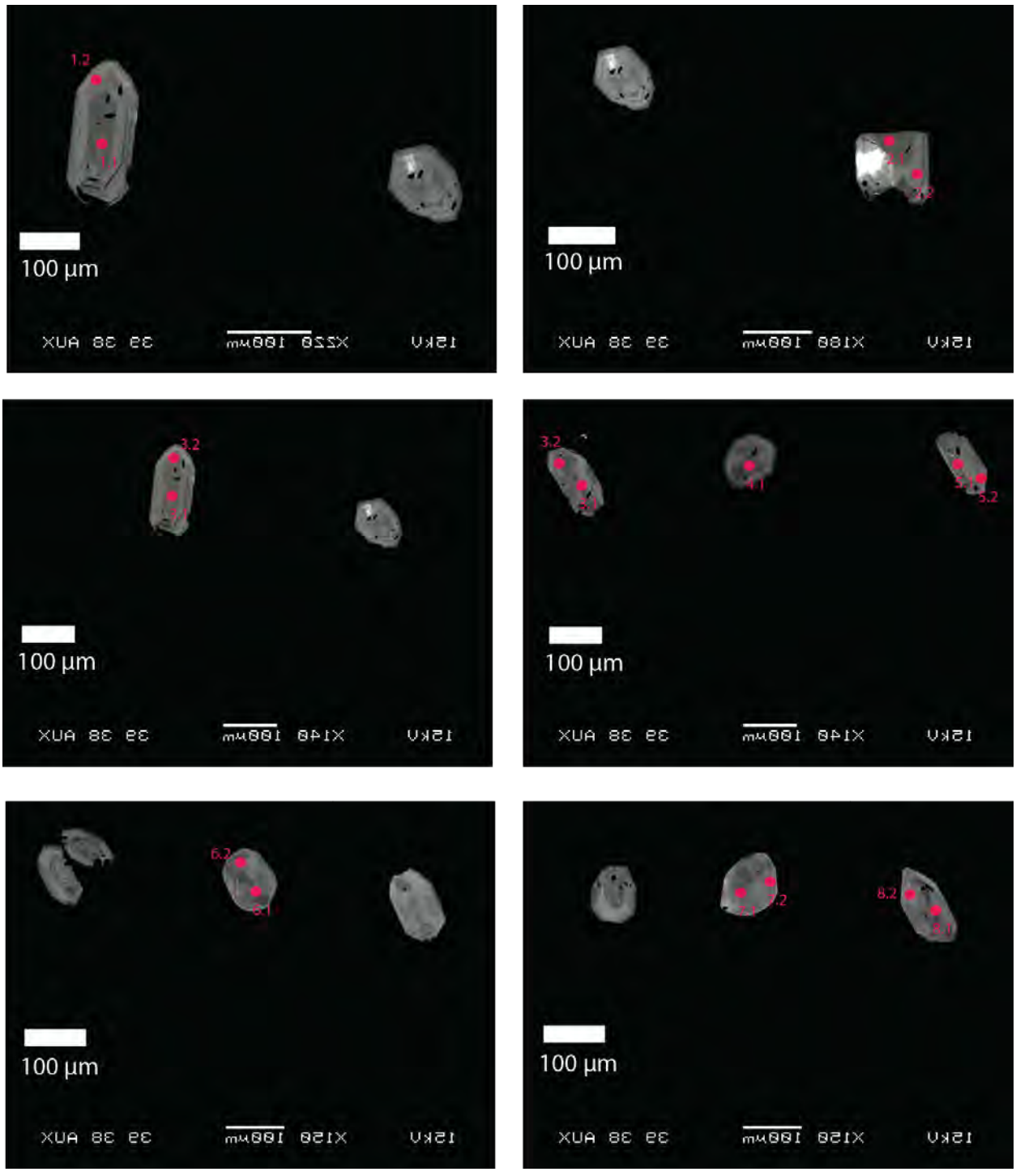

Fig. S15: CL images of SHRIMP and oxygen isotope spots from sample PX10-76. Spots are denoted by red dots with the spot number nearby.

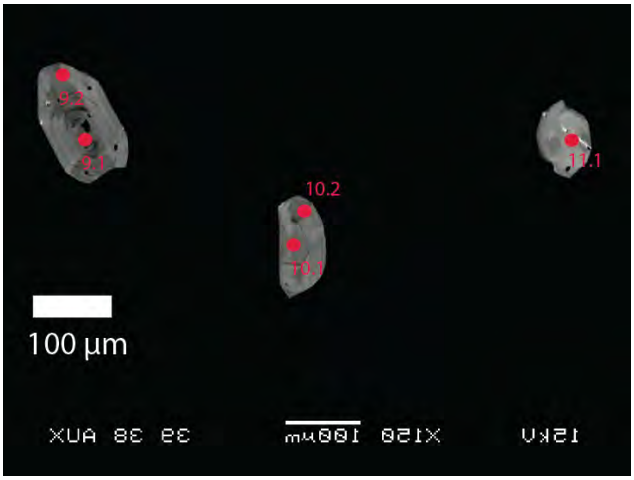

Fig. S16: CL images of SHRIMP and oxygen isotope spots from sample PX10-76. Spots are denoted by red dots with the spot number nearby.

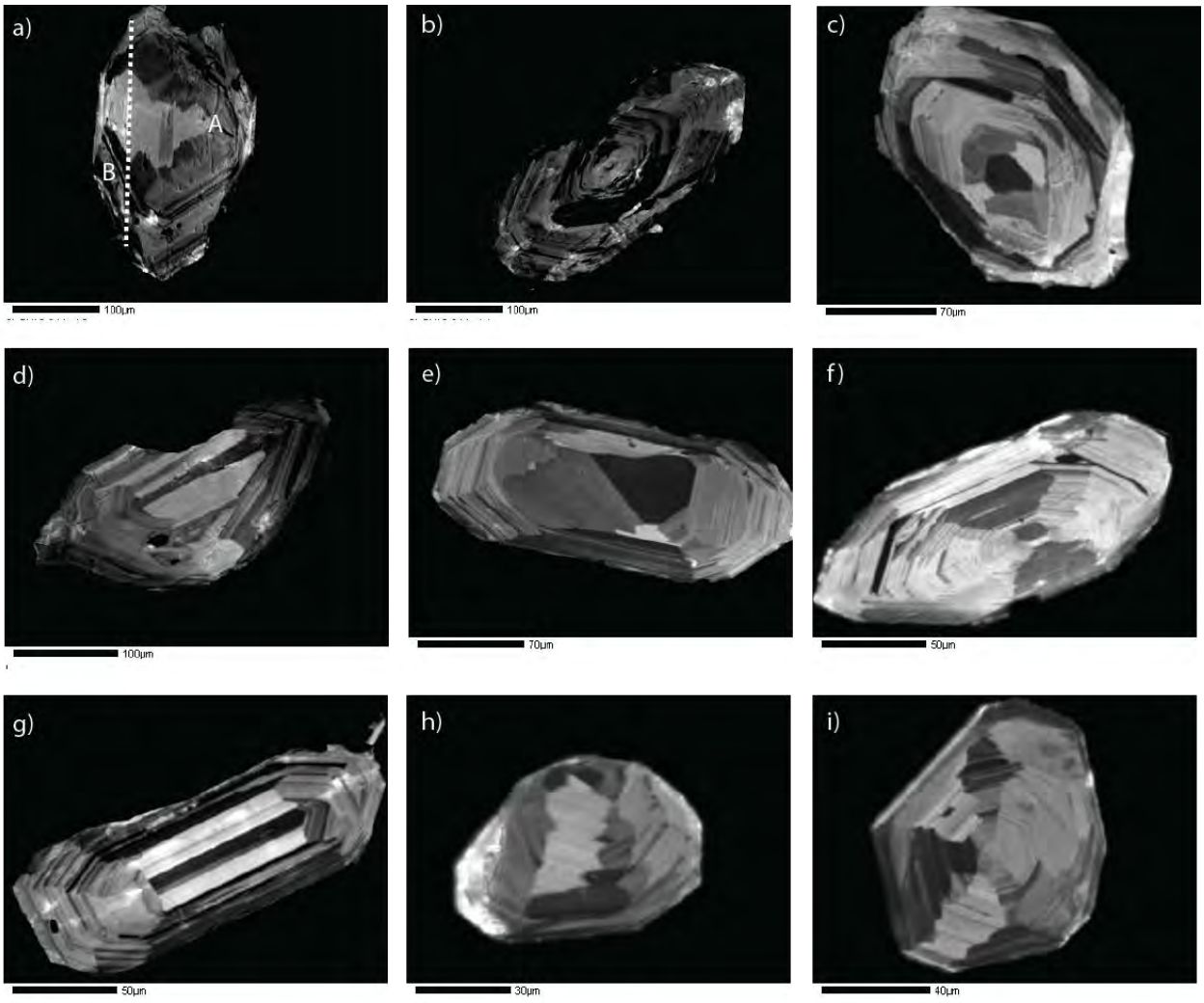

Fig. S17: CL images of representative grains from sample PX10-34A. Asterisk indicates dated grain. a) zL3A*, zL3B b) zL4 c) zM4 d) zM6 e)-k) representative grains

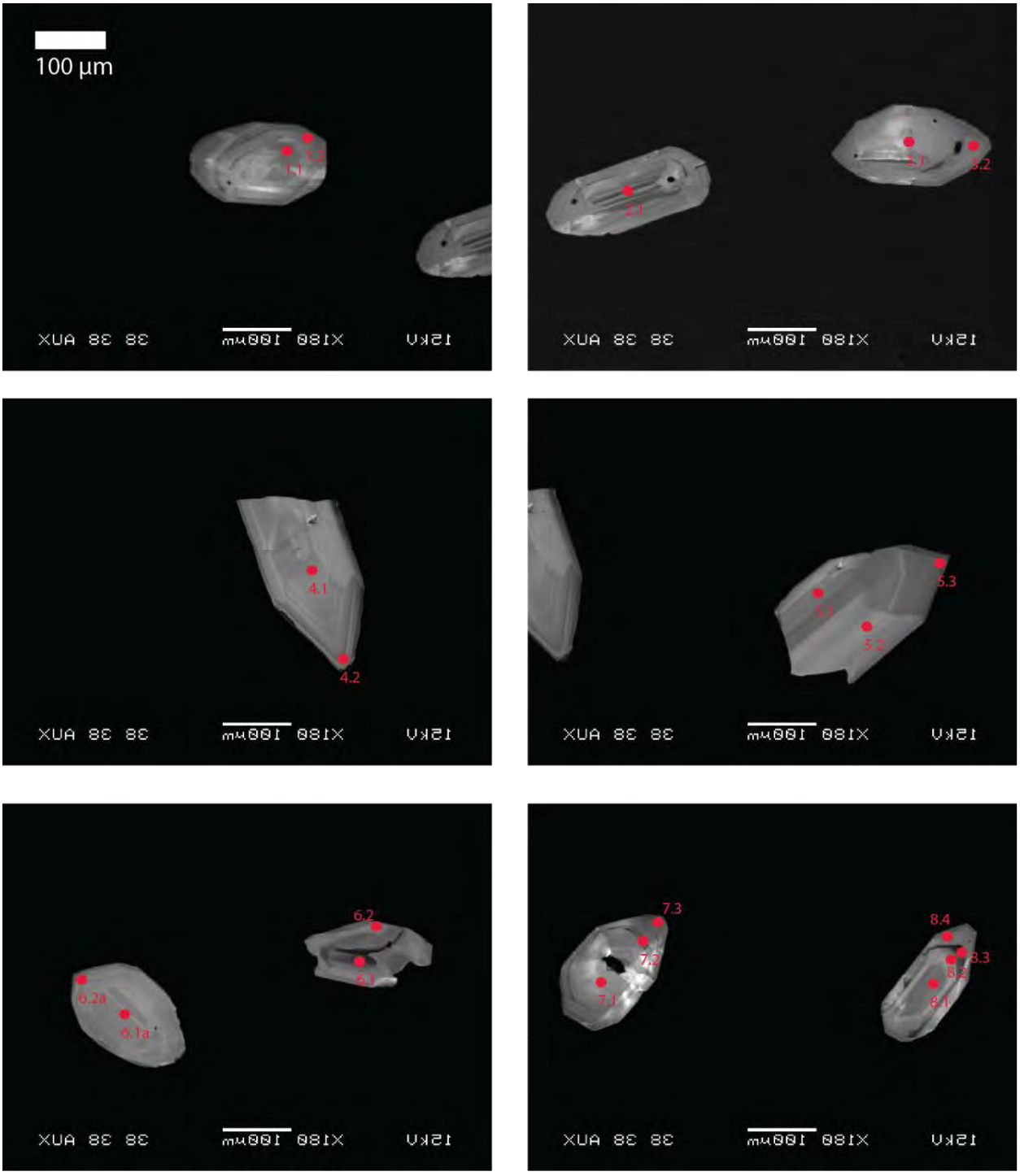

Fig. S18: CL images of SHRIMP spots from sample PX10-34A. Spots are denoted by red dots with the spot number nearby.

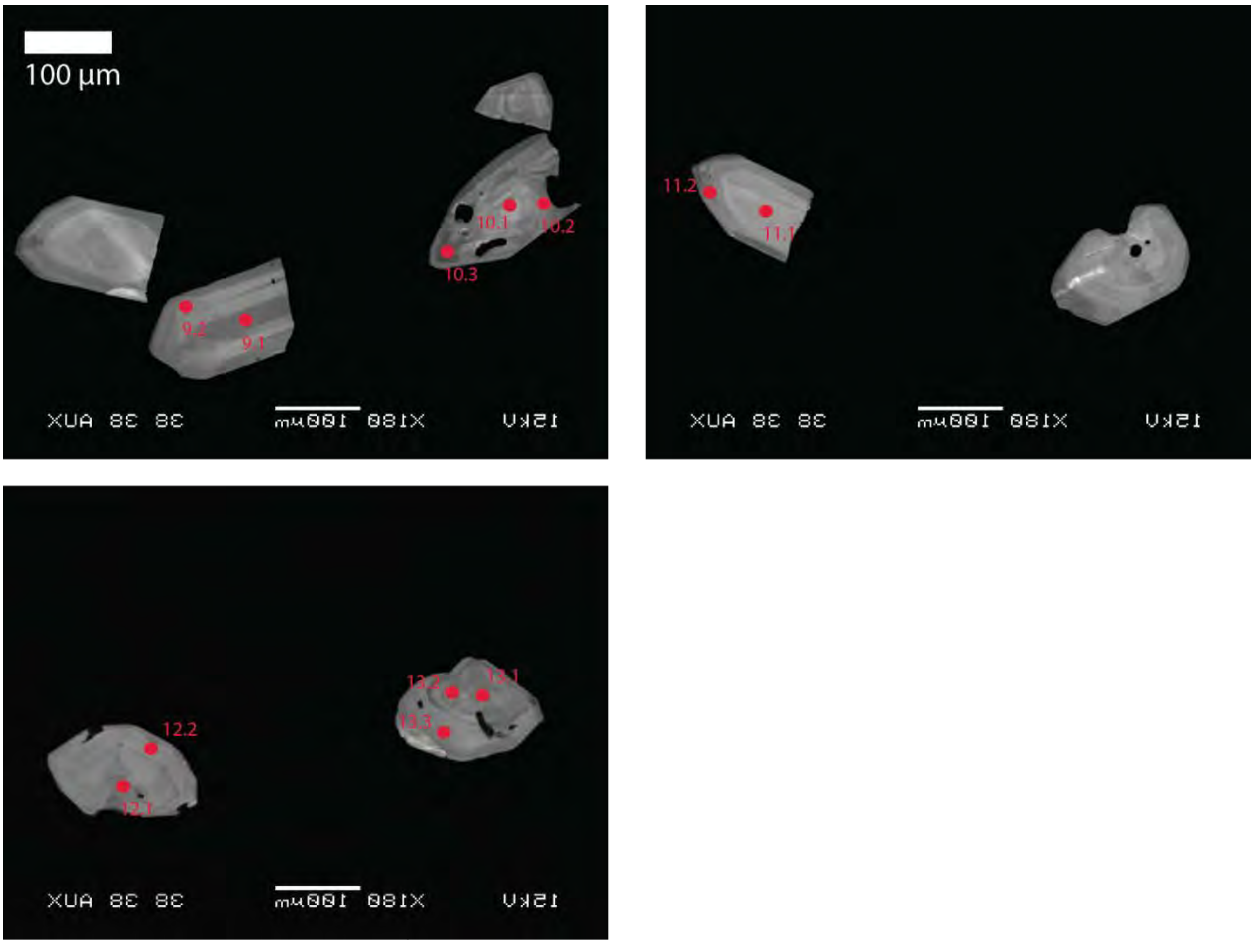

Fig. S19: CL images of SHRIMP spots from sample PX10-34A. Spots are denoted by red dots with the spot number nearby.

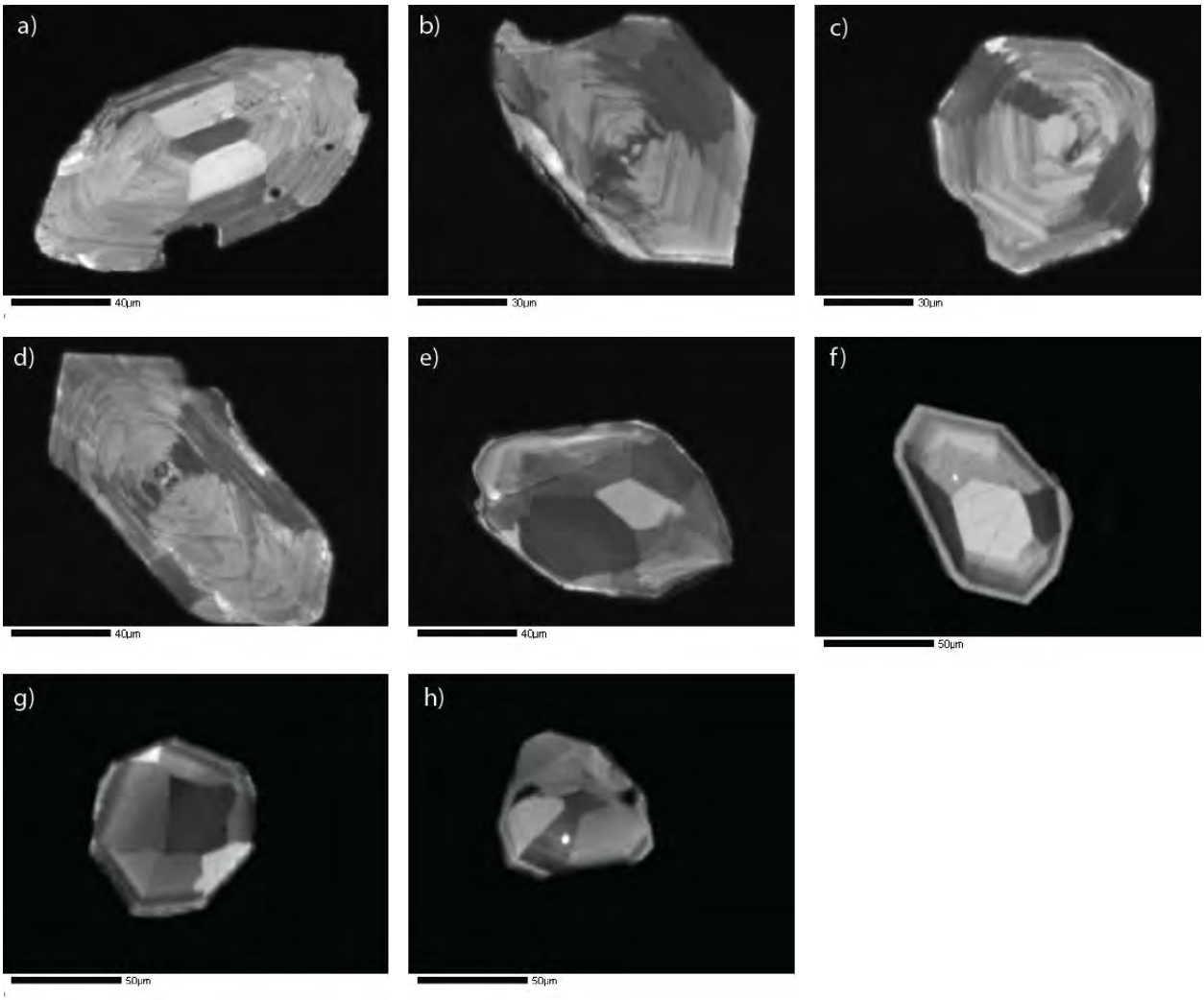

Fig. S20: CL images of representative grains from sample GP-322. a)-h) representative grains

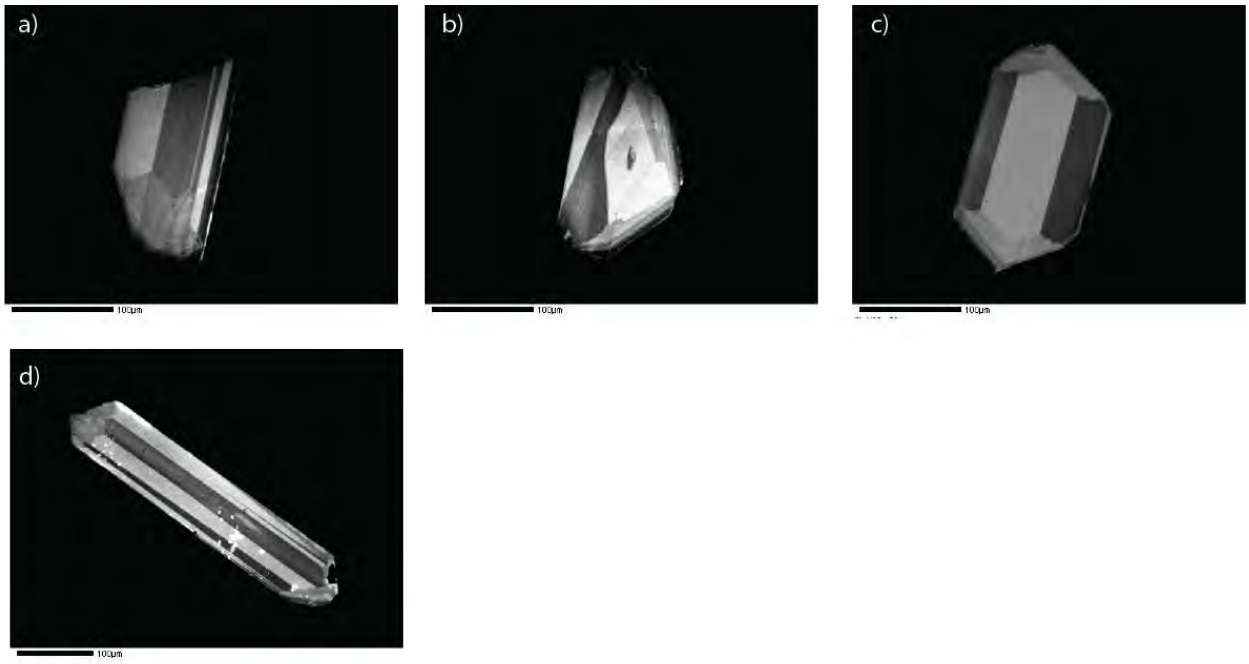

Fig. S21: CL images of representative grains from K26. a)-d) representative grains.

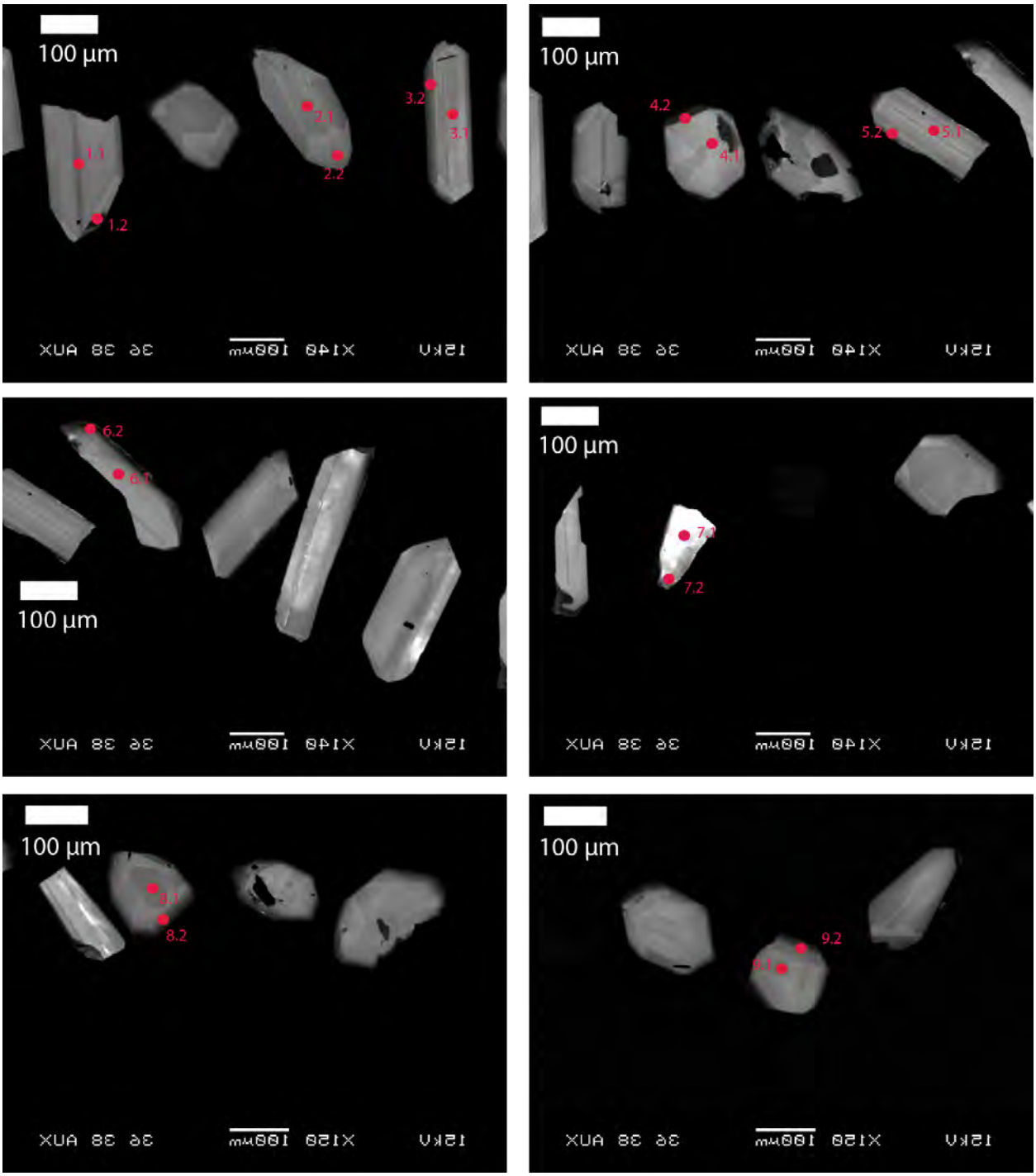

Fig. S22: CL images of SHRIMP spots from sample K26. Spots are denoted by red dots with the spot number nearby.

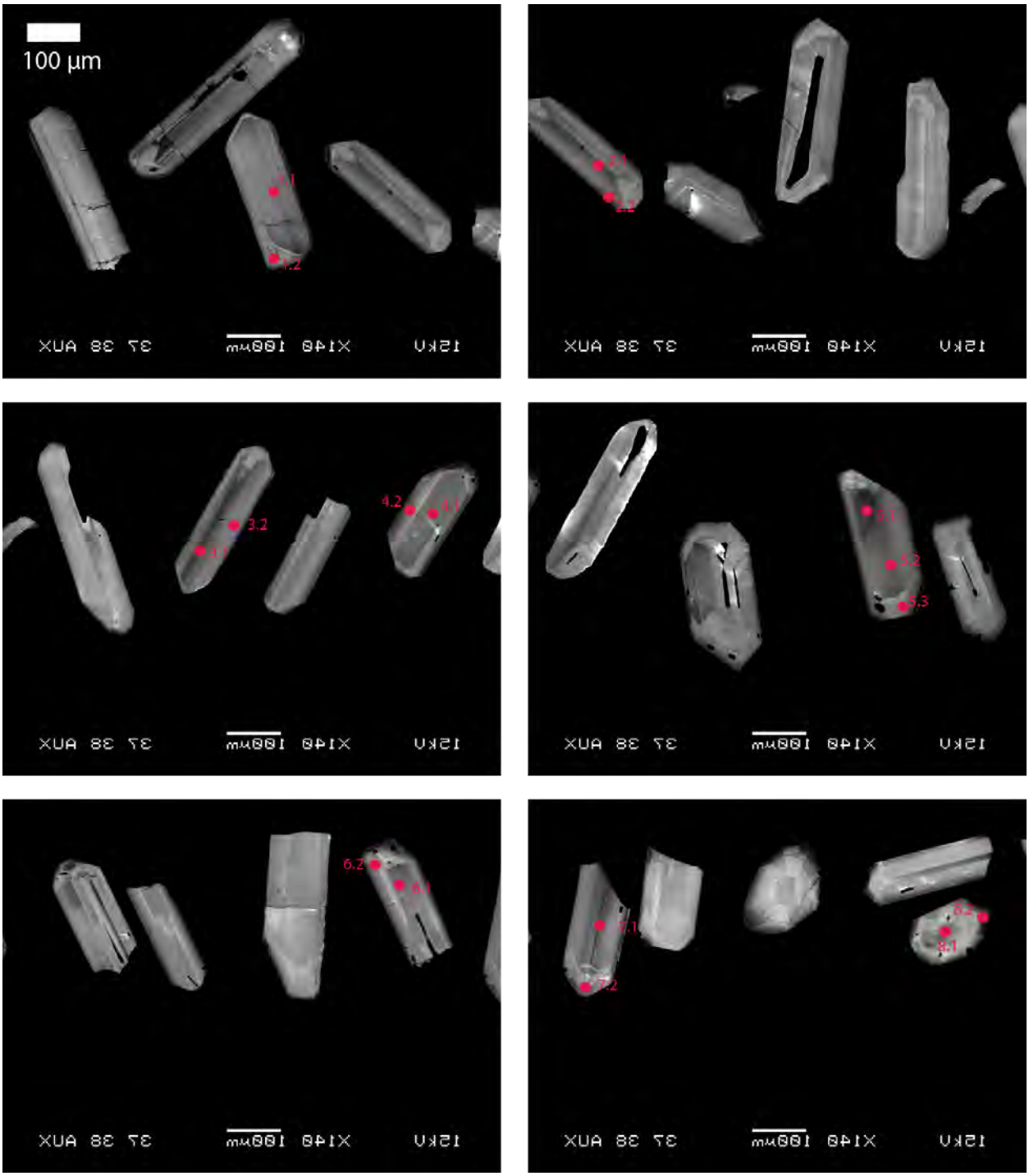

Fig. S23: CL images of SHRIMP spots from sample K55. Spots are denoted by red dots with the spot number nearby.

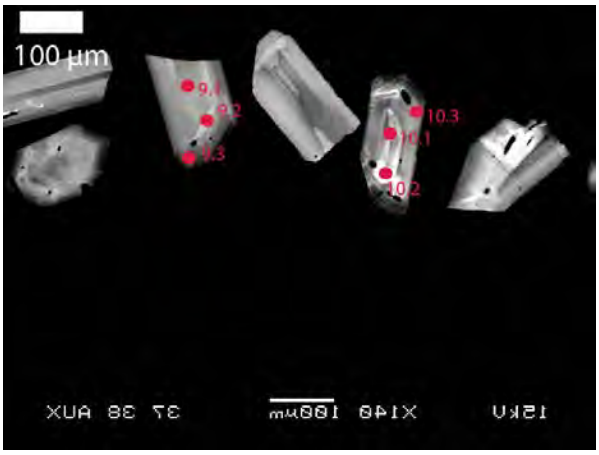

Fig. S24: CL images of SHRIMP spots from sample K55. Spots are denoted by red dots with the spot number nearby.

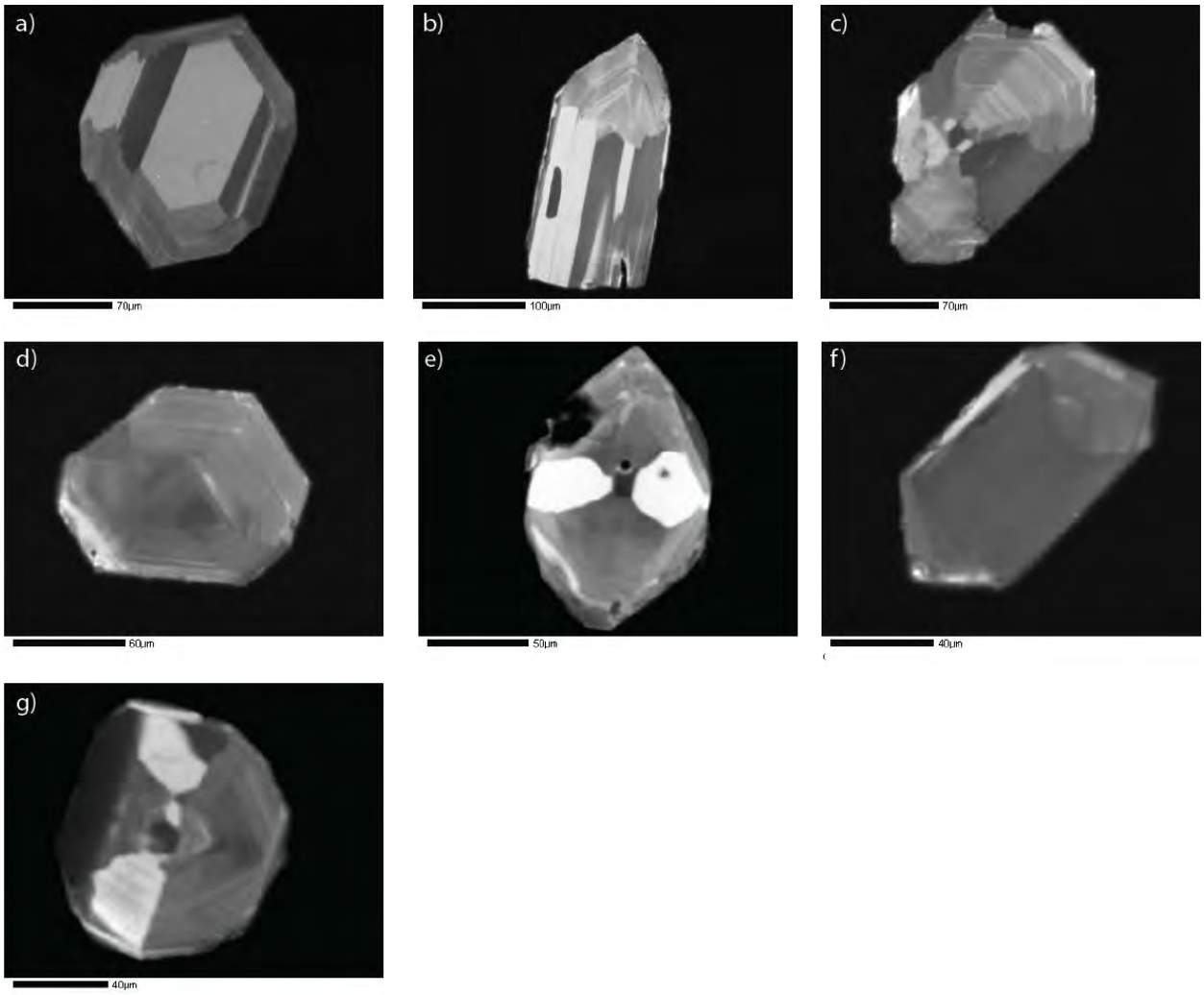

Fig. S25: CL images of dated grains from PX10-251. a) zL1 b) zM2 c) zM4 d) zM6 e) zS1 f) zS6 g) zS7

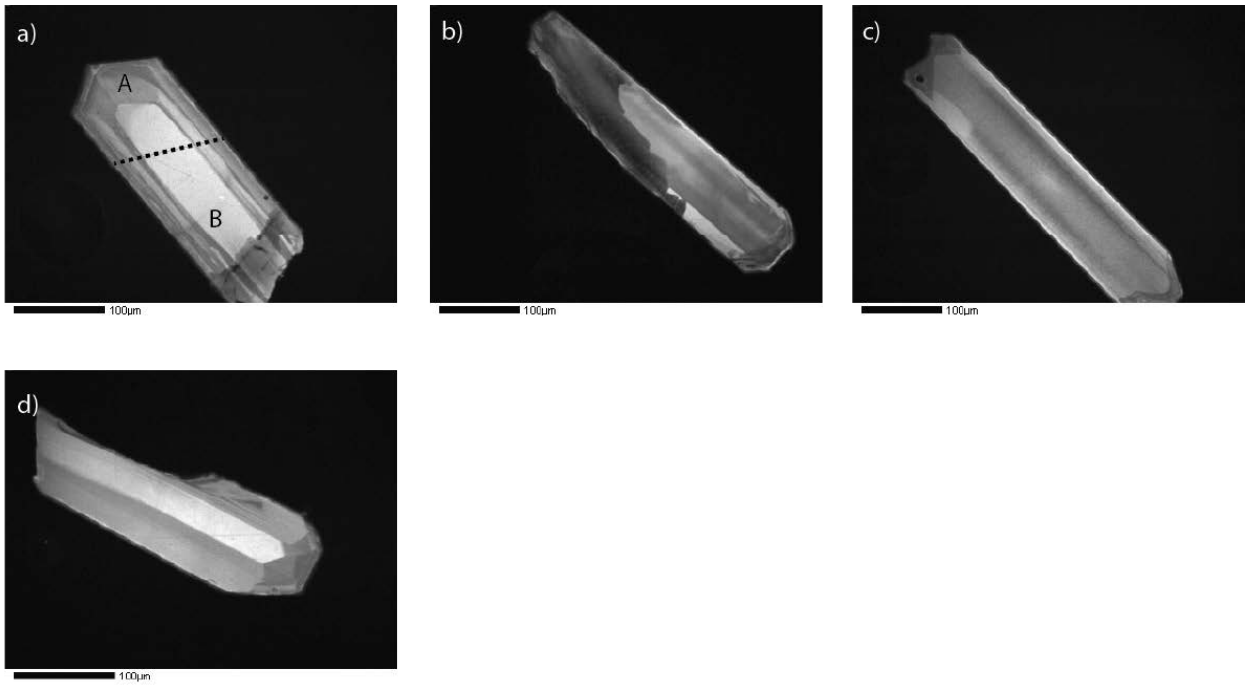

Fig. S26: CL images of dated grains from K16B. a) zL4A*, zL4B b) zL5 c) zL11 d) zL12

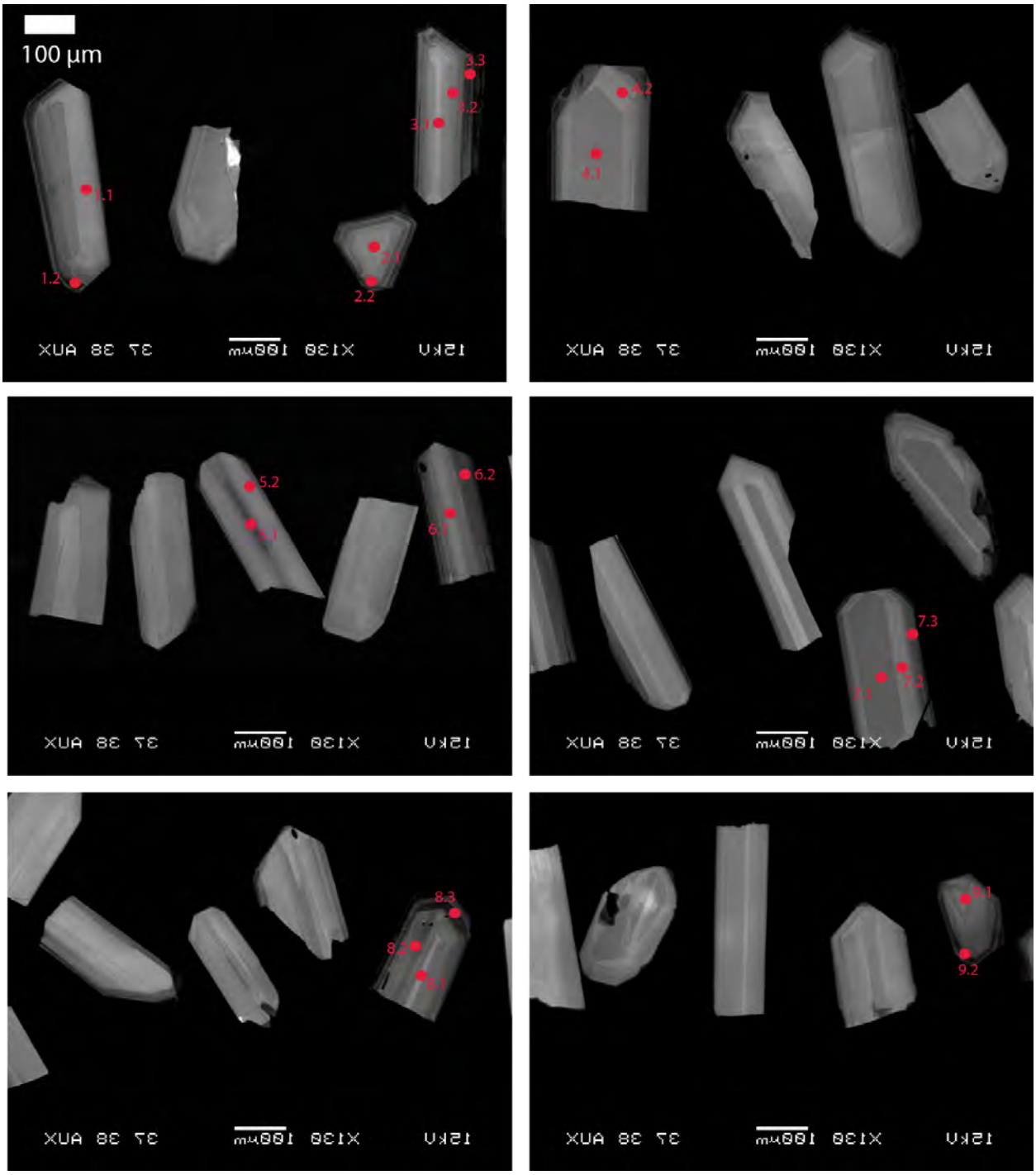

Fig. S27: CL images of SHRIMP spots from sample K16B. Spots are denoted by red dots with the spot number nearby.

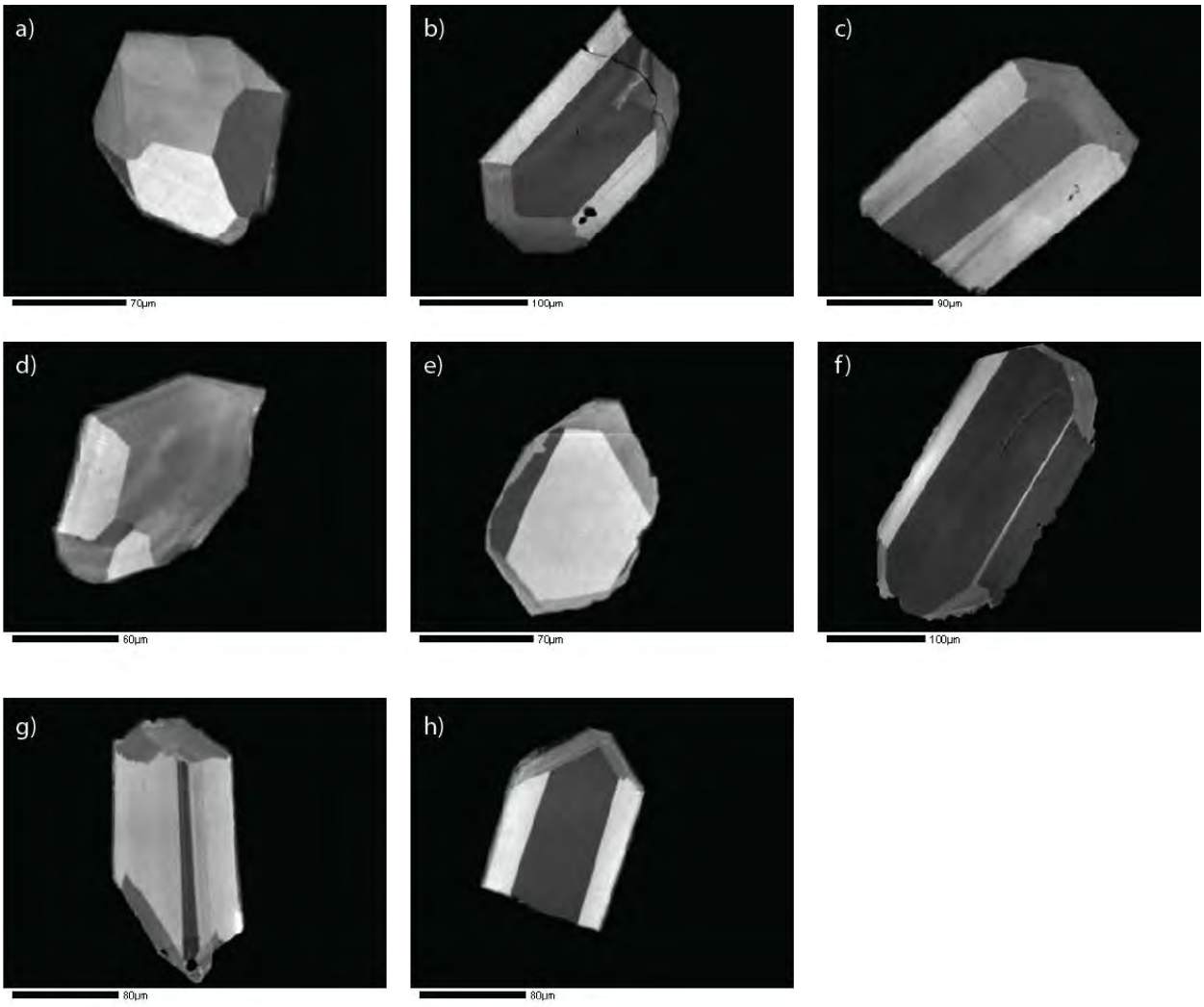

Fig. S28: CL images of dated grains from sample PX10-236. a) zL2 b) zL4 c) zL8 d) zL9 e) zM1 f) zM3 g) zM10 h) zM11

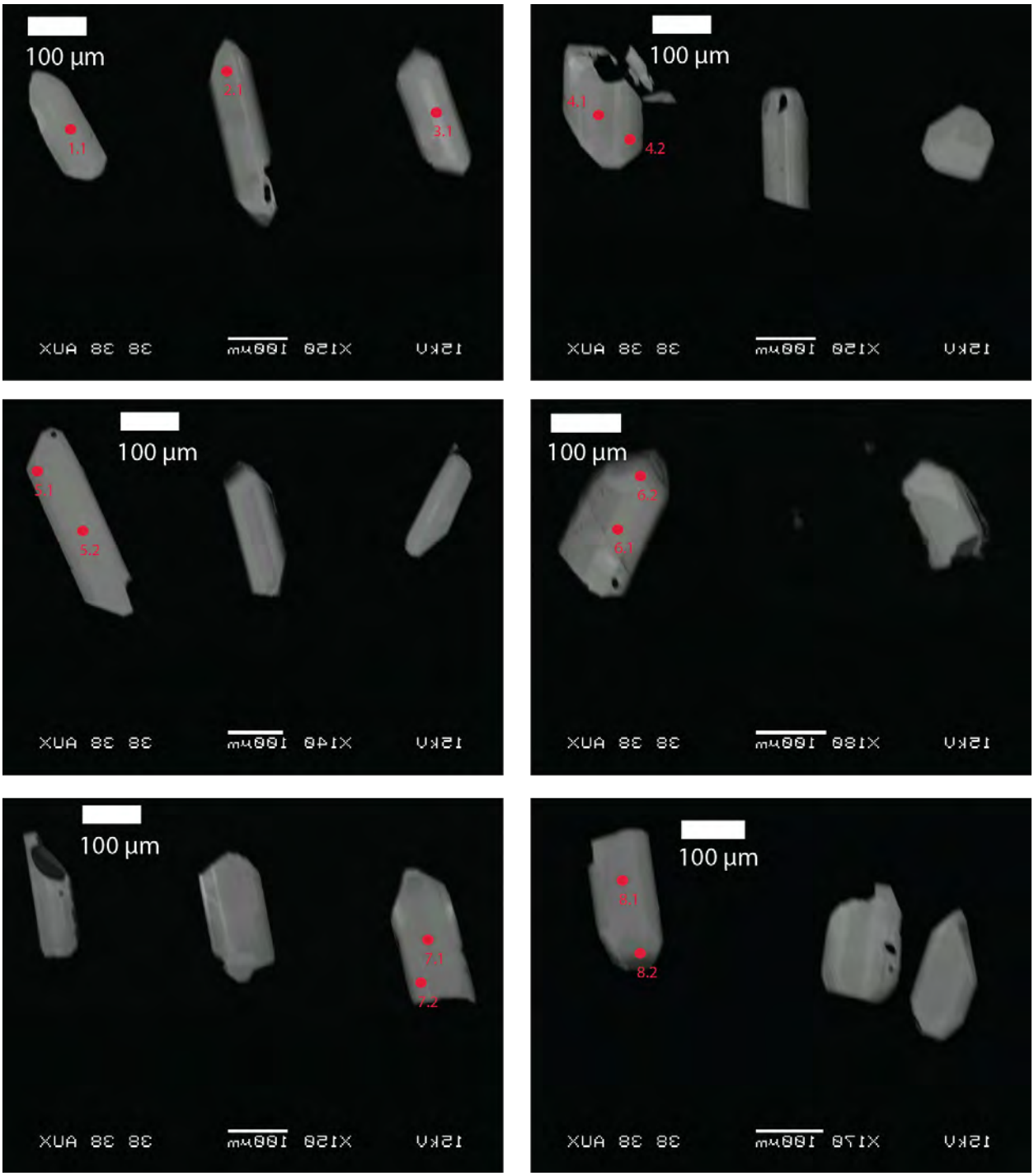

Fig. S29: CL images of SHRIMP spots from sample PX10-236. Spots are denoted by red dots with the spot number nearby.

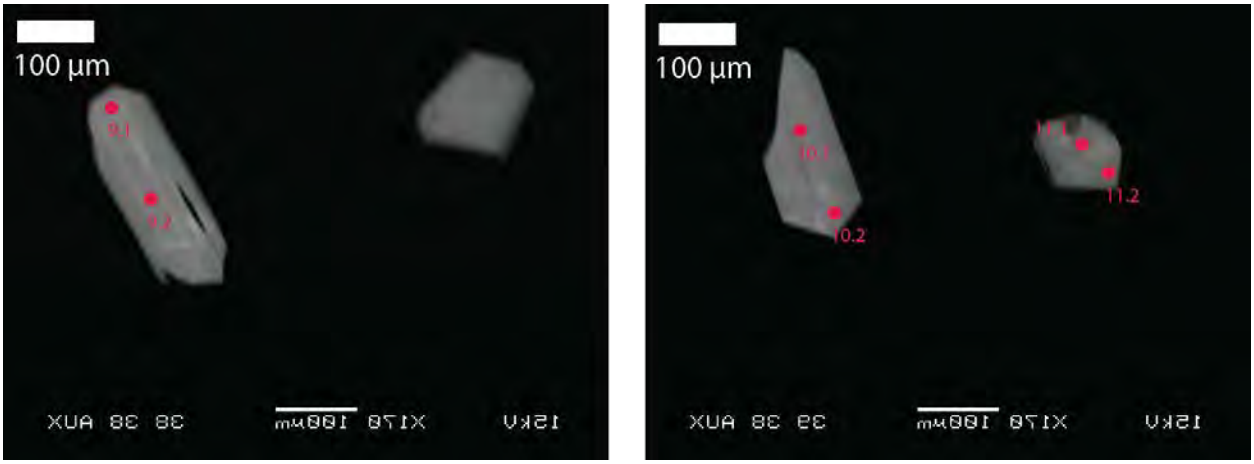

Fig. S30: CL images of SHRIMP spots from sample PX10-236. Spots are denoted by red dots with the spot number nearby.

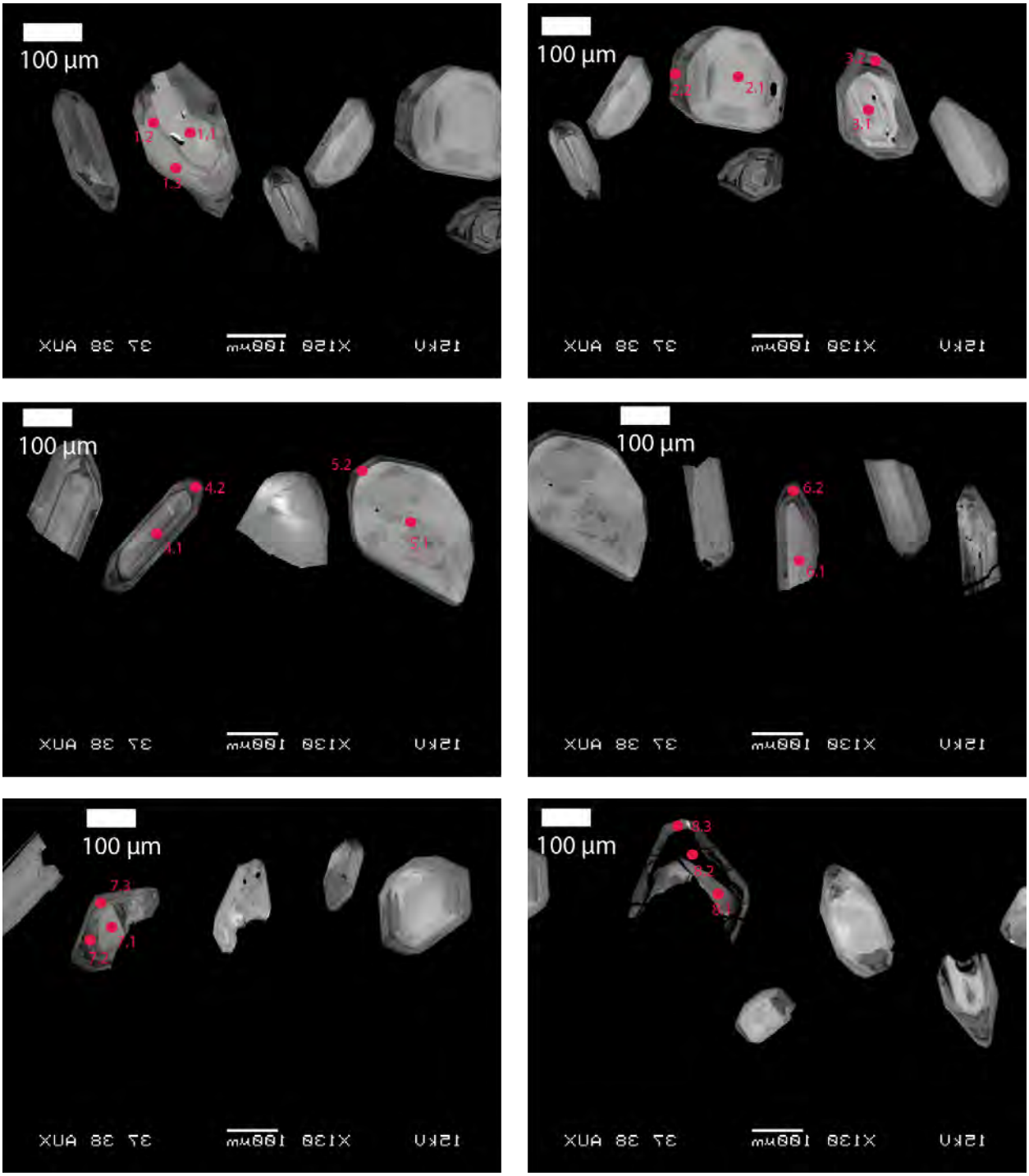

Fig. S31: CL images of SHRIMP spots from sample K42B. Spots are denoted by red dots with the spot number nearby.

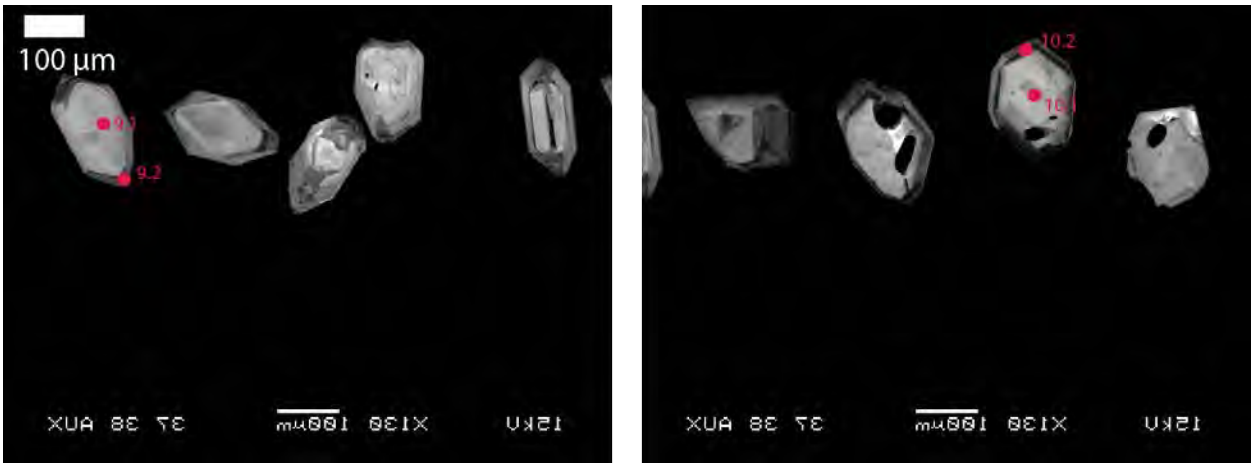

Fig. S32: CL images of SHRIMP spots from sample K42B. Spots are denoted by red dots with the spot number nearby.

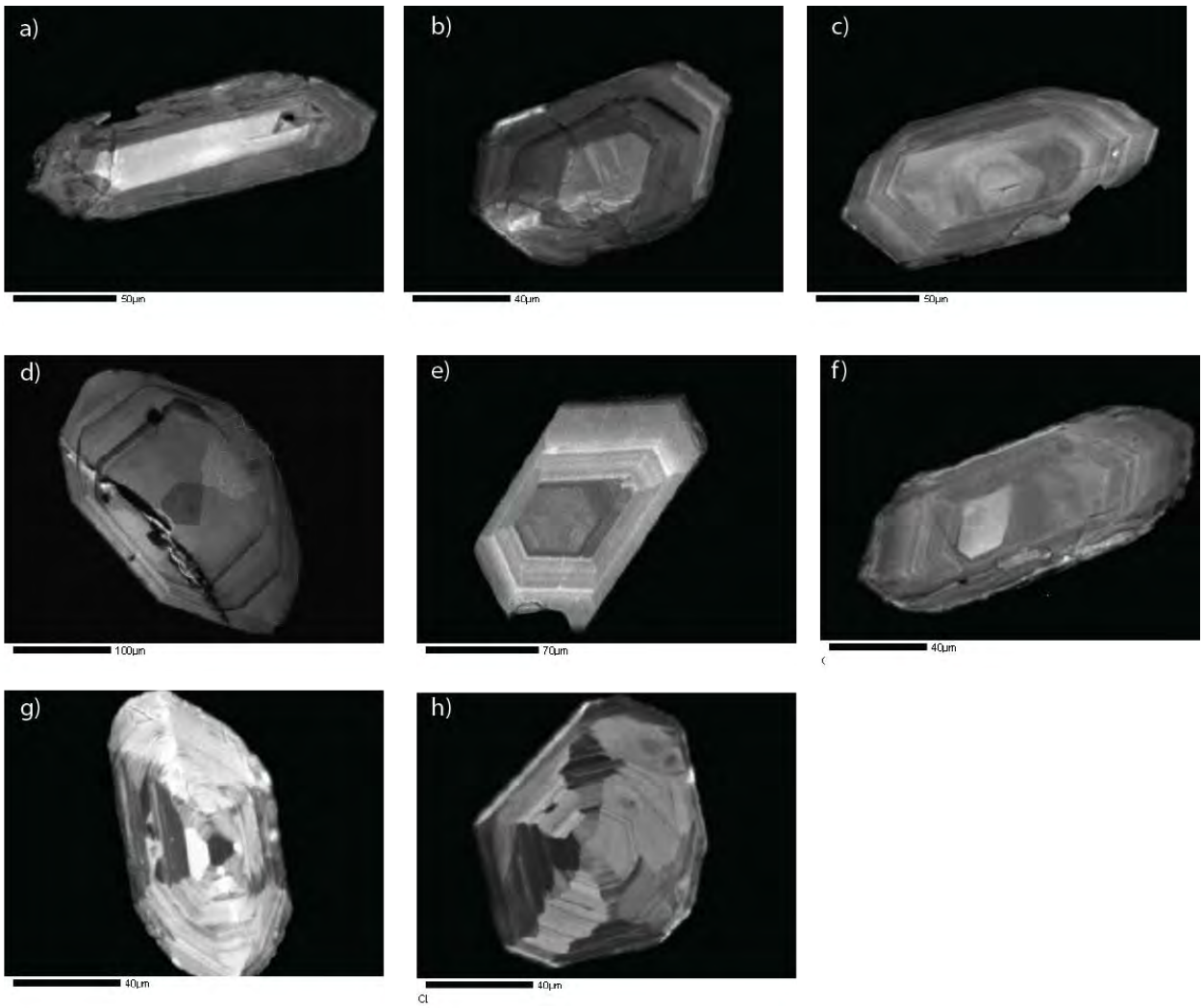

Fig. S33: CL images of dated grains from sample PX10-86. a) zM1 b) zM5 c) zM8 d) zM9 e) zM10 f) zS1 g)-h) representative grains

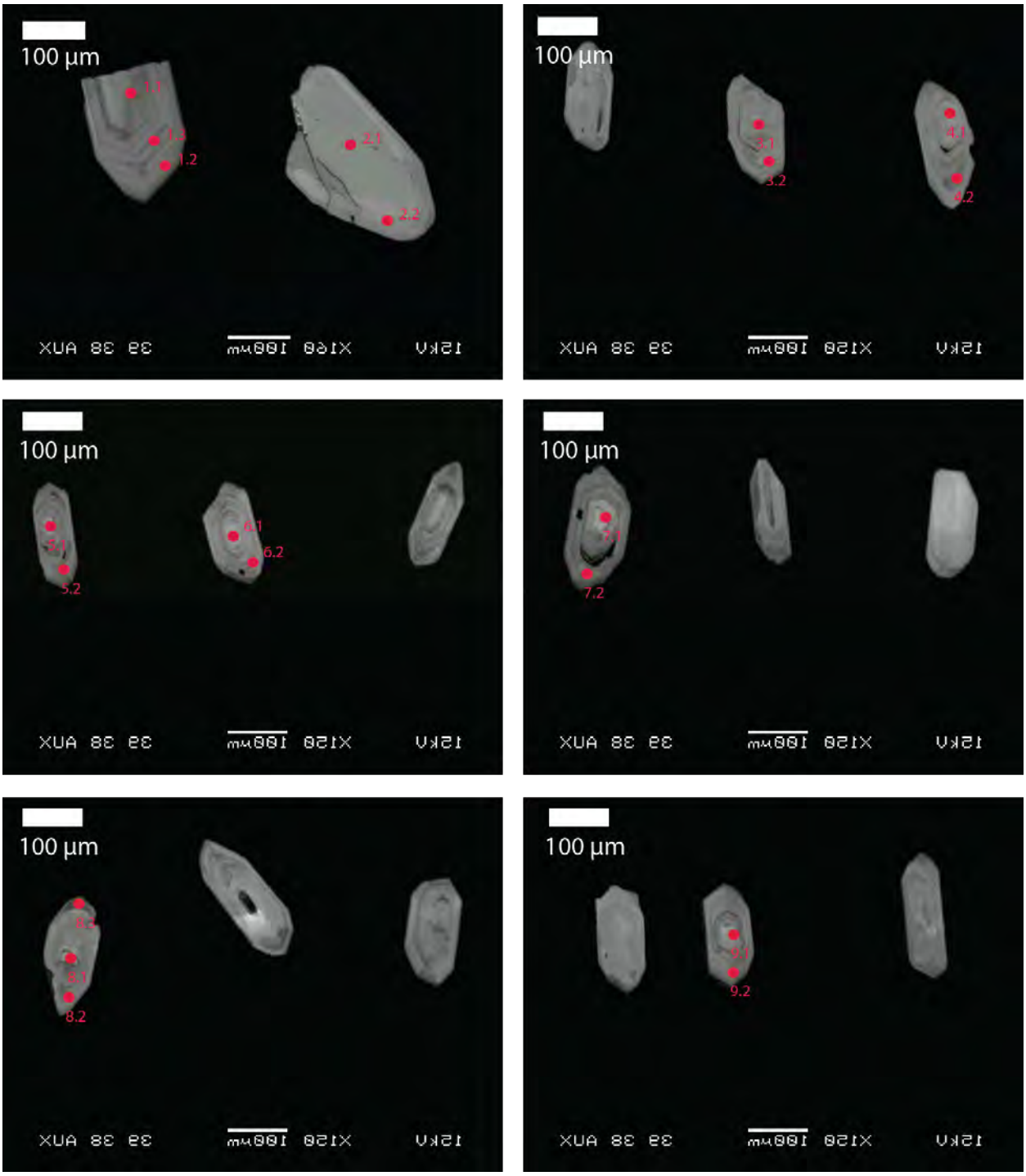

Fig. S34: CL images of SHRIMP and oxygen isotope spots from sample PX10-86. Spots are denoted by red dots with the spot number nearby.

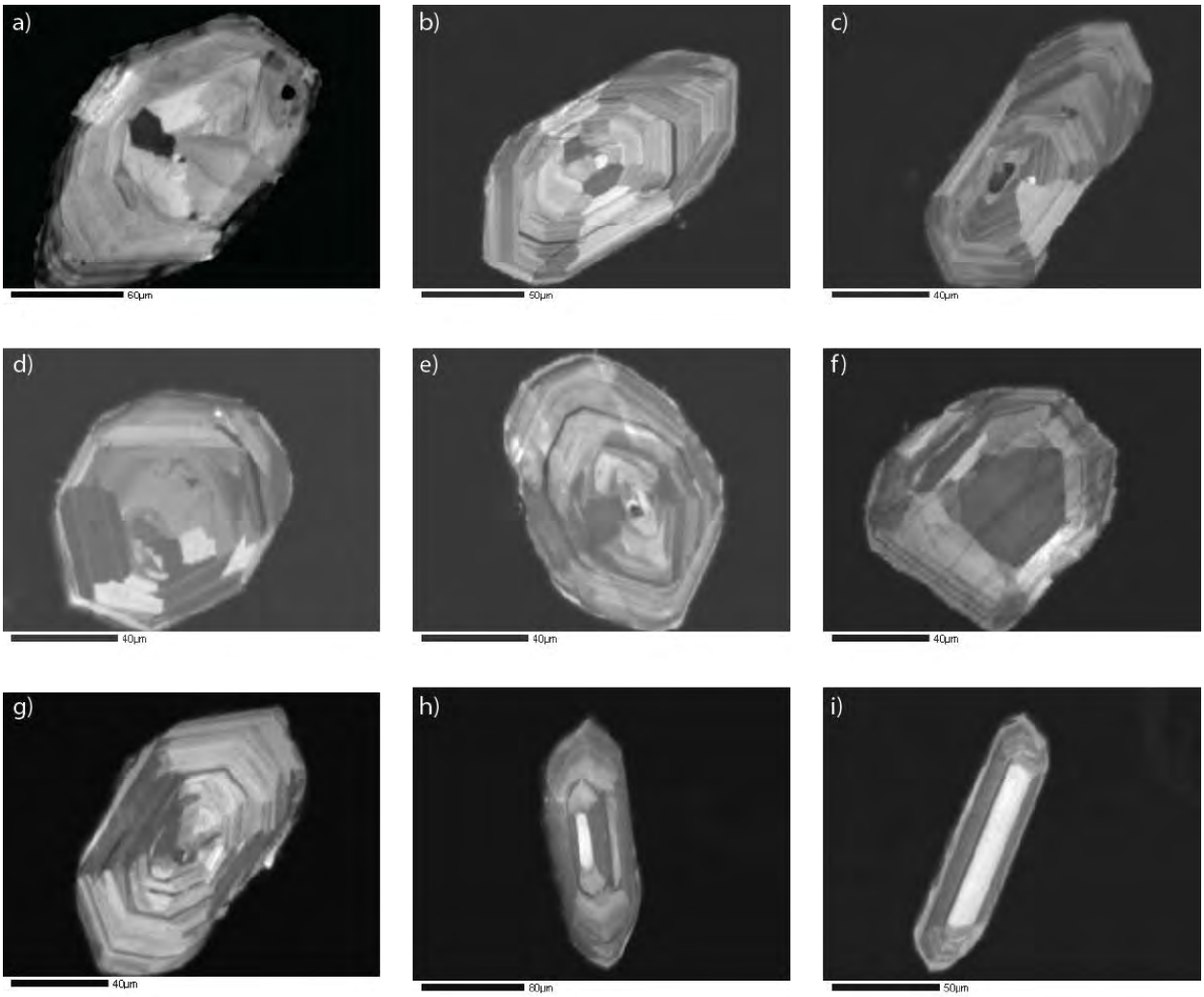

Fig. S35: CL images of dated and representative grains from sample GP309-1. Asterisk indicates dated grain. a) zM1* b)-i) representative grains.

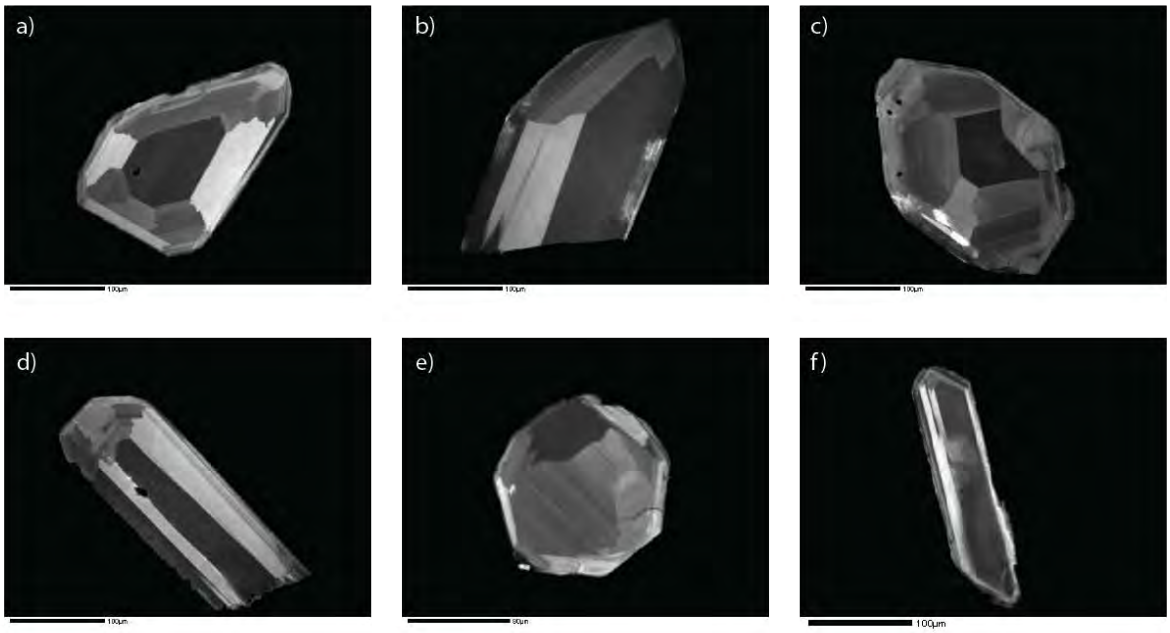

Fig. S36: CL images of representative grains from sample PX11-261A. a)-f) representative grains

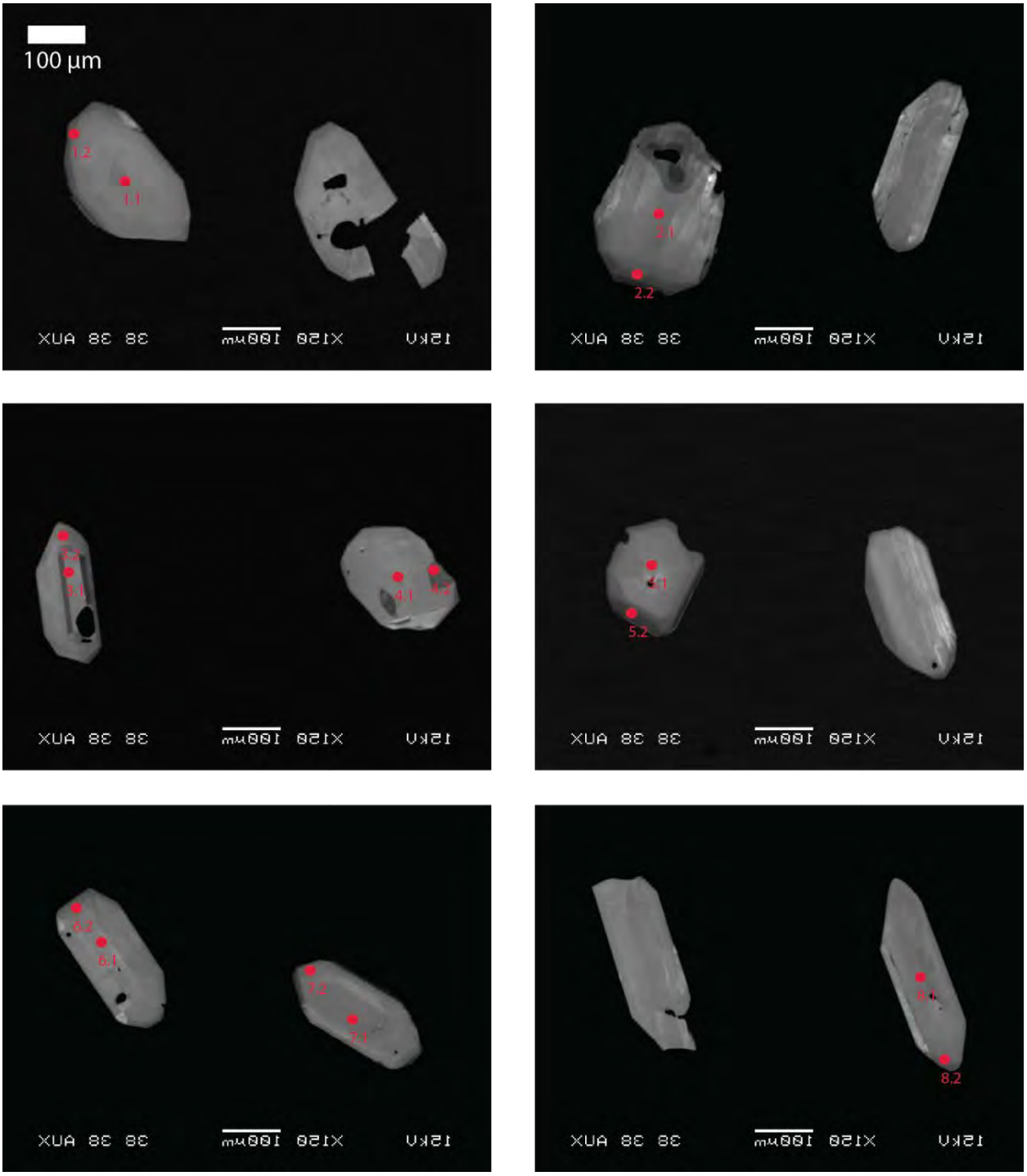

Fig. S37: CL images of SHRIMP spots from sample PX10-261A. Spots are denoted by red dots with the spot number nearby.

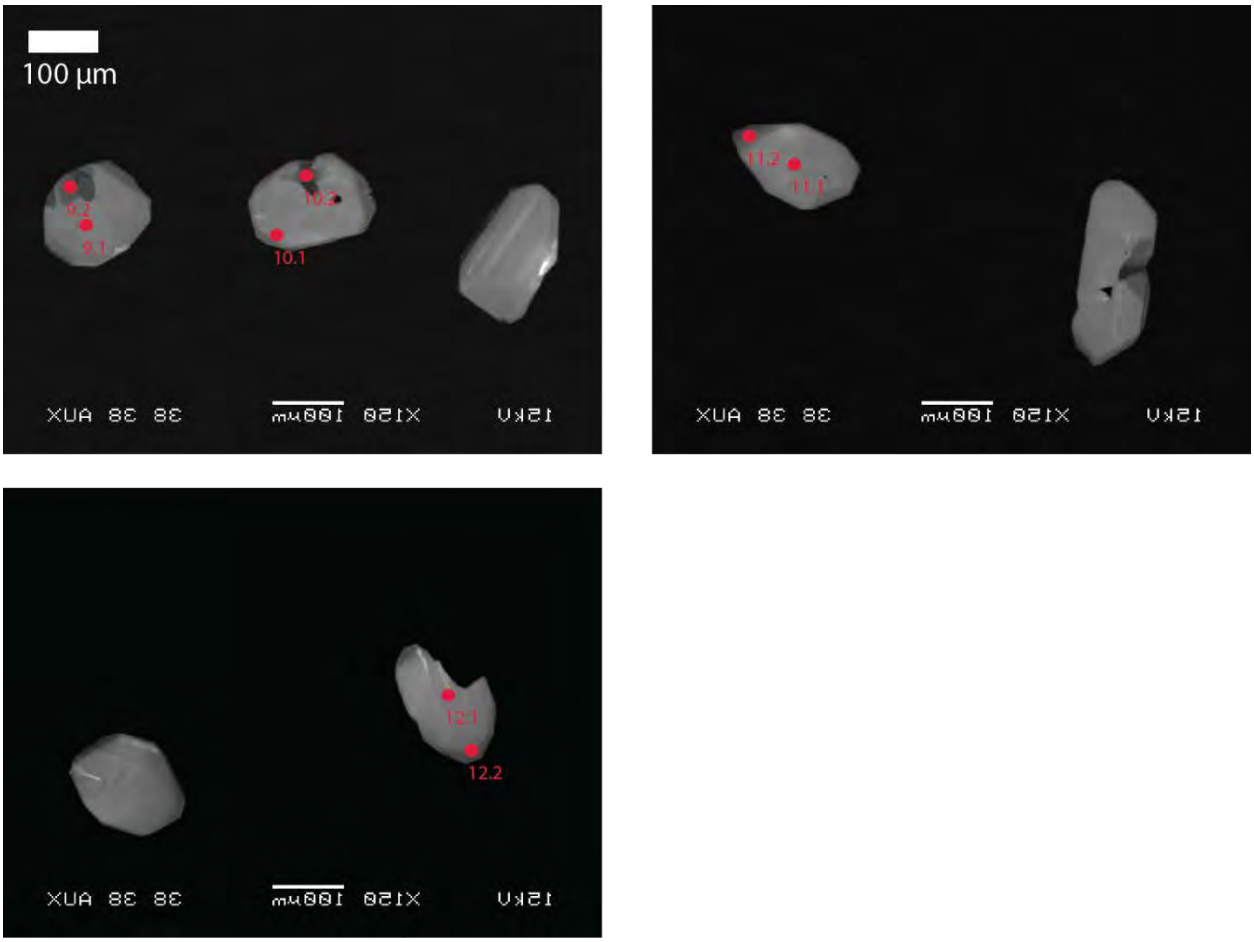

Fig. S38: CL images of SHRIMP spots from sample PX10-261A. Spots are denoted by red dots with the spot number nearby.

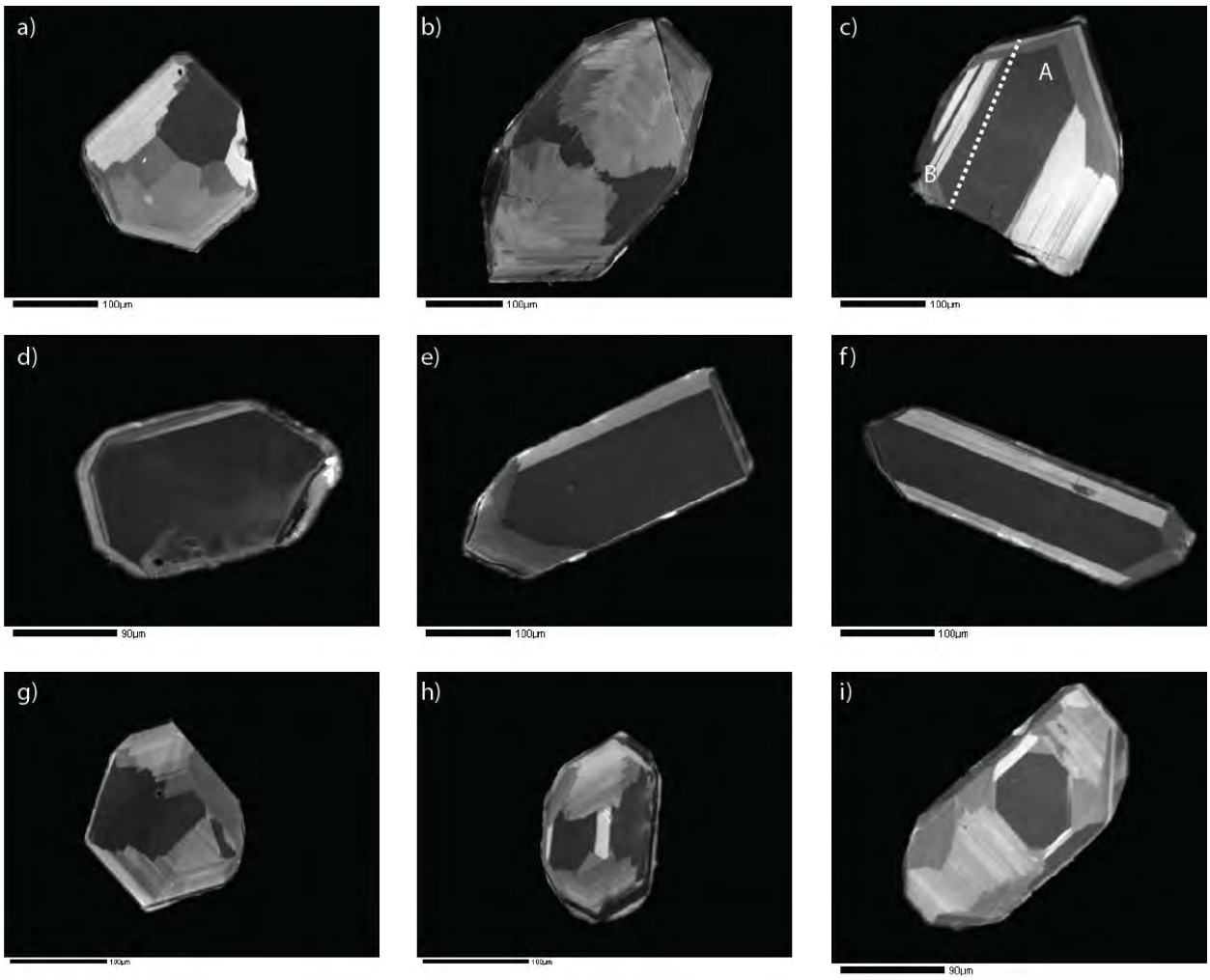

Fig. S39: CL images of dated and representative grains from sample PX11-209. Asterisk indicates dated grain. a) zL1* b) zL2* c) zL4A*, zL4B d)-i) representative grains

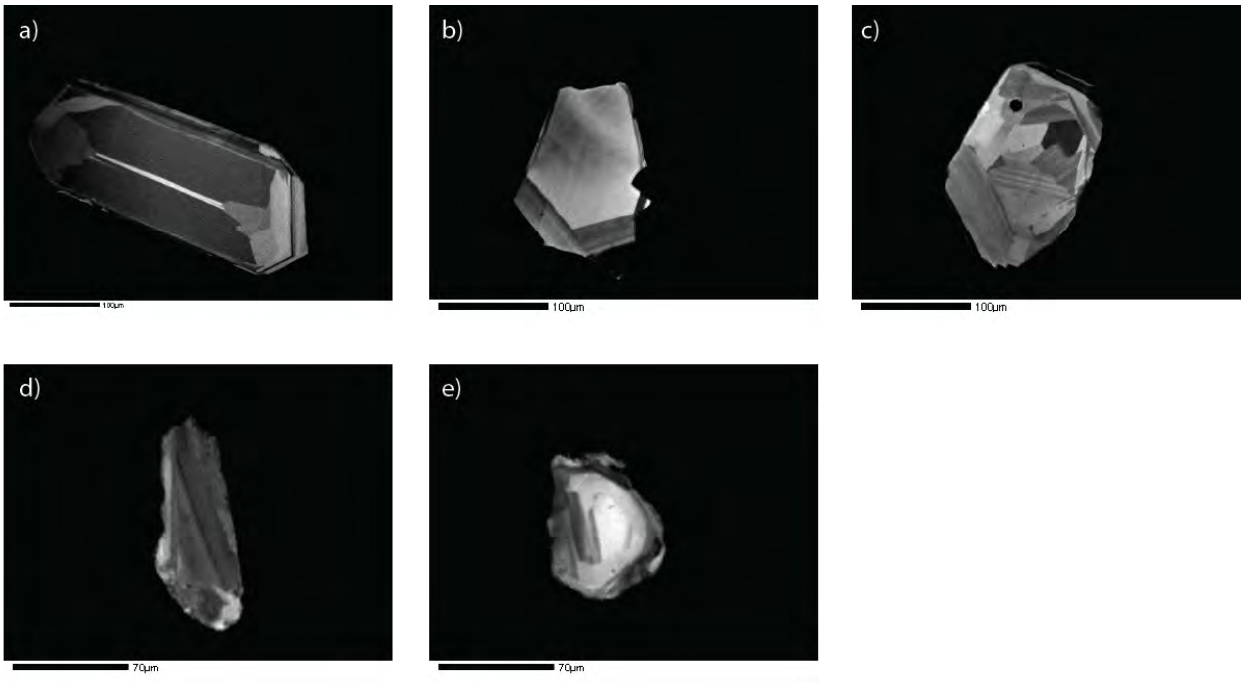

Fig. S40: CL images of representative grains from sample PX11-263c. a)-e) representative grains

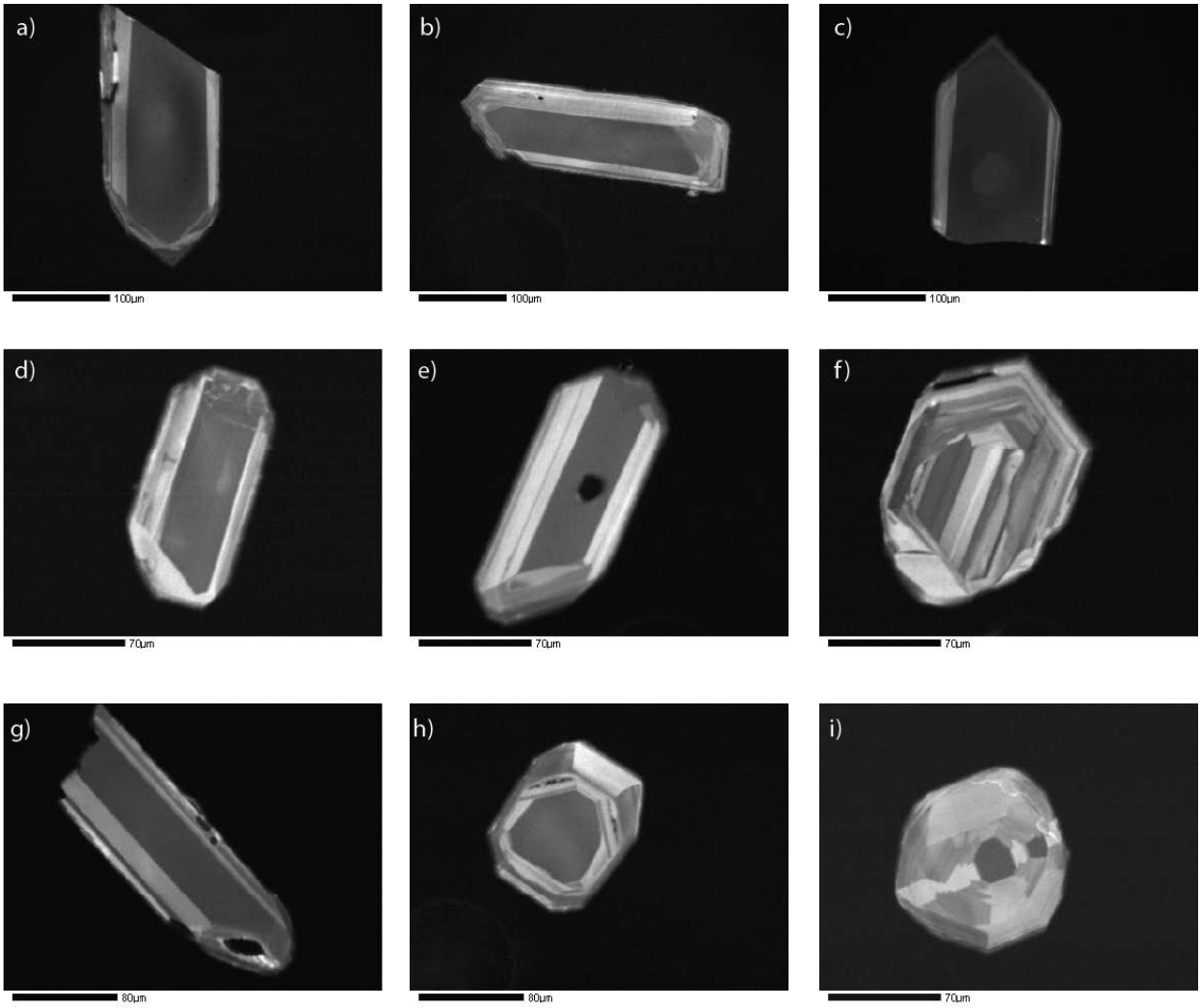

Fig. S41: CL images of dated and representative grains from sample PX11-284. Asterisk indicates dated grain. a) zL1* b) zL3* c) zL5* d) zM1* e)-i) representative grains

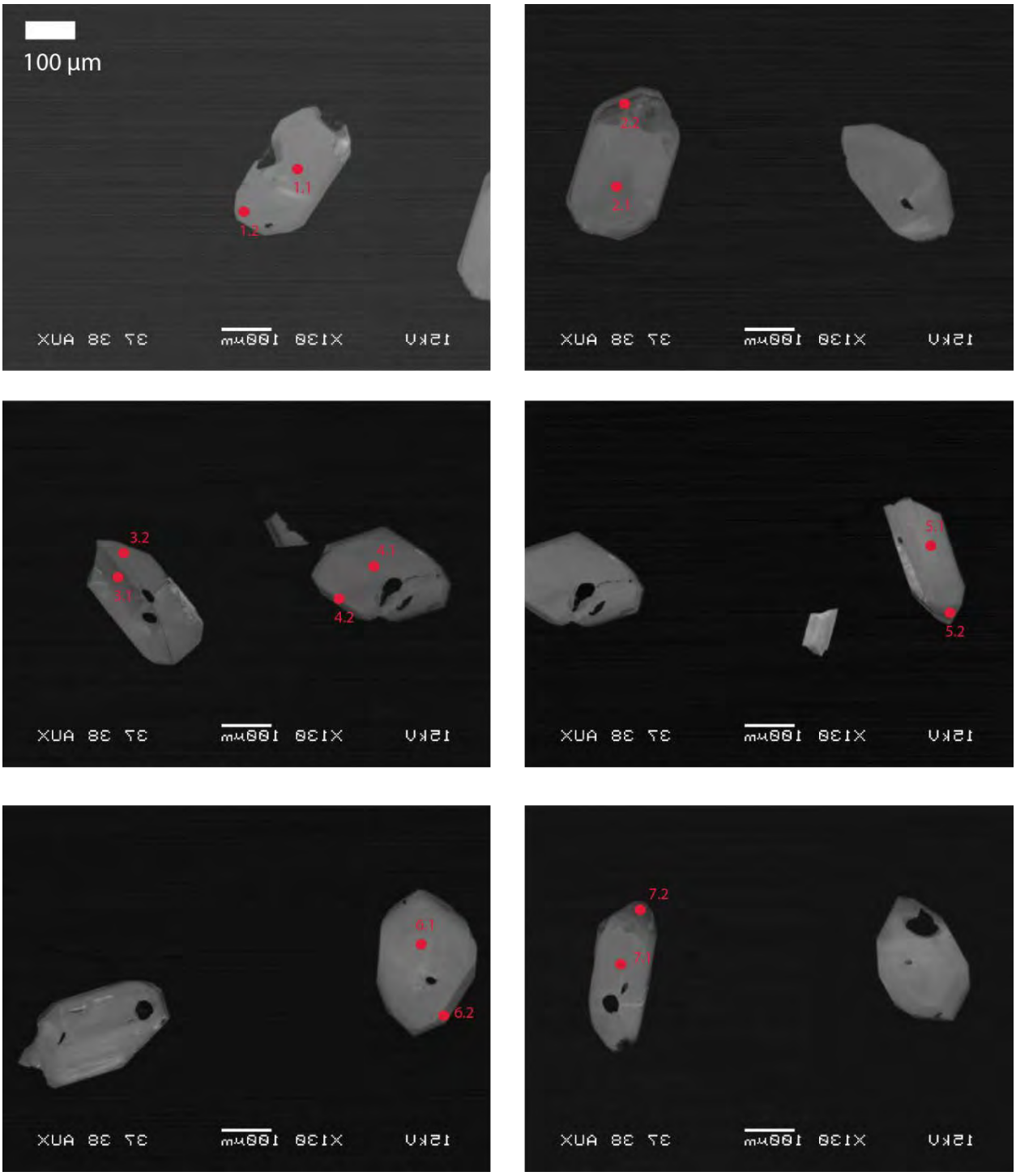

Fig. S42: CL images of SHRIMP spots from sample PX10-284. Spots are denoted by red dots with the spot number nearby.

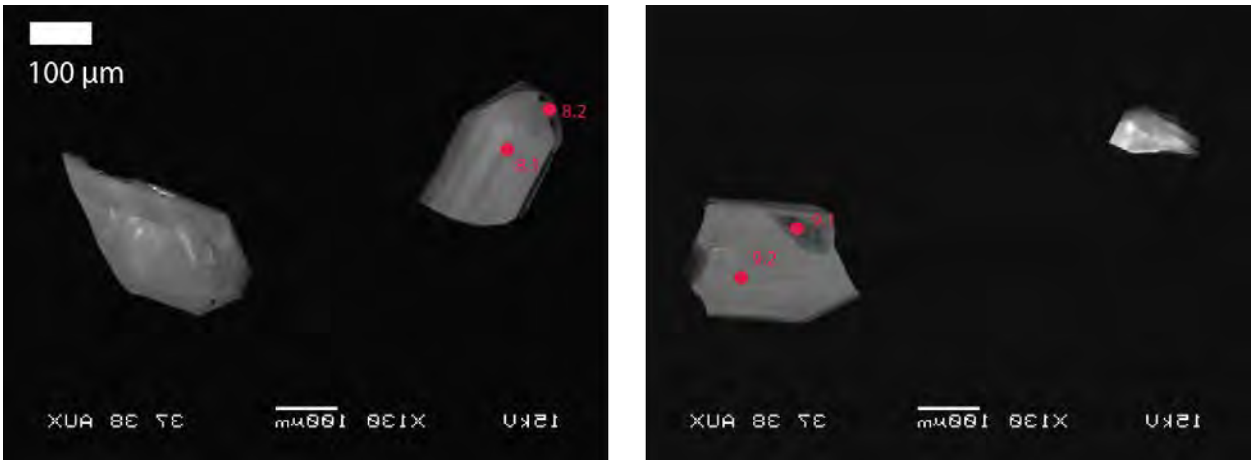

Fig. S43: CL images of SHRIMP spots from sample PX10-284. Spots are denoted by red dots with the spot number nearby.

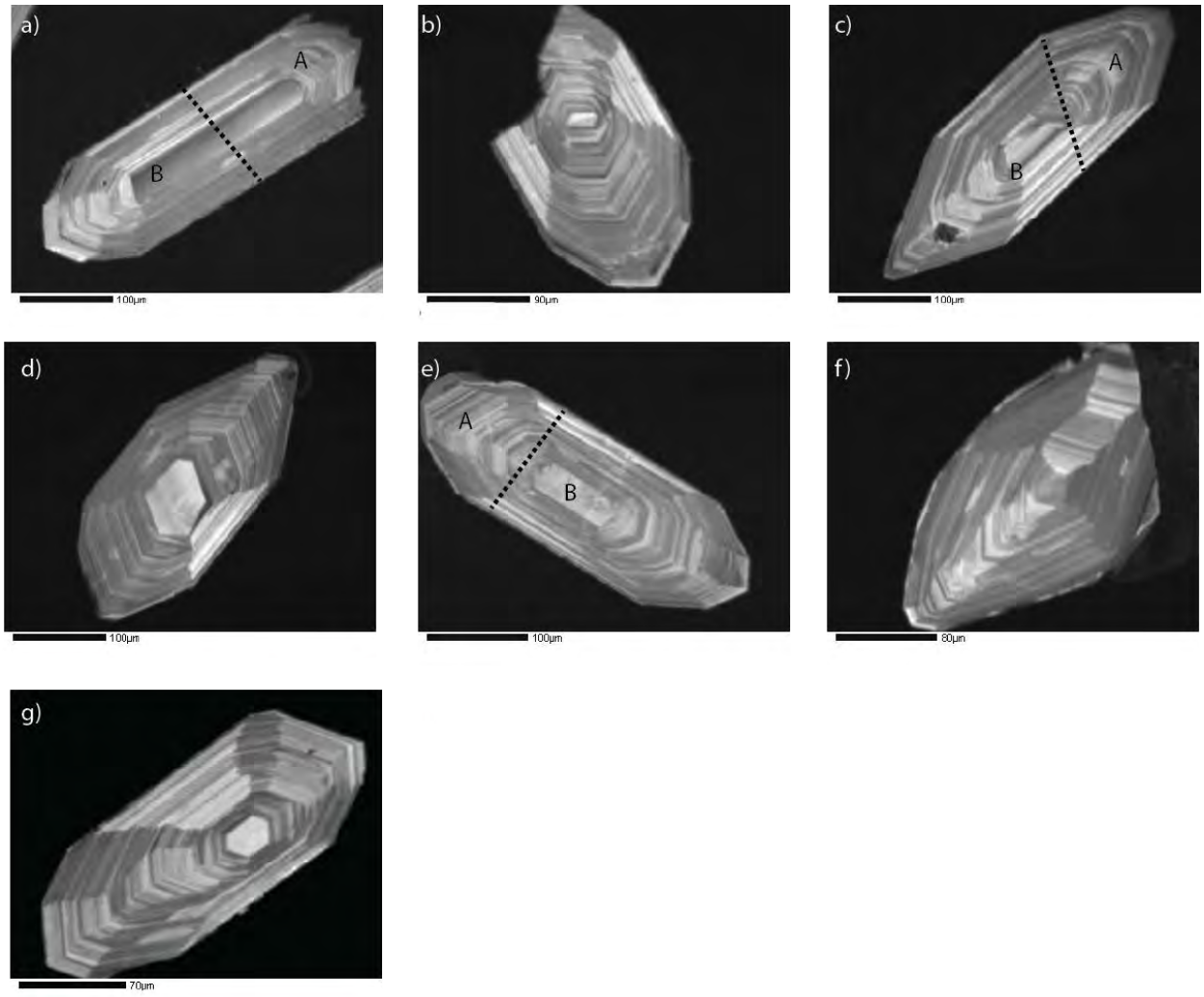

Fig. S44: CL images of dated grains from PX10-96. Asterisk indicates dated grain. Dashed line indicates a sub-divided grain with pieces indicated. a) zL2a*, zL2b* b) zL3 c) zL4a*, zL4b d) zL5 e) zL8a*, zL8b* f) zL9* g) zM4*

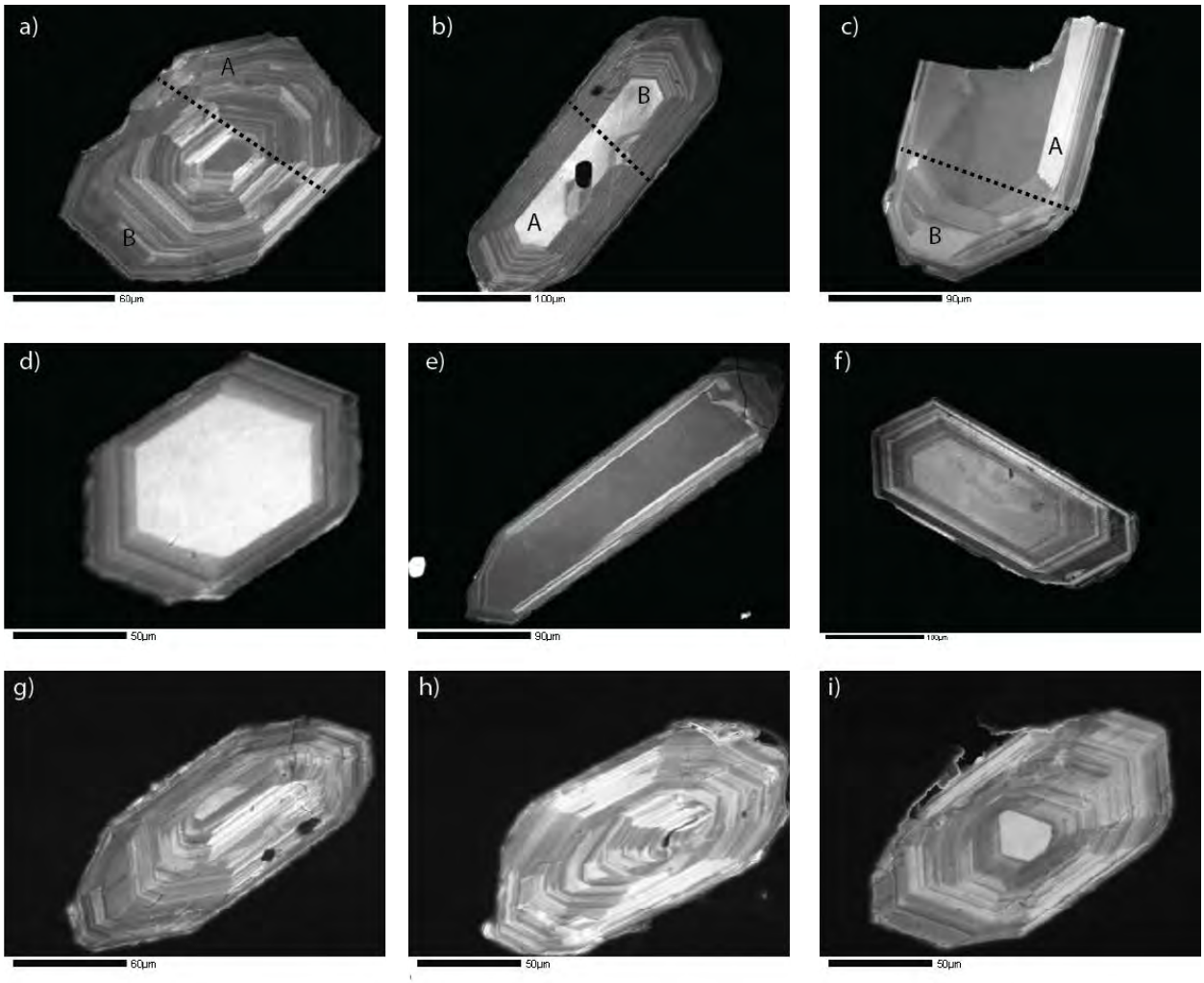

Fig. S45: CL images of dated and representative grains from sample PX10-103B. Asterisk indicates dated grain. Dashed line indicates a sub-divided grain with pieces indicated. a) zL4A, zL4B* b) zL6A*, zL6B* c) zL7A*, zL7B d)-i) representative grains

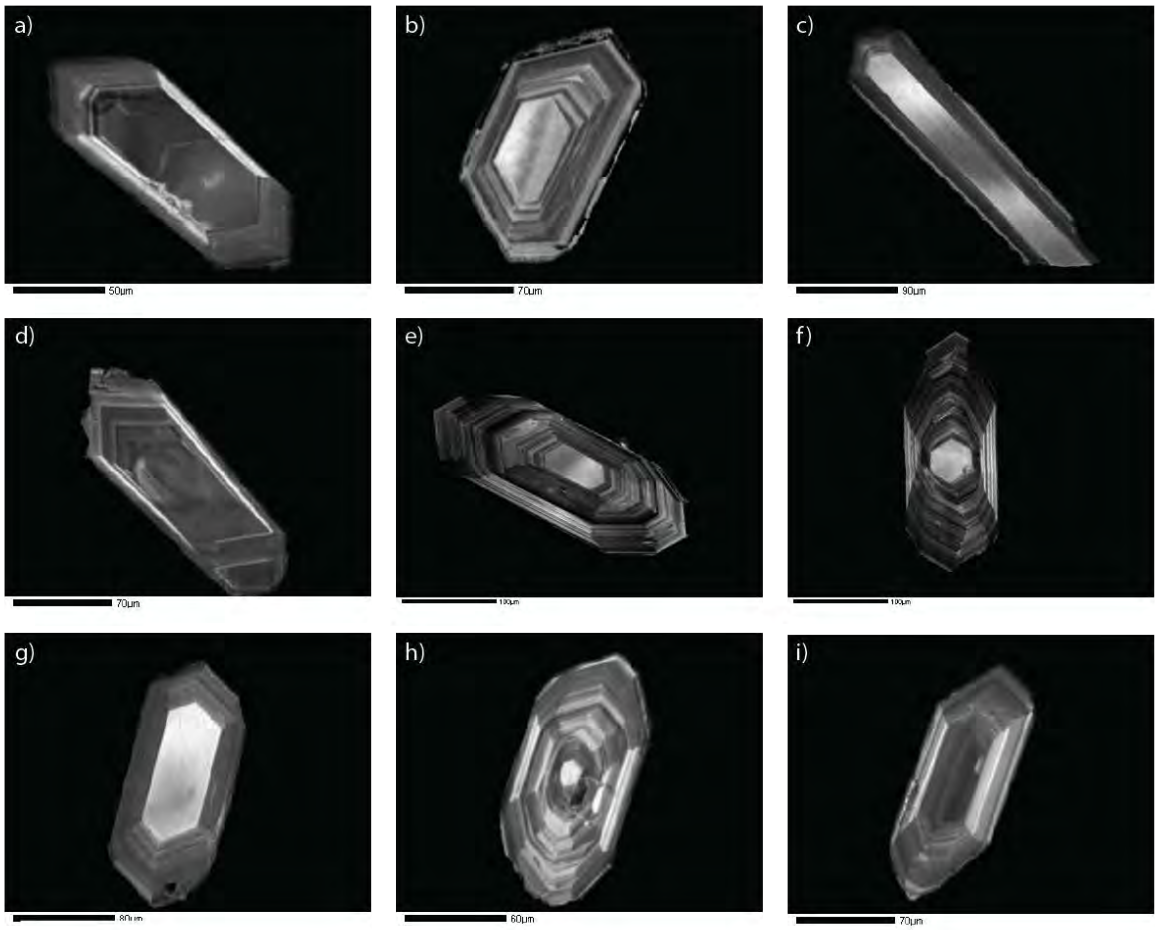

Fig. S46: CL images of dated and representative grains from sample GP-158-10. Asterisk indicates dated grain. a) zS1* b) zS3* c) zS4* d) zS6* e)-i) representative grains

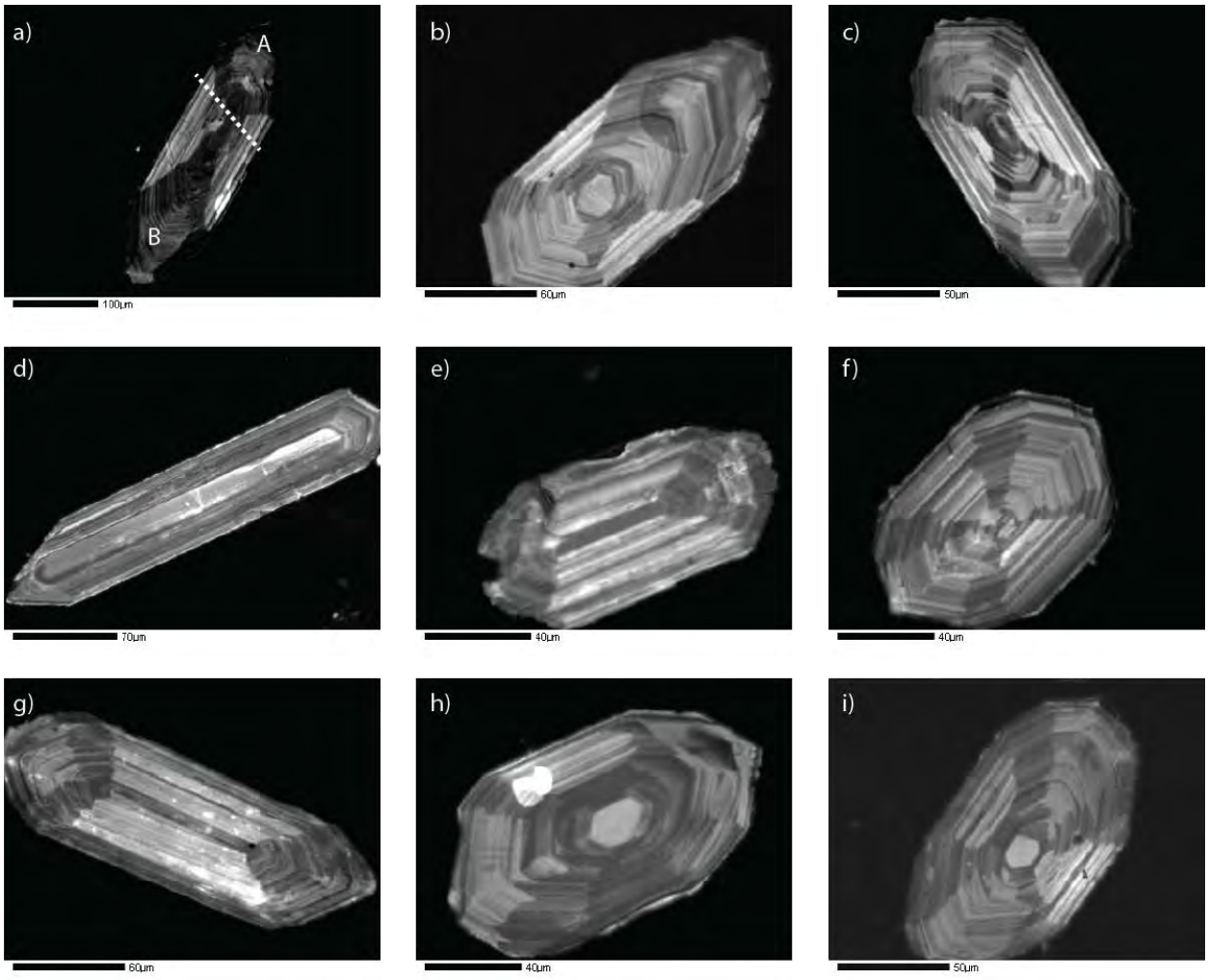

Fig. S47: CL images of dated and representative grains from sample SCP. Asterisk indicates dated grain. a) zM1A, zM1B* b)-i) representative grains

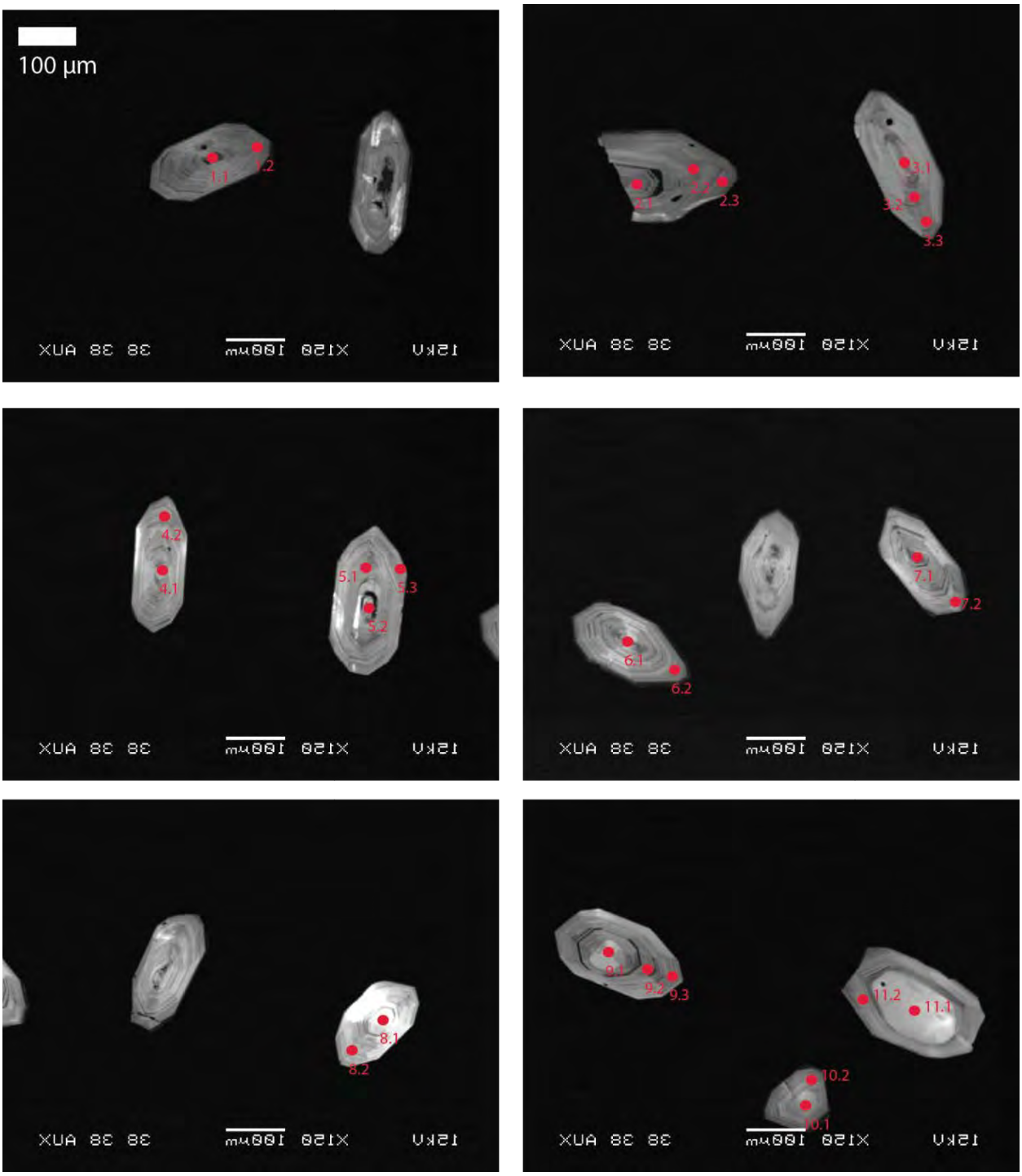

Fig. S48: CL images of SHRIMP spots from sample SCP. Spots are denoted by red dots with the spot number nearby.

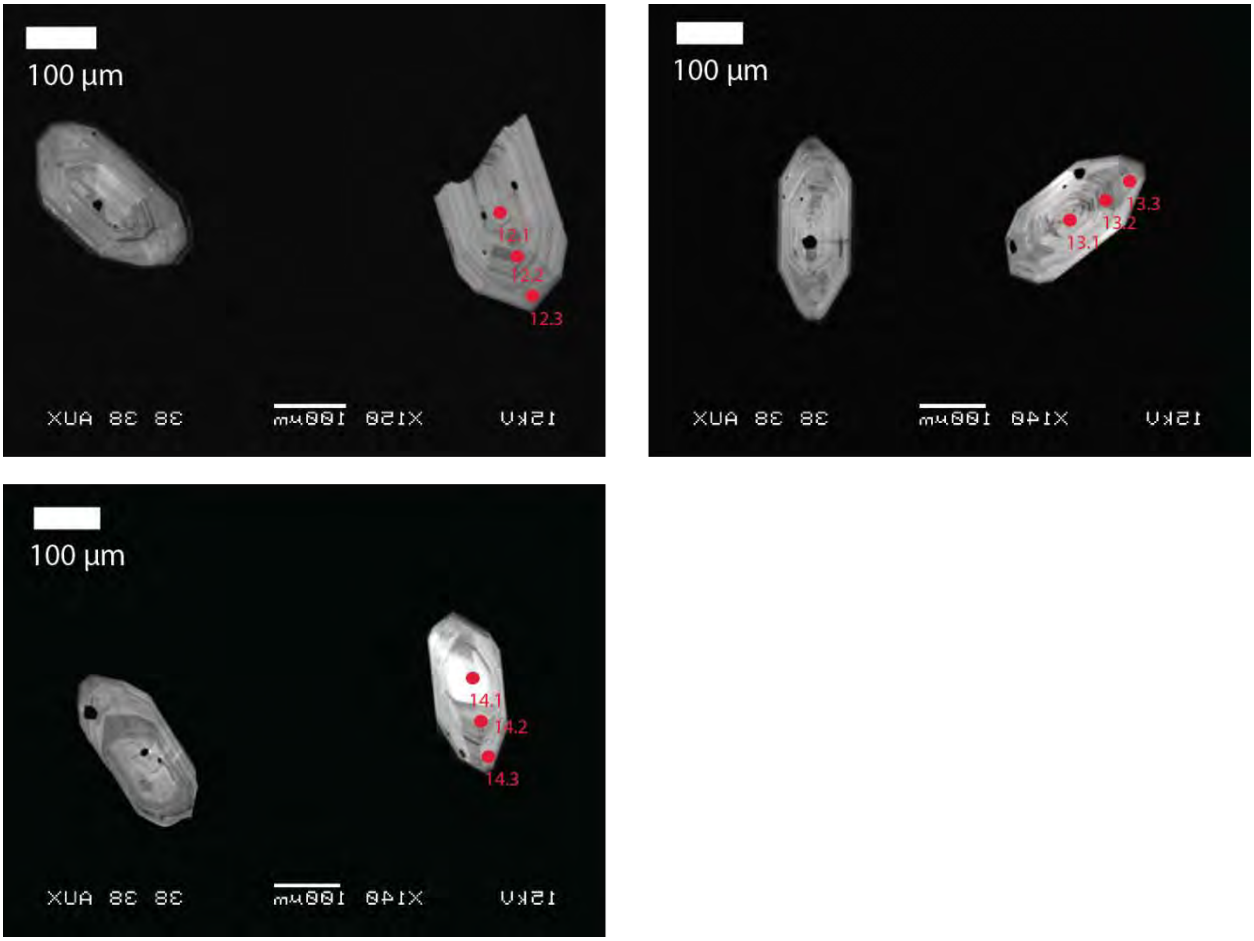

Fig. S49: CL images of SHRIMP spots from sample SCP. Spots are denoted by red dots with the spot number nearby.

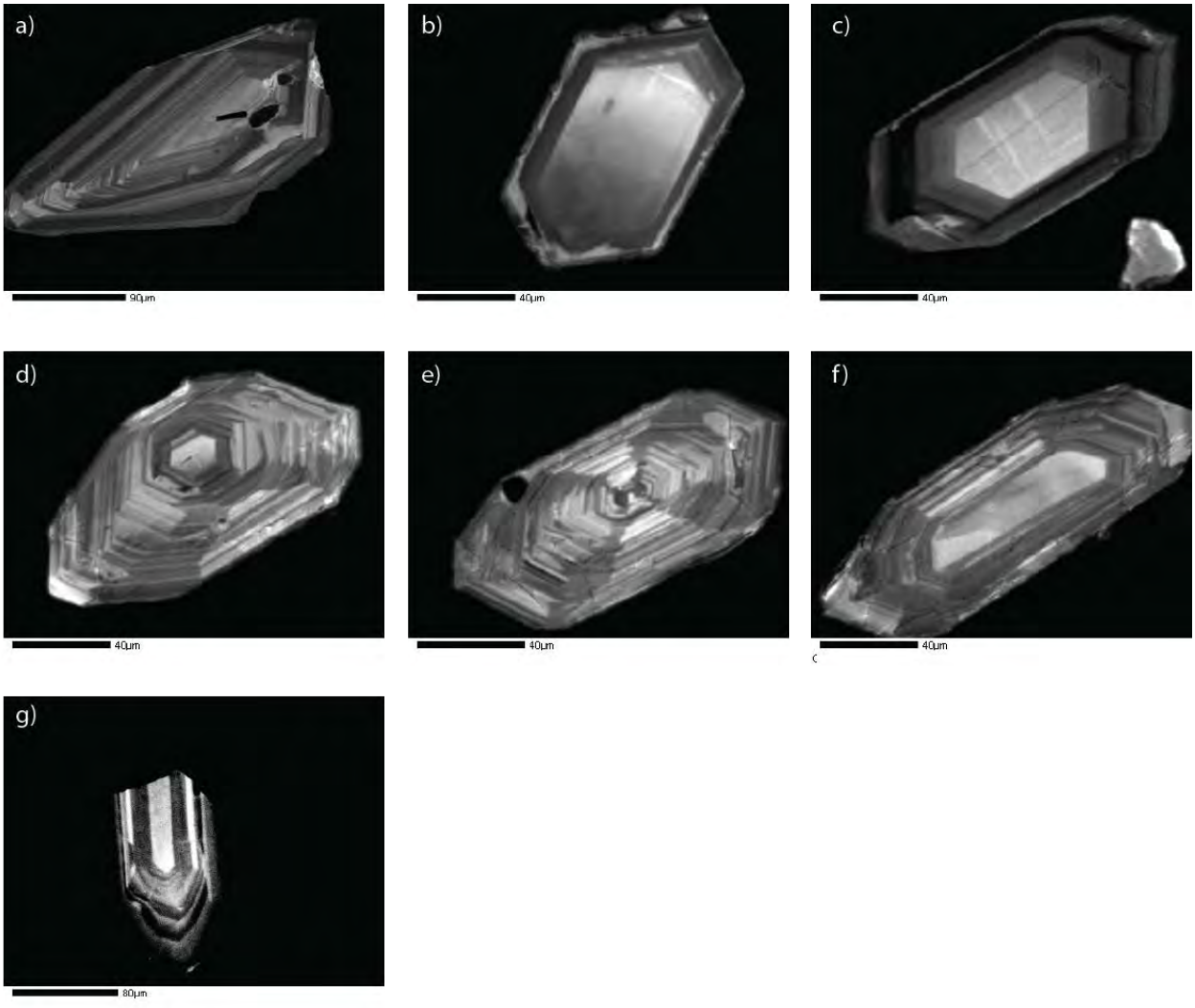

Fig. S50: CL images of dated and representative grains from sample PX10-221. Asterisk indicates dated grain. a) zL1* b)-g) representative grains

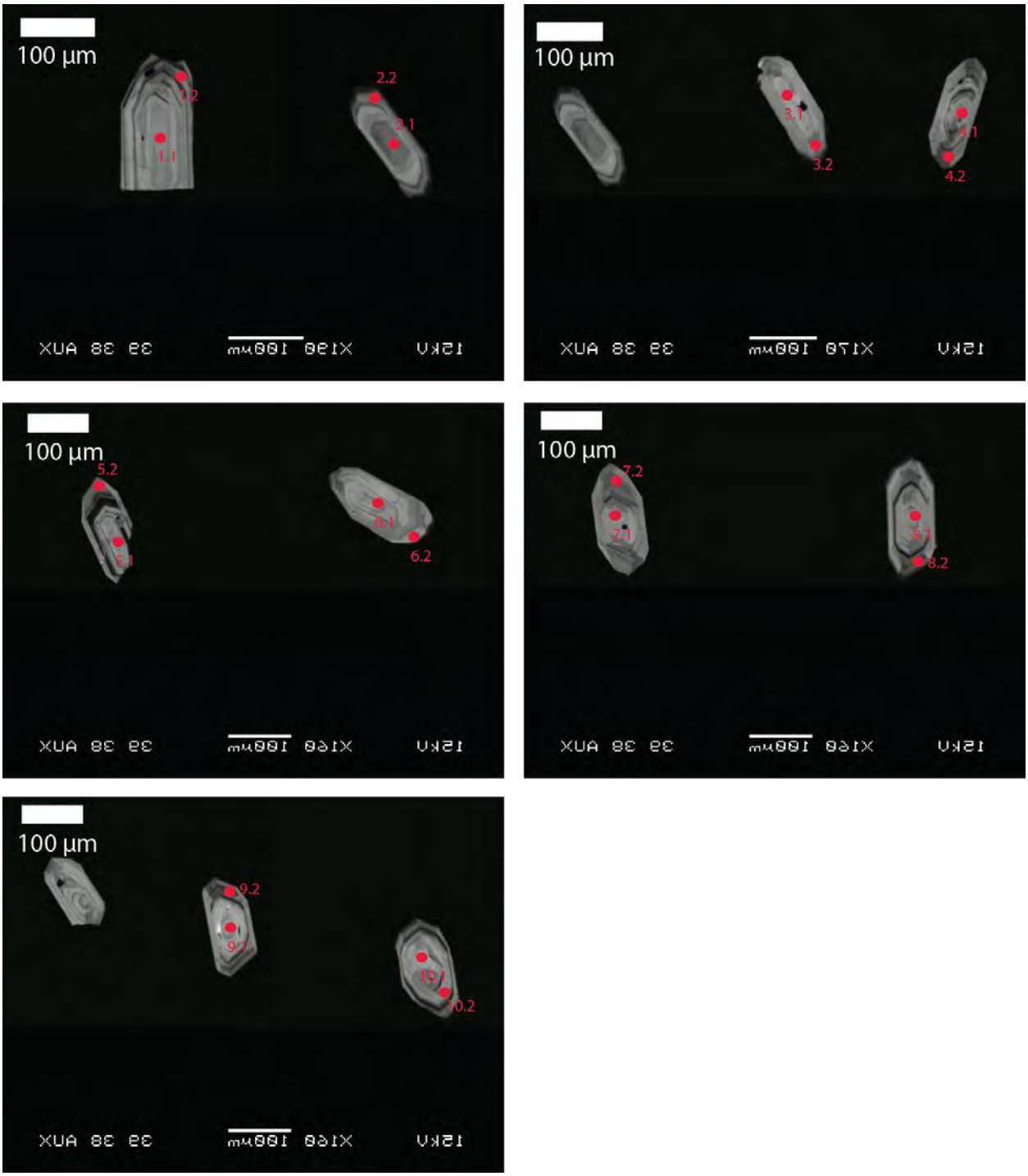

Fig. S51: CL images of SHRIMP and oxygen isotope spots from sample PX10-221. Spots are denoted by red dots with the spot number nearby.

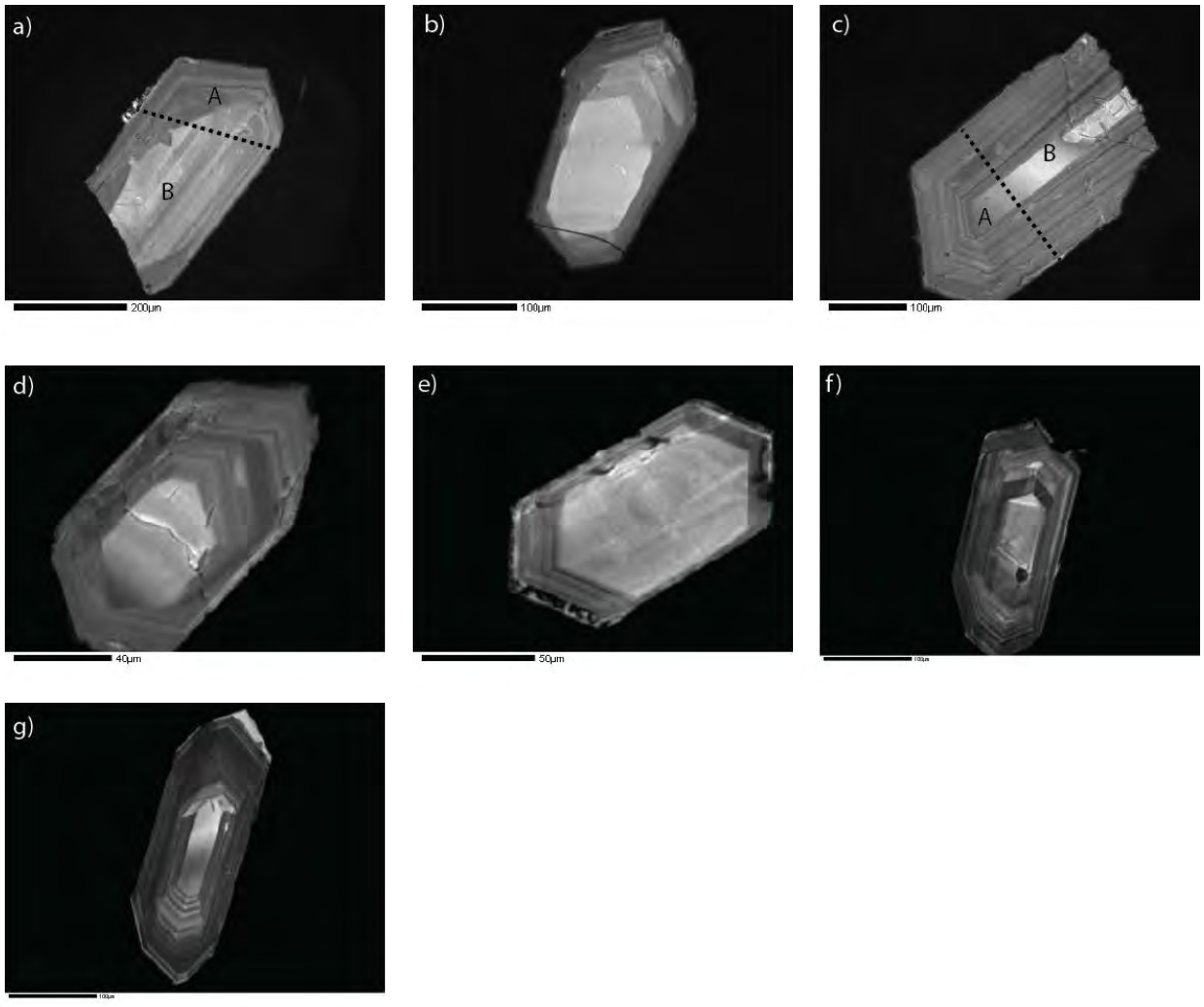

Fig. S52: CL images of dated and representative grains from sample PX10-103A. Asterisk indicates dated grain. Dashed line indicates a sub-divided grain with pieces indicated. a) zXL1a*, zXL1b* b) zXL2* c) zXL3a*, zXL3b* d) zM1* e)-g) representative grains

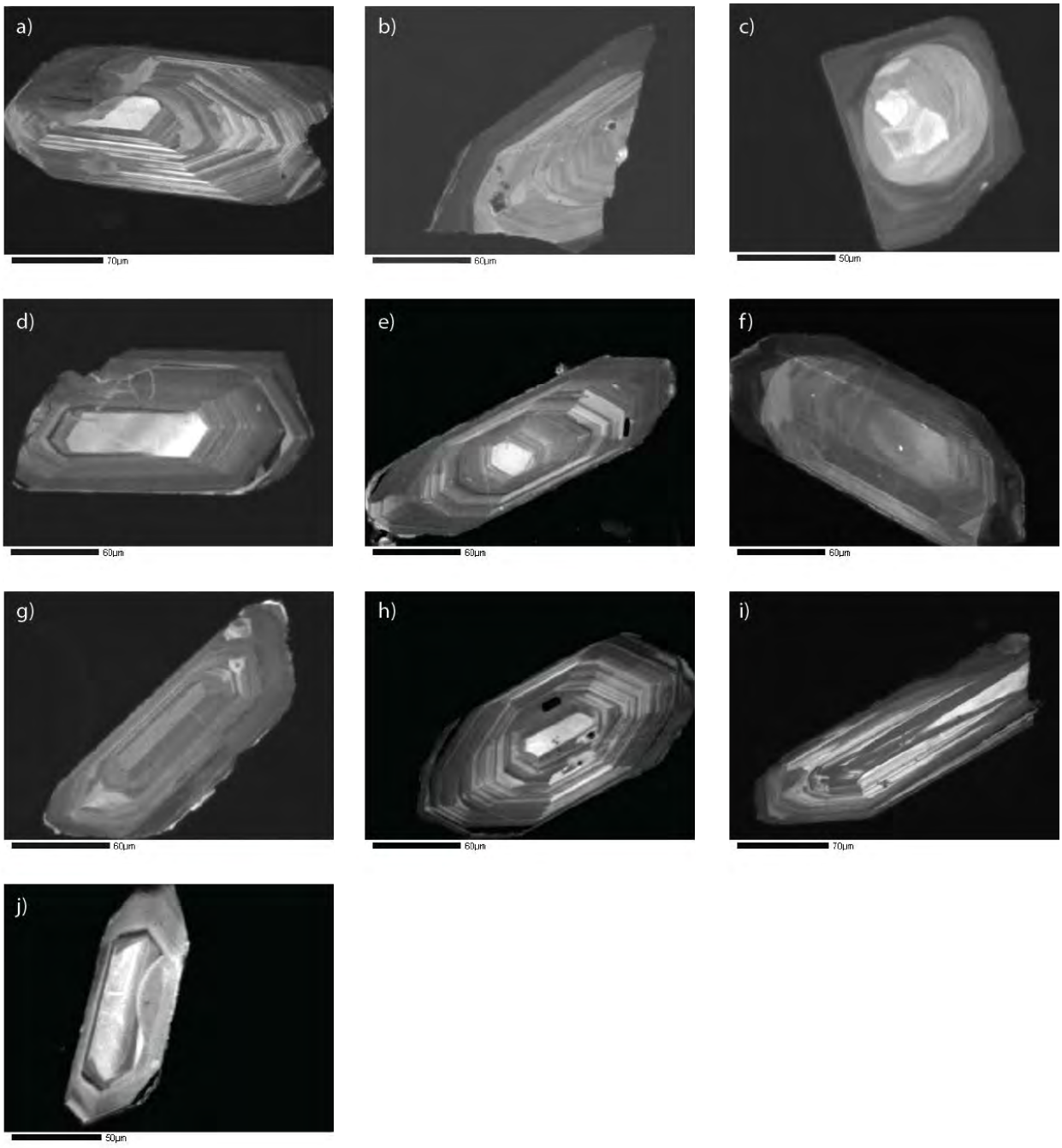

Fig. S53: CL images of dated and representative grains from sample WCG. Asterisk indicates dated grain. a) zL1* b) zL6* c) zM4* d) zM9* e)-j) representative grains

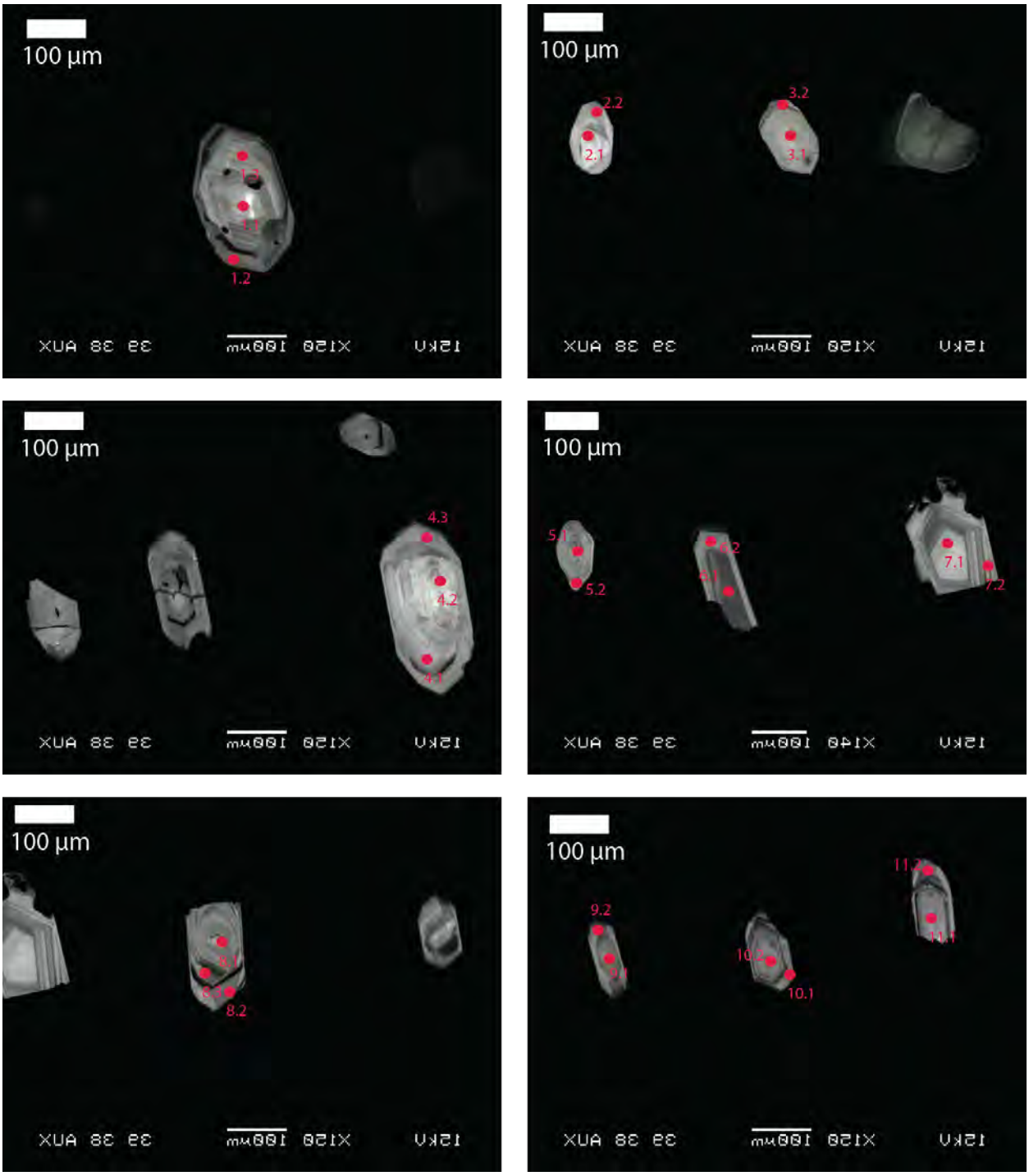

Fig. S54: CL images of SHRIMP spots from sample WCG. Spots are denoted by red dots with the spot number nearby.

Fig. S55: CL images of SHRIMP spots from sample WCG. Spots are denoted by red dots with the spot number nearby.

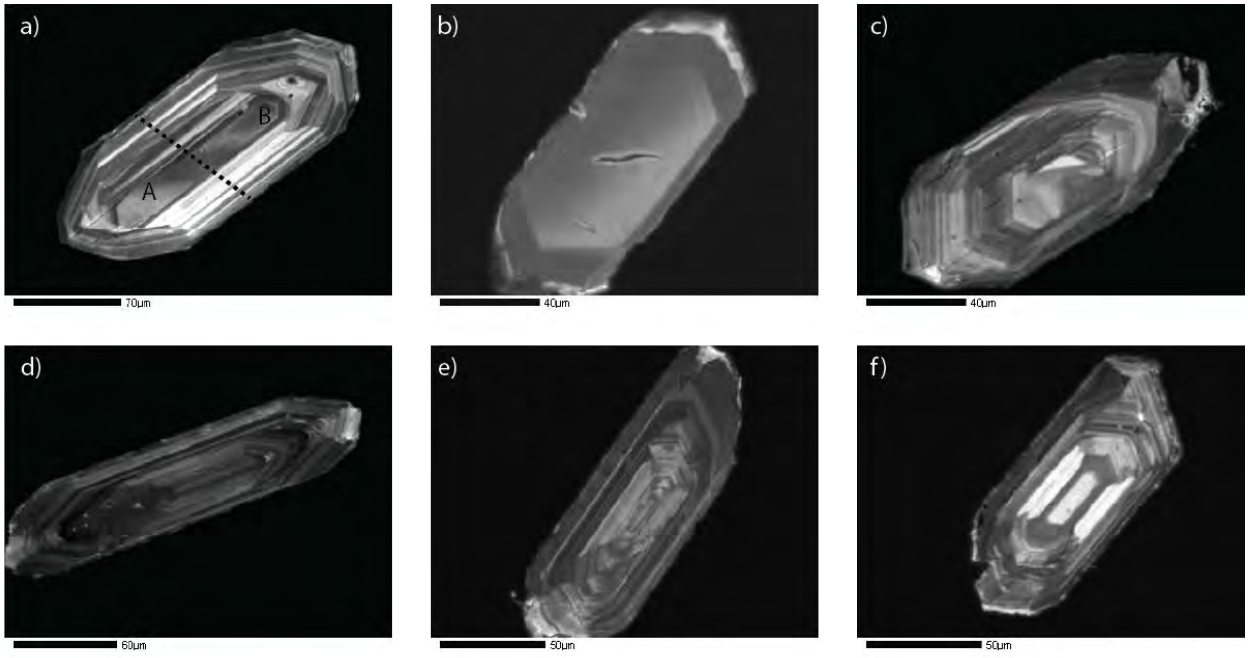

Fig. S56: CL images of dated and representative grains from sample PX10-175. Asterisk indicates dated grain. Dashed line indicates a sub-divided grain with pieces indicated. a) zL2a, zL2b* b)-f) representative grains

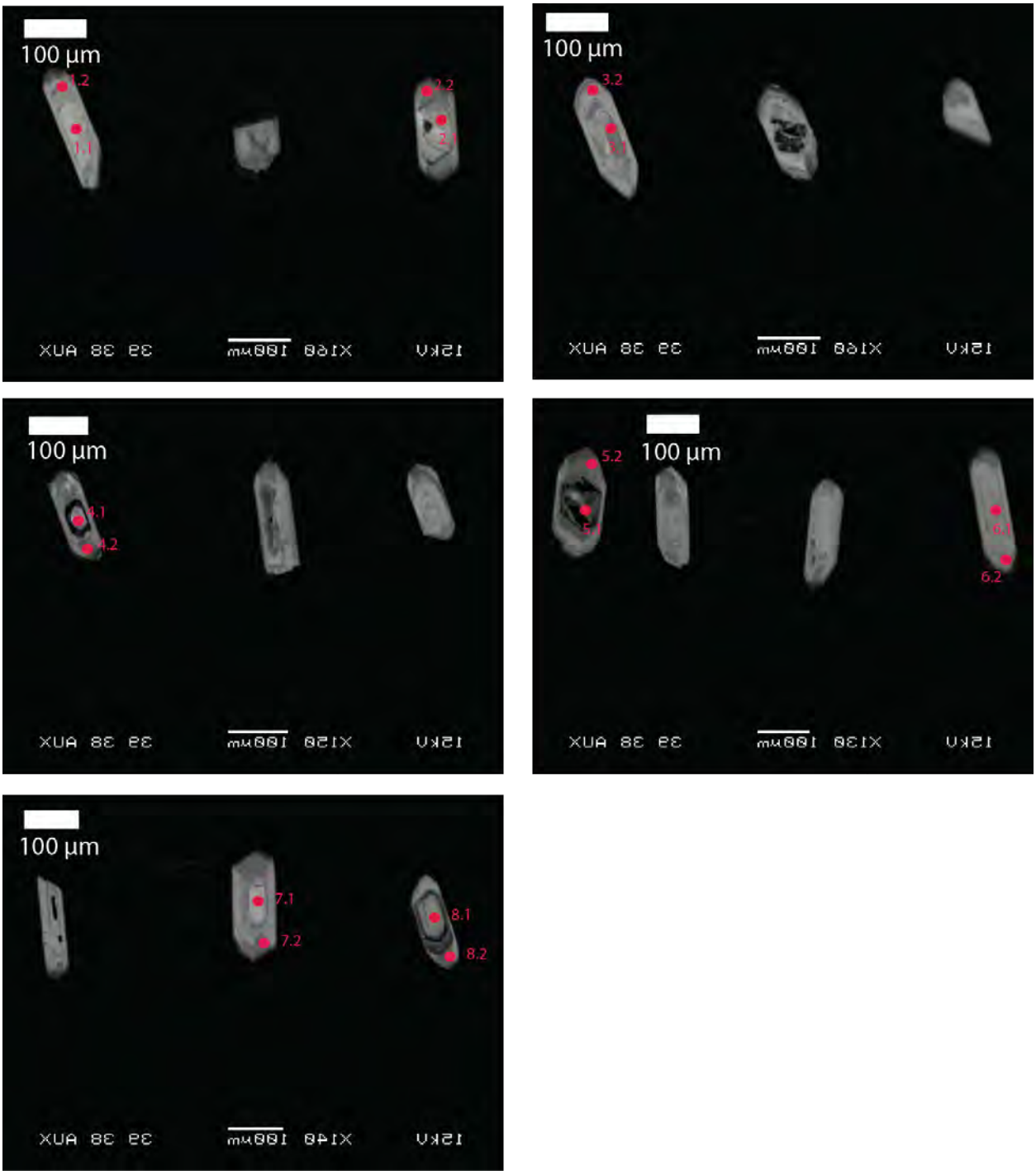

Fig. S57: CL images of SHRIMP and oxygen isotope spots from sample PX10-175. Spots are denoted by red dots with the spot number nearby.

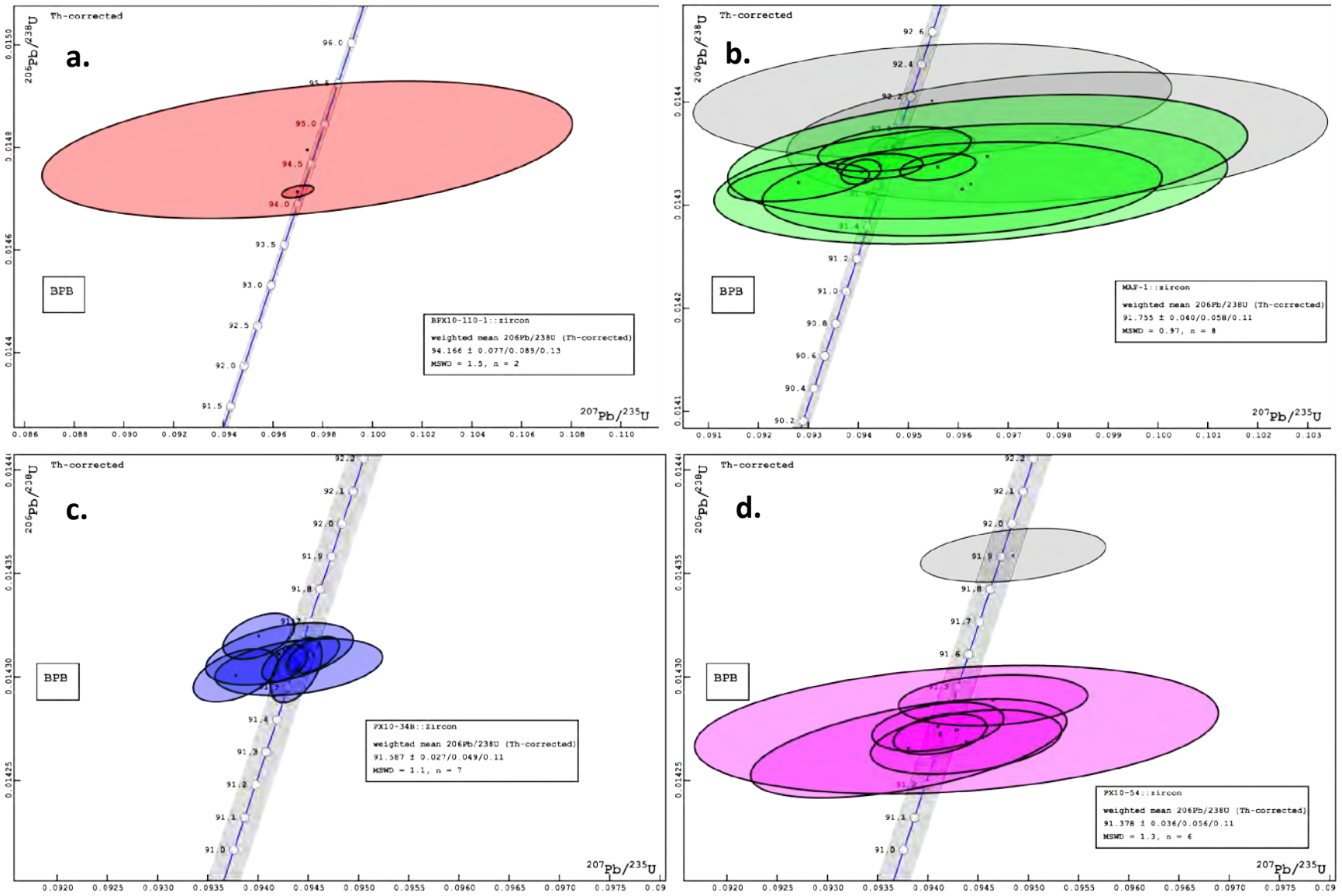
a.
Th-corrected
BPB
BPX10-110-1::zircon
weighted mean 206Pb/238U (Th-corrected)
94.166 ± 0.077/0.089/0.13
MSWD = 1.5, n = 2
b.
Th-corrected
BPB
MAF-1::zircon
weighted mean 206Pb/238U (Th-corrected)
91.755 ± 0.040/0.058/0.11
MSWD = 0.97, n = 8
c.
Th-corrected
BPB
PX10-348::zircon
weighted mean 206Pb/238U (Th-corrected)
91.587 ± 0.027/0.049/0.11
MSWD = 1.1, n = 7
d.
Th-corrected
BPB
PX10-54::zircon
weighted mean 206Pb/238U (Th-corrected)
91.378 ± 0.036/0.056/0.11
MSWD = 1.3, n = 6
207Pb/235U
206Pb/238U

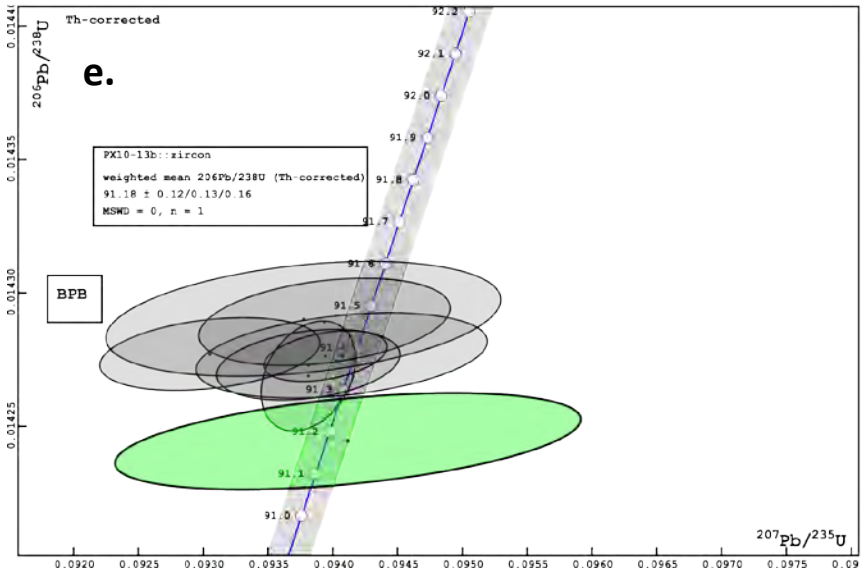

Figure S58: U-Pb concordia diagrams from the Midnight Peak Formation and the Crescent Peak unit. Analyses that are not included in the calculation of the weighted mean or single-grain $^{206}Pb/^{238}U$ age are represented by grey ellipses. a) BPX10-110-1 b) MAF-1 c) PX10-34B d) PX10-54 e) PX10-13b

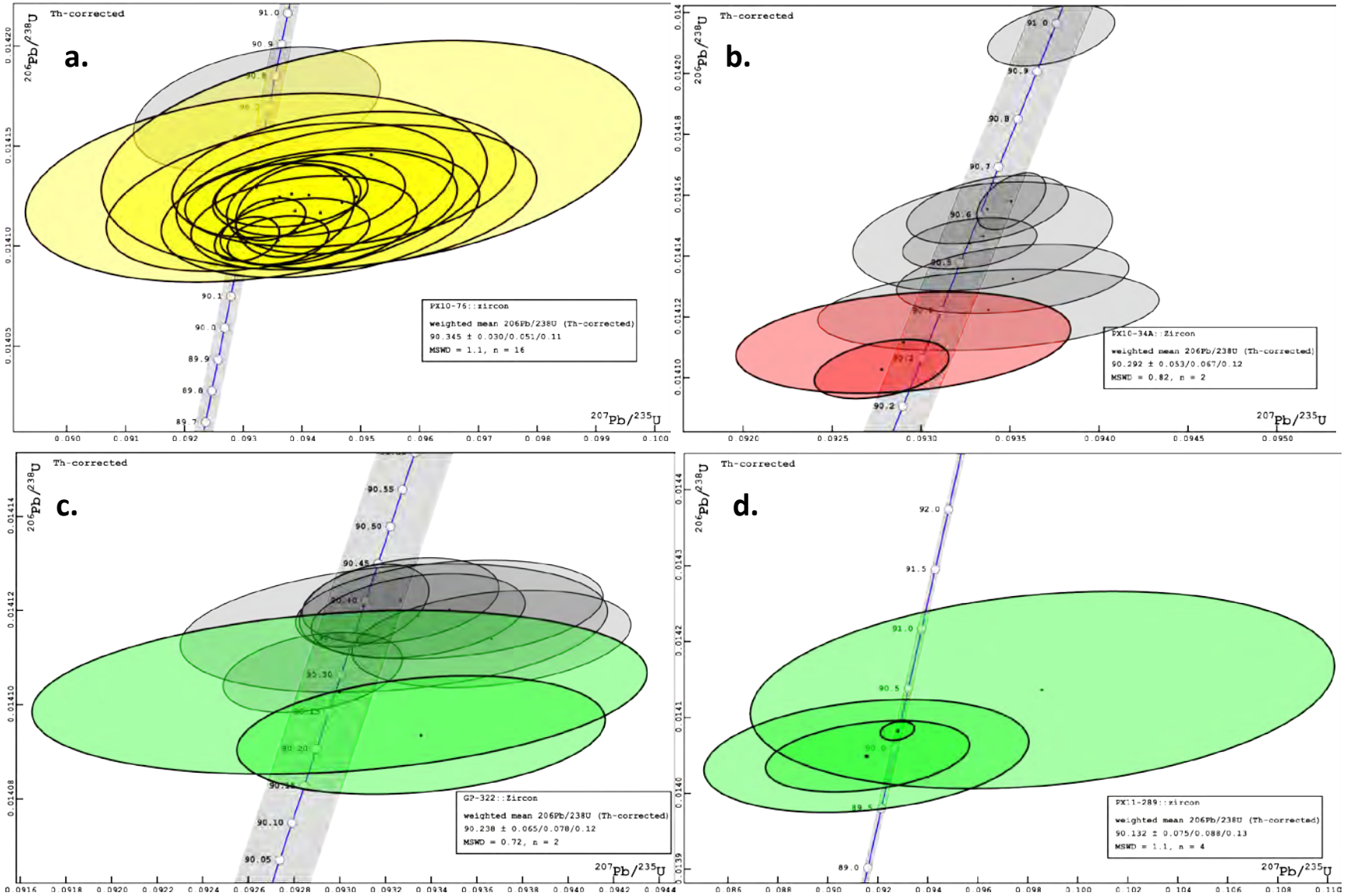
a.
Th-corrected
PX10-76::zircon
weighted mean 206Pb/238U (Th-corrected)
90.345 ± 0.030/0.051/0.11
MSWD = 1.1, n = 16
b.
Th-corrected
PX10-34A::Zircon
weighted mean 206Pb/238U (Th-corrected)
90.292 ± 0.053/0.067/0.12
MSWD = 0.82, n = 2
c.
Th-corrected
G9-322::Zircon
weighted mean 206Pb/238U (Th-corrected)
90.238 ± 0.065/0.078/0.12
MSWD = 0.72, n = 2
d.
Th-corrected
PX11-289::zircon
weighted mean 206Pb/238U (Th-corrected)
90.132 ± 0.075/0.088/0.13
MSWD = 1.1, n = 4
206Pb/238U
207Pb/235U

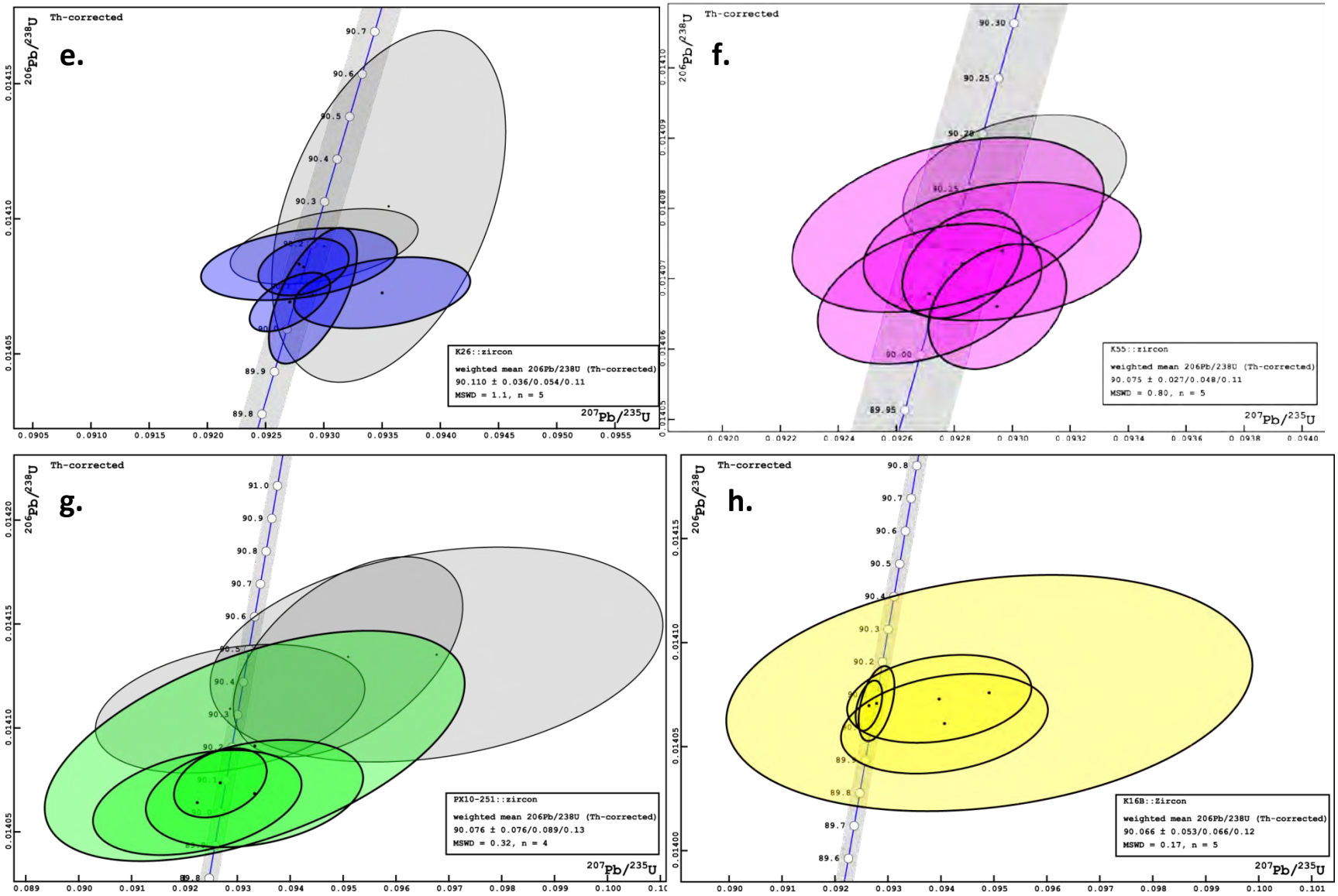
e.
Th-corrected
K26::zircon
weighted mean 206Pb/238U (Th-corrected)
90.110 ± 0.036/0.054/0.11
MSWD = 1.1, n = 5
f.
Th-corrected
K55::zircon
weighted mean 206Pb/238U (Th-corrected)
90.075 ± 0.027/0.048/0.11
MSWD = 0.80, n = 5
g.
Th-corrected
PX10-251::zircon
weighted mean 206Pb/238U (Th-corrected)
90.076 ± 0.076/0.089/0.13
MSWD = 0.32, n = 4
h.
Th-corrected
K16B::Zircon
weighted mean 206Pb/238U (Th-corrected)
90.066 ± 0.053/0.066/0.12
MSWD = 0.17, n = 5

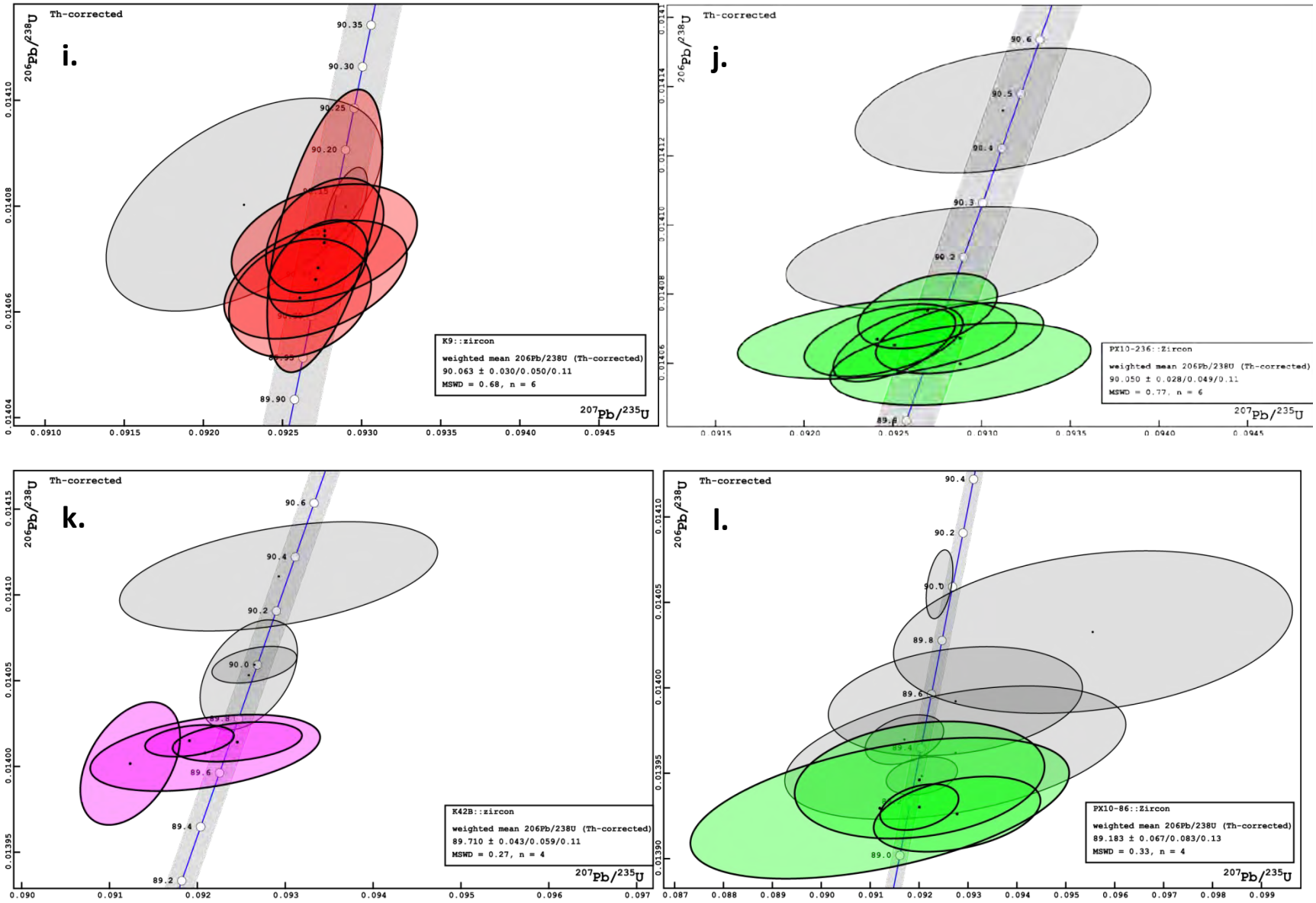
i.
Th-corrected
K9::zircon
weighted mean 206Pb/238U (Th-corrected)
90.063 ± 0.030/0.050/0.11
MSWD = 0.68, n = 6
j.
Th-corrected
PX10-236::Zircon
weighted mean 206Pb/238U (Th-corrected)
90.050 ± 0.028/0.049/0.11
MSWD = 0.77, n = 6
k.
Th-corrected
K42B::zircon
weighted mean 206Pb/238U (Th-corrected)
89.710 ± 0.043/0.059/0.11
MSWD = 0.27, n = 4
l.
Th-corrected
PX10-86::Zircon
weighted mean 206Pb/238U (Th-corrected)
89.183 ± 0.067/0.083/0.13
MSWD = 0.33, n = 4
206Pb/238U
207Pb/235U

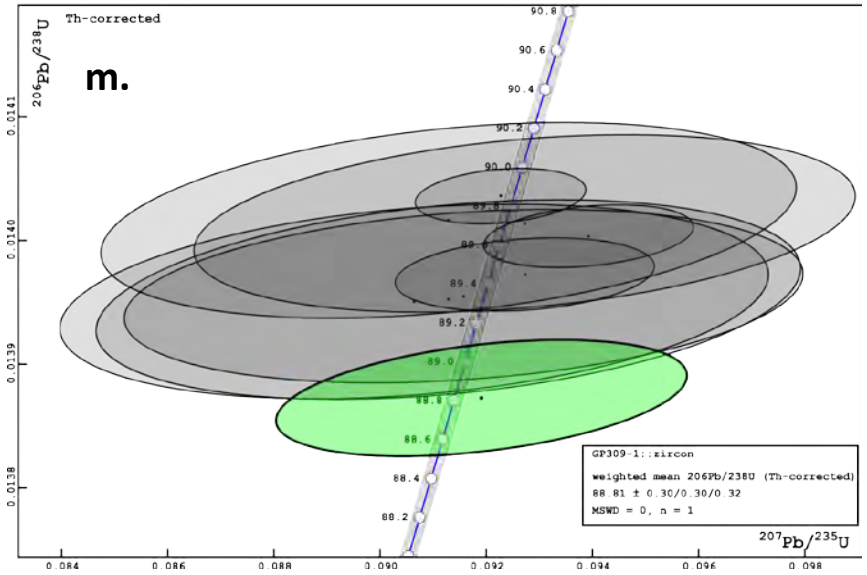

Figure S59: U-Pb concordia diagrams from the Stiletto Mtn unit. Analyses that are not included in the calculation of the weighted mean or single-grain $^{206}Pb/^{238}U$ age are represented by grey ellipses. a) PX10-76 b) PX10-34A c) GP-322 d) PX11-289 e) K26 f) K55 g) PX10-251 h) K16B i) K9 j) PX10-236 k) K42B l) PX10-86 m) GP309-1

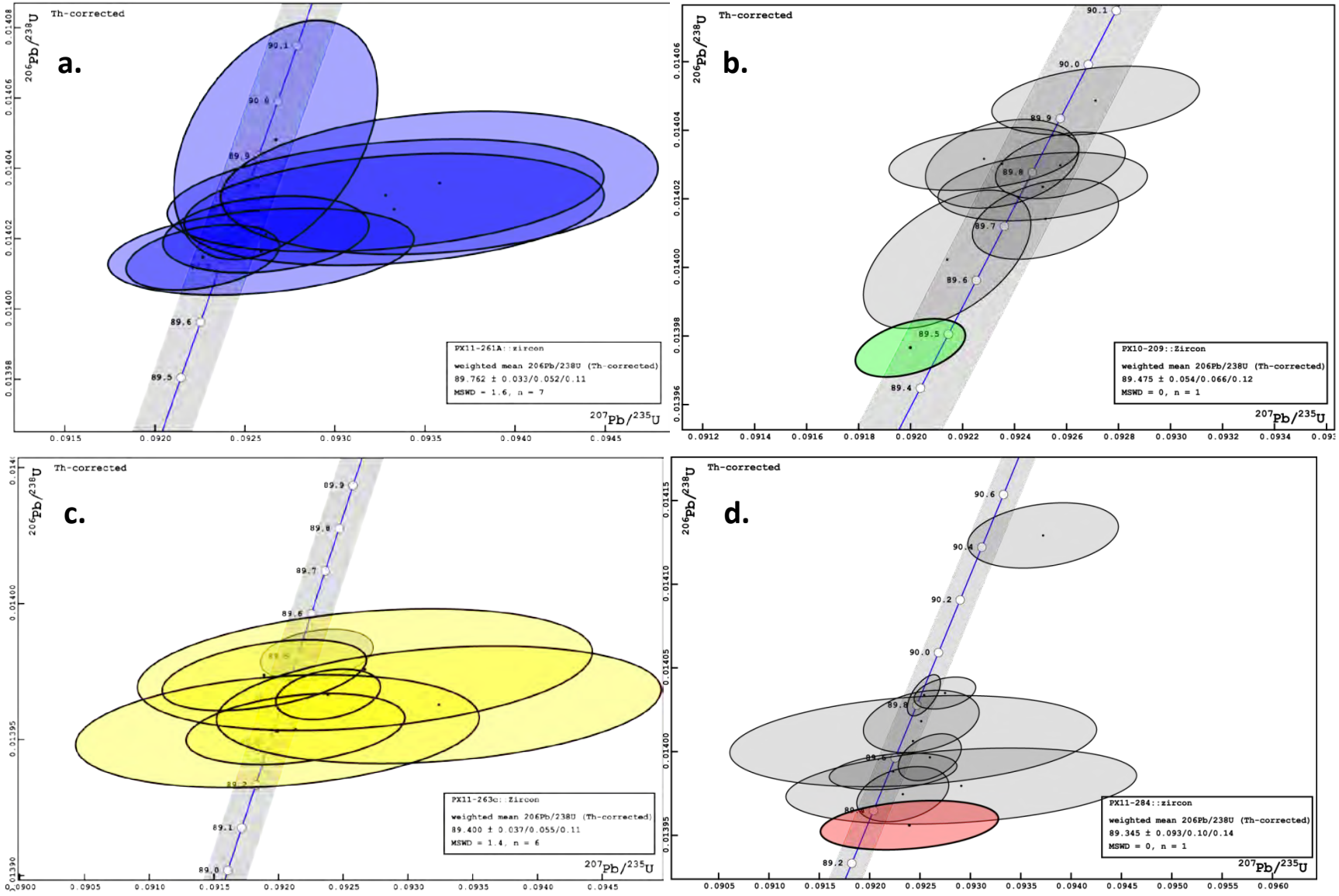
a.
Th-corrected
206Pb/238U
207Pb/235U
PX11-261A::zircon
weighted mean 206Pb/238U (Th-corrected)
89.762 ± 0.033/0.052/0.11
MSWD = 1.6, n = 7
b.
Th-corrected
206Pb/238U
207Pb/235U
PX10-209::Zircon
weighted mean 206Pb/238U (Th-corrected)
89.475 ± 0.054/0.066/0.12
MSWD = 0, n = 1
c.
Th-corrected
206Pb/238U
207Pb/235U
PX11-263c::Zircon
weighted mean 206Pb/238U (Th-corrected)
89.400 ± 0.037/0.055/0.11
MSWD = 1.4, n = 6
d.
Th-corrected
206Pb/238U
207Pb/235U
PX11-284::zircon
weighted mean 206Pb/238U (Th-corrected)
89.345 ± 0.093/0.10/0.14
MSWD = 0, n = 1

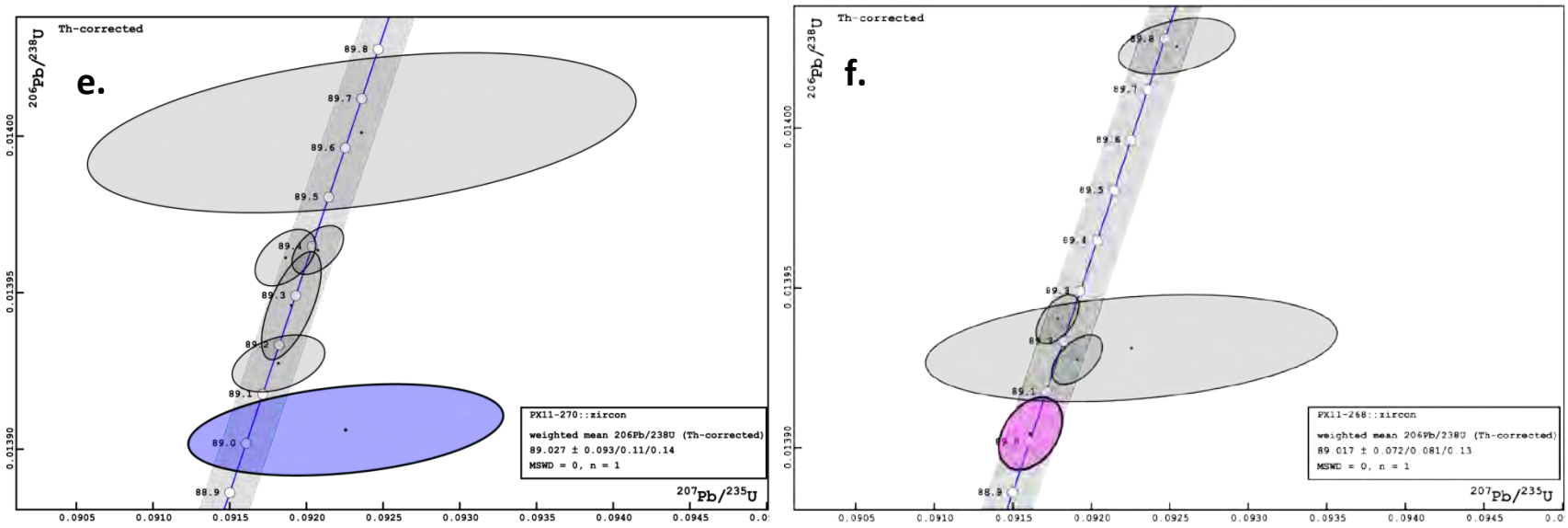

Figure S60: U-Pb concordia diagrams from the Stiletto Mtn unit and the Louis Lake heterogeneous zone. Analyses that are not included in the calculation of the weighted mean or single-grain $^{206}Pb/^{238}U$ age are represented by grey ellipses. a) PX11-261A b) PX10-209 c) PX11-263C d) PX11-284 e) PX11-270 f) PX11-268

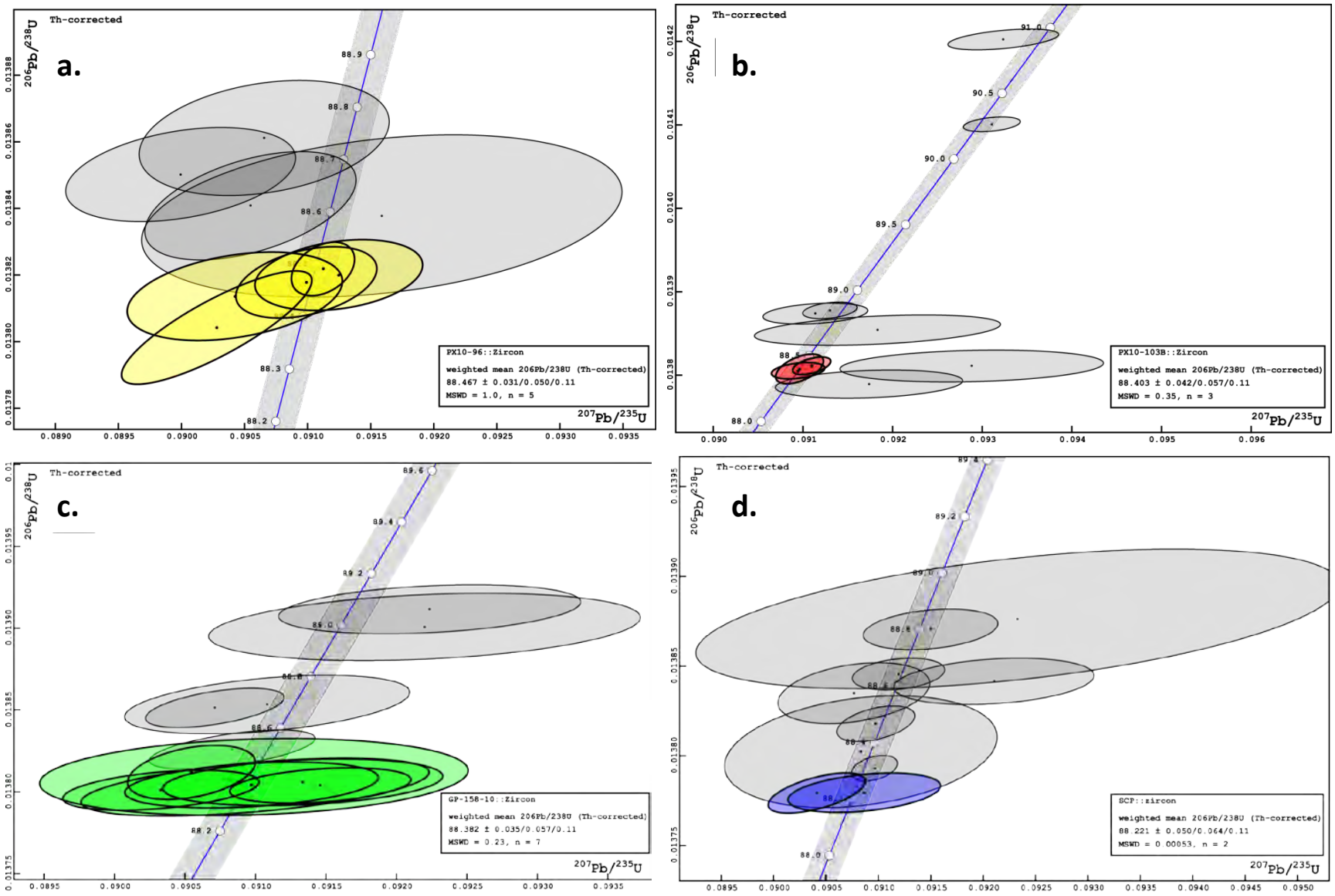
a.
Th-corrected
PX10-96::Zircon
weighted mean 206Pb/238U (Th-corrected)
88.467 ± 0.031/0.050/0.11
MSWD = 1.0, n = 5
b.
Th-corrected
PX10-103B::Zircon
weighted mean 206Pb/238U (Th-corrected)
88.403 ± 0.042/0.057/0.11
MSWD = 0.35, n = 3
c.
Th-corrected
GP-158-10::Zircon
weighted mean 206Pb/238U (Th-corrected)
88.382 ± 0.035/0.057/0.11
MSWD = 0.23, n = 7
d.
Th-corrected
SCP::zircon
weighted mean 206Pb/238U (Th-corrected)
88.221 ± 0.050/0.064/0.11
MSWD = 0.00053, n = 2
207Pb/235U
206Pb/238U

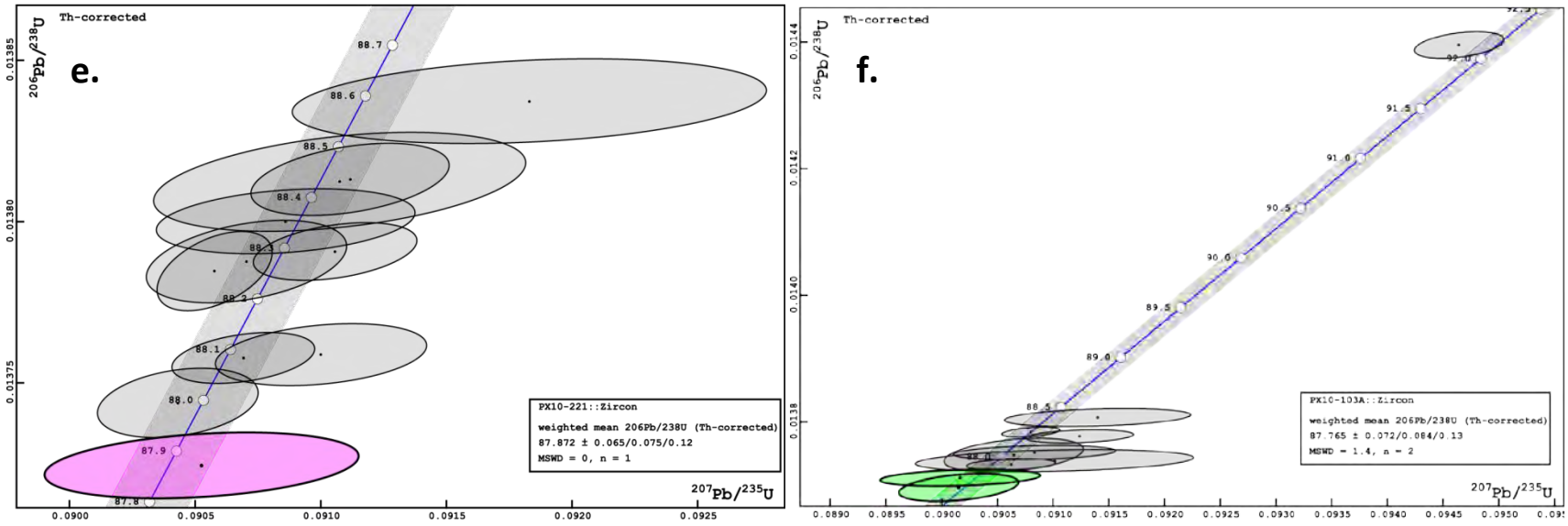

Figure S61: U-Pb concordia diagrams from the Reynolds Peak unit. Analyses that are not included in the calculation of the weighted mean or single-grain $^{206}Pb/^{238}U$ age are represented by grey ellipses. a) PX10-96 b) PX10-103B c)) GP-158-10 d) SCP e) PX10-221 f) PX10-103A

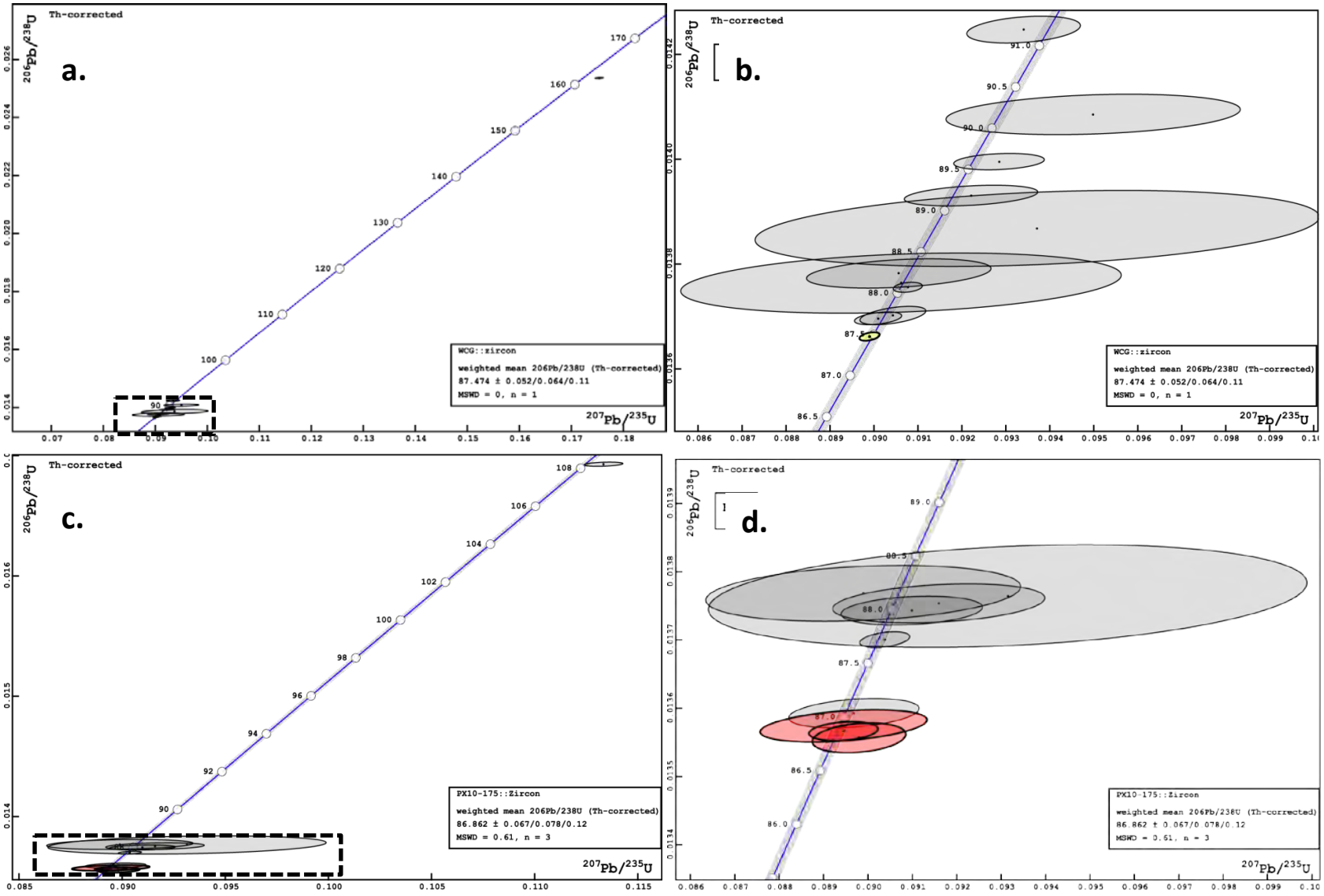
a.
Th-corrected
WCG::zircon
weighted mean 206Pb/238U (Th-corrected)
87.474 ± 0.052/0.064/0.11
MSWD = 0, n = 1
b.
Th-corrected
WCG::zircon
weighted mean 206Pb/238U (Th-corrected)
87.474 ± 0.052/0.064/0.11
MSWD = 0, n = 1
c.
Th-corrected
PX10-175::Zircon
weighted mean 206Pb/238U (Th-corrected)
86.862 ± 0.067/0.078/0.12
MSWD = 0.61, n = 3
d.
Th-corrected
PX10-175::Zircon
weighted mean 206Pb/238U (Th-corrected)
86.862 ± 0.067/0.078/0.12
MSWD = 0.61, n = 3

Figure S62: U-Pb concordia diagrams from the War Creek unit. Analyses that are not included in the calculation of the weighted mean or single-grain $^{206}Pb/^{238}U$ age are represented by grey ellipses. a) WCG b) WCG (zoom on dashed box in a)) c) PX10-175 d) PX10-175 (zoom on dashed box in c))

Table S1: In-situ zircon Ti and Hf data (ppm). Each number represents the zircon # followed by the spot number, e.g., 1.1 represents zircon 1 spot 1.

Crescent Mtn. Unit

Sample	**MAF-1**								
	Core								
Spot	*1.1*	*1.2*	*2.1*	*3.1*	*4.1*	*4.2*	*5.1*	*6.1*	*7.1*
Ti	10.34	9.98	16.10	21.56	14.35	25.04	24.67	23.20	10.88
Hf	7907.68	7053.17	7445.92	9593.09	9286.94	8629.98	9455.19	7914.57	7165.71
	Rim								
Spot	*2.2*	*3.2*	*5.2*	*6.2*					
Ti	18.54	14.31	25.29	21.94					
Hf	7216.55	10255.56	9512.68	7272.30					

Stiletto Mtn. Unit

Sample	**PX10-76**									
	Core									
Spot	*1.1*	*2.1*	*3.1*	*4.1*	*5.1*	*6.1*	*7.1*	*8.1*	*10.1*	*11.1*
Ti	6.87	6.61	8.55	8.41	7.99	7.54	6.98	8.18	7.63	13.53
Hf	10280.85	10554.39	10053.46	10479.44	10018.45	10974.50	10927.73	10605.41	10158.11	8621.38
	Rim									
Spot	*1.2*	*2.2*	*3.2*	*5.2*	*7.2*	*8.2*	*9.2*	*10.2*		
Ti	8.17	8.79	8.52	8.67	8.18	8.76	8.22	7.04		
Hf	9613.97	9934.69	9666.93	9862.57	10169.53	9250.83	10157.52	10774.15		

Sample	**PX10-34A**													
	Core													
Spot	*2.1*	*3.1*	*4.1*	*5.1*	*6.1*	*6.1a*	*7.1*	*8.1*	*9.1*	*10.1*	*11.1*	*12.1*	*13.1*	
Ti	16.28	16.64	14.07	17.85	11.70	16.25	19.88	9.70	12.52	15.67	19.59	21.28	16.51	
Hf	9627.45	8834.31	7585.48	7428.24	7345.36	9866.47	9610.56	9386.94	9562.28	9318.90	9243.61	8833.17	8887.58	
	Mid													
Spot	*1.1*	*5.2*	*7.2*	*13.2*	*8.2*	*8.3*								
Ti	12.81	10.88	5.32	16.87	11.48	8.64								
Hf	10103.44	7562.27	11773.91	8827.80	9241.85	9873.58								
	Rim													
Spot	*1.2*	*2.2*	*3.2*	*4.2*	*5.3*	*6.2*	*6.2a*	*7.3*	*8.4*	*9.2*	*10.2*	*10.3*	*11.2*	*12.2*	*13.2*
Ti	6.13	6.43	3.21	13.01	18.97	8.42	7.01	4.43	5.19	12.36	11.06	17.85	7.61	10.89	6.97
Hf	11032.06	11527.09	12616.89	10344.17	9356.59	10513.13	10558.59	11980.37	11433.85	9364.44	10480.53	7636.86	10353.38	9678.61	10359.17

Sample	**K26**								
	Core								
Spot	*1.1*	*2.1*	*3.1*	*4.1*	*5.1*	*6.1*	*7.1*	*8.1*	*9.1*

Ti	22.41	18.01	17.24	22.60	14.76	14.69	17.29	15.25	14.33
Hf	9802.61	10607.44	11113.16	9830.21	10979.22	10579.51	10381.31	10653.81	10908.83
	Rim								
Spot	*1.2*	*2.2*	*3.2*	*4.2*	*5.2*	*6.2*	*7.2*	*8.2*	*9.2*
Ti	4.39	12.26	9.82	4.78	11.01	5.00	6.76	4.75	5.74
Hf	15429.90	12289.75	12447.74	19536.55	11743.83	19792.64	15160.66	17108.08	16473.45

Sample	**K9**									
	Core									
Spot	*1.1*	*2.1*	*3.1*	*4.1*	*5.1*	*6.1*	*7.1*	*8.1*	*9.1*	
Ti	18.06	20.32	16.95	12.85	16.62	13.66	13.99	9.11	13.99	
Hf	9690.30	9665.24	10040.49	10927.58	10406.61	10740.30	11272.24	11266.53	10820.97	
	Mid									
Spot	*7.2*	*8.2*								
Ti	13.31	12.07								
Hf	10738.09	11138.93								
	Rim									
Spot	*1.2*	*3.3*	*4.2*	*4.3*	*5.2*	*5.3*	*6.2*	*8.3*	*9.2*	*9.3*
Ti	8.29	4.98	11.05	6.00	10.72	5.37	7.52	3.96	11.72	5.08
Hf	9825.44	16933.94	10992.67	15308.53	11414.81	12303.04	12797.29	11901.18	11247.15	14207.54

Sample	**K16B**								
	Core								
Spot	*1.1*	*2.1*	*3.1*	*4.1*	*5.1*	*6.1*	*7.1*	*8.1*	*9.1*
Ti	11.58	11.80	14.33	14.50	26.13	15.10	11.06	12.24	12.84
Hf	11688.24	11796.70	11088.78	10411.36	9668.22	10966.32	11209.04	11238.39	11209.55
	Mid								
Spot	*3.2*	*7.2*	*8.2*						
Ti	8.27	10.94	5.68						
Hf	11969.13	11878.77	14222.68						
	Rim								
Spot	*1.2*	*2.2*	*3.3*	*4.2*	*5.2*	*6.2*	*7.3*	*8.3*	
Ti	6.11	6.90	2.40	9.72	16.86	3.65	9.79	4.60	
Hf	14308.16	13801.52	15250.35	11653.69	10462.00	15853.56	17594.85	14855.38	

Sample	**PX10-236**											
	Core											
Spot	*1.1*	*2.1*	*3.1*	*4.1*	*4.2*	*5.2*	*6.1*	*7.1*	*8.1*	*9.2*	*10.1*	*11.1*
Ti	13.37	15.03	12.61	14.31	10.13	14.64	13.90	19.81	12.89	16.96	15.56	19.23
Hf	10603.91	10518.51	10966.69	10881.61	11883.04	10895.16	11050.24	9658.85	10903.15	10434.73	10566.96	9711.00
	Rim											
Spot	*3.2*	*5.1*	*9.1*	*6.2*	*7.2*	*8.2*	*10.2*	*11.2*				
Ti												
Hf												

Ti	9.67	13.69	18.41	6.77	12.86	6.43	15.50	13.93		
Hf	11520.26	10687.10	9682.02	14571.24	11044.63	14896.16	10271.94	11155.06		

Sample	**K55**									
	Core									
Spot	*1.1*	*2.1*	*3.1*	*4.1*	*5.2*	*6.1*	*7.1*	*8.1*	*9.1*	*10.1*
Ti	20.65	22.00	24.15	20.34	22.49	20.13	22.22	19.03	13.50	20.24
Hf	9737.16	9695.94	9484.54	9734.61	9496.50	9594.44	9335.49	9530.04	10998.42	9932.00
	Mid									
Spot	*5.1*	*9.2*	*10.2*							
Ti	23.00	13.66	11.99							
Hf	9460.85	10566.84	12158.33							
	Rim									
Spot	*1.2*	*2.2*	*3.2*	*4.2*	*5.3*	*6.2*	*7.2*	*9.3*	*10.3*	
Ti	9.58	7.11	21.31	6.12	5.86	12.81	10.87	4.71	7.18	
Hf	11917.33	14667.89	9663.16	15034.91	14954.54	11352.40	12637.99	14927.35	13891.31	

Sample	**K42B**									
	Core									
Spot	*1.1*	*2.1*	*3.1*	*4.1*	*5.1*	*6.1*	*7.1*	*8.1*	*9.1*	*10.1*
Ti	16.47	14.84	18.33	20.08	21.13	9.11	10.29	18.24	15.41	17.26
Hf	10223.51	10565.53	10791.70	9445.62	9634.93	8192.71	12127.31	10801.00	8705.63	10353.71
	Mid									
Spot	*1.2*	*7.2*	*8.2*	*1.3*	*2.2*					
Ti	16.63	5.33	4.27	15.59	3.78					
Hf	10204.16	12043.36	17608.11	10278.51	12331.86					
	Rim									
Spot	*3.2*	*4.2*	*5.2*	*6.2*	*7.3*	*8.3*	*9.2*	*10.2*		
Ti	4.68	5.11	4.67	4.78	3.33	4.30	4.05	4.79		
Hf	12175.14	11955.98	11401.68	11773.03	9634.59	11901.62	12351.03	13398.21		

Sample	**PX11-261A**											
	Core/Mid											
Spot	*1.1*	*2.1*	*3.1*	*4.1*	*5.1*	*6.1*	*7.1*	*8.1*	*9.1*	*10.1*	*11.1*	*12.1*
Ti	17.23	16.94	18.50	24.56	20.45	18.43	12.97	22.41	17.66	14.30	20.46	17.37
Hf	9319.86	9754.74	9338.24	9437.33	9487.77	9945.67	10329.04	9277.56	9476.38	10567.03	9100.03	9550.02
	Rim											
Spot	*1.2*	*2.2*	*3.2*	*4.2*	*5.2*	*6.2*	*7.2*	*8.2*	*9.2*	*10.2*	*11.2*	*12.2*
Ti	11.95	5.46	12.88	0.76	2.65	5.98	10.79	9.56	1.91	1.68	4.00	8.16
Hf	11002.65	12049.33	10102.21	10856.24	15963.24	11960.01	11053.03	11450.72	17276.95	15817.32	12839.69	12121.32

Sample	**PX11-284**
	Core

Spot	*1.1*	*2.1*	*4.1*	*5.1*	*6.1*	*7.1*	*8.1*	*9.1*
Ti	13.35	15.93	18.68	16.87	20.09	19.11	16.94	3.66
Hf	9499.26	9813.09	9423.24	9561.06	9023.29	9226.70	9697.87	14684.56
	Rim							
Spot	*1.2*	*2.2*	*4.2*	*5.2*	*6.2*	*7.2*	*8.2*	*9.2*
Ti	13.14	2.11	16.77	2.47	2.42	3.29	3.53	16.42
Hf	10896.63	16636.44	9635.88	15889.02	15822.13	14011.70	14281.06	9746.45

Sample	**PX10-86**								
	Core								
Spot	*1.1*	*2.1*	*3.1*	*4.1*	*5.1*	*6.1*	*7.1*	*8.1*	*9.1*
Ti	10.39	13.00	5.71	3.73	8.26	3.71	12.16	2.97	7.81
Hf	9403.08	10124.54	11145.55	11468.64	10781.33	10783.51	8436.31	13025.97	10257.07
	Mid								
Spot	*1.3*	*8.2*							
Ti	2.06	4.44							
Hf	13025.15	11518.42							
	Rim								
Spot	*1.2*	*2.2*	*3.2*	*4.2*	*5.2*	*6.2*	*7.2*	*8.3*	*9.2*
Ti	4.45	10.71	3.57	4.17	5.00	6.01	3.68	1.55	3.88
Hf	11319.09	11336.70	11951.03	11549.54	11877.19	11213.01	12049.64	13618.52	11587.10

Reynolds Peak Unit

Sample	**SCP**													
	Core													
Spot	*1.1*	*2.1*	*3.1*	*4.1*	*5.1*	*6.1*	*7.1*	*8.1*	*9.1*	*10.1*	*11.1*	*12.1*	*13.1*	*14.1*
Ti	8.24	3.32	18.23	5.42	3.04	6.93	6.53	6.06	10.78	3.81	16.48	11.04	5.23	15.54
Hf	11222.63	11514.87	11467.03	11280.06	12497.92	11022.12	11104.07	10587.30	9919.56	12038.94	10900.28	10141.33	11170.38	9774.84
	Mid													
Spot	*2.2*	*3.2*	*5.2*	*9.2*	*12.2*	*13.2*	*14.2*							
Ti	3.10	6.74	8.14	3.60	4.60	4.62	3.83							
Hf	12619.25	10345.78	11041.42	12464.83	11289.93	11421.30	12195.40							
	Rim													
Spot	*1.2*	*2.3*	*3.3*	*4.2*	*5.3*	*6.2*	*7.2*	*8.2*	*9.3*	*10.2*	*11.2*	*12.3*	*13.3*	*14.3*
Ti	3.69	1.60	3.55	4.72	3.35	2.55	5.54	3.68	4.72	5.53	4.14	4.45	4.93	4.47
Hf	12146.86	14077.56	12366.26	12047.95	12445.54	13045.35	11135.49	11804.16	11581.88	11273.16	11513.44	11813.32	11761.01	11586.73

Sample	**PX10-221**									
	Core									
Spot	*1.1*	*2.1*	*3.1*	*4.1*	*5.1*	*6.1*	*7.1*	*8.1*	*9.1*	*10.1*
Ti	3.24	3.46	5.63	6.05	4.47	4.17	10.10	4.70	4.92	5.77
Hf	11718.82	13008.56	10577.68	10279.61	11894.17	11509.04	10857.56	10535.24	11796.06	10286.47

	Rim									
Spot	*1.2*	*2.2*	*3.2*	*4.2*	*5.2*	*6.2*	*7.2*	*8.2*	*9.2*	*10.2*
Ti	2.88	2.71	3.62	4.62	3.41	2.16	2.33	3.60	3.34	2.75
Hf	12937.98	15023.99	12225.71	10995.13	11025.14	13442.19	12100.45	12240.68	12338.56	12813.37

War Creek Unit

Sample	**WCG**											
	Core											
Spot	*1.1*	*2.1*	*4.2*	*5.1*	*7.1*	*8.1*	*9.1*	*10.1*	*11.1*	*12.1*	*13.1*	
Ti	5.60	5.25	8.37	7.89	11.58	4.18	4.50	1.14	6.07	5.77	1.35	
Hf	9021.67	10118.83	9224.01	10431.03	10969.86	11217.75	11423.63	15922.77	10888.43	11396.51	13687.07	
	Mid											
Spot	*1.3*	*4.1*	*8.3*									
Ti	5.18	2.86	1.71									
Hf	9206.07	13048.60	15298.82									
	Rim											
Spot	*1.2*	*2.2*	*3.2*	*4.3*	*5.2*	*6.2*	*7.2*	*8.2*	*9.2*	*10.2*	*11.2*	*13.2*
Ti	1.24	1.02	2.09	1.12	4.38	0.84	3.48	1.13	0.89	4.14	3.73	1.26
Hf	13844.00	16195.19	15856.46	16133.17	11414.42	19157.92	12242.20	14748.38	15879.02	12132.96	13580.52	13547.20

Sample	**PX10-175**						
	Core						
Spot	*1.1*	*2.1*	*3.1*	*4.1*	*6.1*	*7.1*	*8.1*
Ti	5.92	8.80	28.96	6.55	2.05	4.70	2.95
Hf	9993.59	10415.32	8122.42	10357.86	12366.19	10876.74	11663.10
	Rim						
Spot	*1.2*	*2.2*	*4.2*	*5.2*	*6.2*	*7.2*	*8.2*
Ti	1.64	0.78	1.65	1.03	1.59	1.82	1.55
Hf	14343.92	14547.20	13574.61	14590.31	13790.10	13961.92	13189.81

Table S2: Sm-Nd isotopic data from the BPIC. Data for samples MAF and SCP are taken from Matzel (2004).

Sample #	Sm (ppm)[a]	Nd (ppm)[a]	$\frac{^{147}Sm}{^{144}Nd}$ [b]	$\frac{^{143}Nd}{^{144}Nd}$ [c]	$\varepsilon_{Nd(0)}$ [d]	$\varepsilon_{Nd(t)}$ [d]
MAF	2.6	10.9	0.1448	0.512928	4.4	**6.3**
PX10-13b	5.54	22.37	0.14985	0.512874	4.60	**5.14**
PX10-148	2.98	18.54	0.09726	0.512895	5.01	**6.16**
PX10-148B	4.14	19.62	0.12752	0.512899	5.10	**5.89**
PX10-251	5.05	23.4	0.13053	0.512912	5.34	**6.10**
PX10-236	3.66	17.17	0.12872	0.512904	5.19	**5.97**
SCP	2.1	11.3	0.1094	0.512863	4.4	**5.4**
WCG	2.10	10.82	0.111737	0.512842	3.98	**4.89**

[a] Concentrations determined by isotope dilution

[b] Internal errors in measured $\frac{^{146}Sm}{^{144}Nd}$ are 0.1% (2σ s.e.)

[c] Measured $\frac{^{143}Nd}{^{144}Nd}$ with internal error (2σ s.d.); long-term reproducibility of Nd isotopic standards is 20 ppm (2σ s.d.), which propagates into an average reproducibility of $\varepsilon_{Nd(t)}$ of approximately ± 0.5 epsilon units.

[d] ε_{Nd} was calculated with $\frac{^{147}Sm}{^{144}Nd}$ CHUR = 0.1967 and $\frac{^{143}Nd}{^{144}Nd}$ CHUR = 0.512638 where CHUR is the chondritic uniform reservoir; $\varepsilon_{Nd(t)}$ was calculated at a crystallization age of 90 Ma.

Table S3: In-situ zircon oxygen isotope data from the BPIC.

Sample	Spot Number	$\delta^{18}O$ (‰)	Uncertainty (‰)
MAF-1	*1.1*	6.50	0.05
MAF-1	*2.1*	6.32	0.06
MAF-1	*2.2*	6.45	0.05
MAF-1	*3.1*	6.89	0.06
MAF-1	*4.1*	6.40	0.05
MAF-1	*5.1*	6.65	0.09
MAF-1	*6.1*	6.50	0.04
MAF-1	*7.1*	6.56	0.06
PX10-76	*1.1*	6.67	0.06
PX10-76	*2.1*	6.99	0.04
PX10-76	*3.1*	7.05	0.09
PX10-76	*4.1*	6.31	0.08
PX10-76	*5.1*	6.60	0.06
PX10-76	*6.1*	6.49	0.04
PX10-76	*7.1*	6.23	0.08
PX10-76	*8.1*	6.76	0.10
PX10-76	*9.1*	6.59	0.04
PX10-76	*10.1*	6.60	0.09
PX10-76	*11.1*	7.06	0.06
PX10-86	*1.2*	7.71	0.06
PX10-86	*2.1*	6.94	0.06
PX10-86	*3.1*	6.65	0.05
PX10-86	*4.1*	6.24	0.07
PX10-86	*4.2*	7.46	0.06
PX10-86	*5.1*	6.86	0.05
PX10-86	*6.1*	7.35	0.05
PX10-86	*7.1*	7.05	0.03
PX10-86	*7.2*	7.17	0.05

PX10-86	*8.1*	6.72	0.06
PX10-86	*9.1*	6.71	0.07
PX10-221	*1.1*	6.89	0.06
PX10-221	*2.1*	6.45	0.06
PX10-221	*3.1*	7.12	0.12
PX10-221	*4.1*	6.23	0.05
PX10-221	*4.2*	6.41	0.04
PX10-221	*5.1*	6.98	0.07
PX10-221	*5.2*	6.37	0.04
PX10-221	*6.1*	6.68	0.03
PX10-221	*7.1*	7.09	0.03
PX10-221	*7.2*	6.63	0.05
PX10-221	*8.1*	6.84	0.05
PX10-221	*8.2*	6.68	0.07
PX10-221	*9.1*	6.97	0.06
PX10-221	*10.1*	7.26	0.06
PX10-175	*1.1*	6.79	0.04
PX10-175	*2.1*	6.99	0.05
PX10-175	*3.1*	6.08	0.06
PX10-175	*3.2*	6.27	0.02
PX10-175	*4.1*	6.27	0.06
PX10-175	*4.2*	7.66	0.04
PX10-175	*5.1*	3.47	0.05
PX10-175	*5.2*	7.04	0.05
PX10-175	*6.1*	7.24	0.04
PX10-175	*7.1*	6.91	0.05
PX10-175	*8.1*	6.46	0.04